The morphological effect of bottom vanes

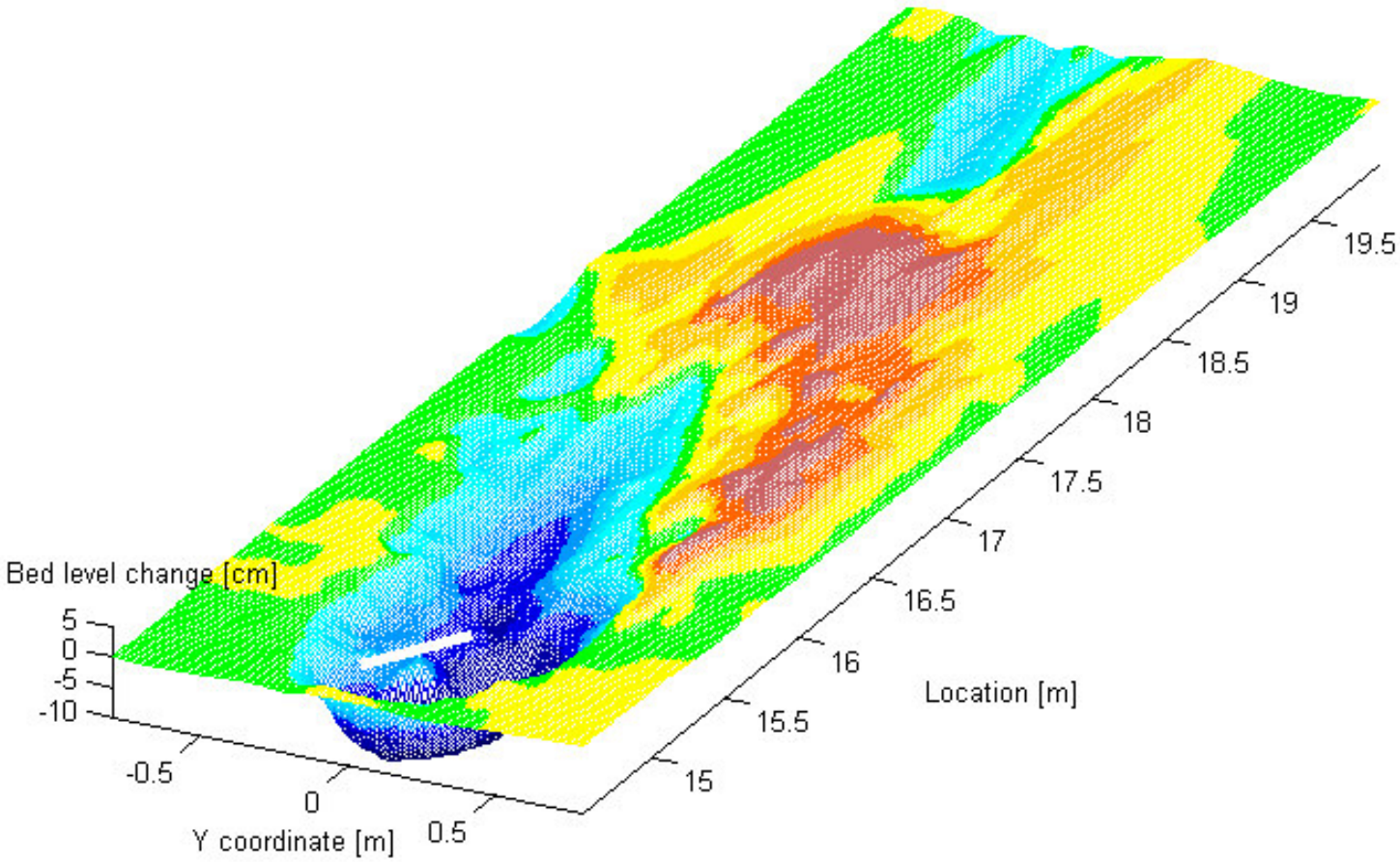

An experimental and a mathematical study

M.Sc. Thesis

By R.Zijlstra

TU Delft

Colophon

Title	The morphological effect of bottom vanes *An experimental and a mathematical study*
Author	R.Zijlstra
Student number	C9999577
Date	24 November 2003
Version	Final
Document	M.Sc. thesis
Contents	78 pages, 39 appendices
Organisation	Delft University of Technology Faculty of Civil Engineering and Geosciences Section of Hydraulic Engineering TU Delft http://www.tudelft.nl/
In co-operation with	WL|Delft Hydraulics Inland Water Systems River Engineering and Morphology WL | delft hydraulics http://www.wldelft.nl/ Bangladesh University of Engineering and Technology Faculty of Civil Engineering Department of Water Resource Engineering http://www.buet.ac.bd/
Graduation committee	prof.dr.ir. H.J. de Vriend dr.ir. H.L. Fontijn dr.ir. E. Mosselman dr.ir. C.J. Sloff
Accompanying document	Measuring report Experimental study of submerged vanes in the outdoor facility of BUET R. Zijlstra and J.A. van Zwol Delft University of Technology, September 2003

Preface

The report you are reading is the final result of my graduation project. With this project I will finish the educational programme for Civil Engineering at the faculty of Civil Engineering and Geosciences of Delft University of Technology.

In November 2002 the project started. After about two months of uncertainty and negotiation, in January 2003, fellow student Boye van Zwol and I finally heard that we could go to Bangladesh to do experiments at Bangladesh University of Engineering and Technology; a unique opportunity to combine graduation with experimental work and going abroad. Of course the circumstances for working in this developing country were far from ideal, but making the challenge even bigger.

After three months working in Bangladesh, we returned to the Netherlands and both worked on the measuring report. After that, in September 2003 I started writing this thesis on the morphological behaviour of a single bottom vane. Without having time to fully explore the theoretical backgrounds of the physics, and with a small, but valuable, dataset obtained during the experiments in Bangladesh, this report was written. Hopefully the reader will see this report as a useful addition to the knowledge on the behaviour of bottom vanes.

Finally I would like to thank the following people and instances for making this project possible; Boye van Zwol for the good co-operation, CICAT for the management in Bangladesh, BUET for making us feel welcome and the good support, Suman Saha for helping us out every day in Bangladesh, the Lamminga foundation for our flight tickets, WL|Delft Hydraulics for providing a working space, the Fluid Mechanics laboratory of TU Delft for the technical support, Erik Mosselman and Kees Sloff for the daily support and help, and finally Harry Fontijn and Huib de Vriend as members of my graduation committee.

Robert Zijlstra,

November 2003

Summary

Bottom vanes are submerged structures placed on the river bed. The foil-like structures are placed under a certain angle of attack to the main flow and have a certain height. The angle of attack can vary from typical values of 10 to 40 degrees. The height of a bottom vane is usually between 0.1 and 0.5 times the local water depth.

A bottom vane induces a secondary circular flow, so called spiral flow. This spiral flow resembles the curvature flow observed in river bends. This vane-induced spiral flow causes morphological changes. So, if placed correctly, bottom vanes can be effective river training work, for instance to prevent a river bank from eroding or to improve navigability in a river bend.

In order to understand and predict the effects of a bottom vane in a real river situation, much research has been done to reveal the working of bottom vanes. However, mainly due to the complex 3D flow around a bottom vane, the working is not yet fully understood. The complex interaction of flow and sediment transport in this 3D flow makes the situation even more difficult.

Odgaard and co-workers [Odgaard & Spoljaric, 1986, Odgaard & Wang, 1991a, 1991b] presented an idealised theory on the working of low angle of attack vanes (typical angles of attack of 10-20 degrees). Later, Marelius and Sinha [1998] executed experiments for a wider range of angles of attack and showed shortcomings in the theory of Odgaard. Also in experiments executed by WL|Delft Hydraulics shortcomings in the theory of Odgaard came to sight.

The current research intended to directly study the morphological effects of single submerged bottom vane for a wide range of angle of attack and various heights. Furthermore the modelling of bottom vanes in the morphological model Delft3D-MOR was investigated.

The main goals were

- Identify the main processes that cause the morphologic development behind a bottom vane in a straight channel, for both low and high angles of attack;
- Determine the influence of vane height and angle of attack on these mechanisms;
- Obtain experimental data to test the modelling of bottom vanes in the morphological model Delft3D-MOR;
- Determine whether the Delft3D-MOR bottom vane model can calculate the effect of a single bottom vane for both low and high angles of attack;
- Investigate how modelling can help understanding the complex flow around bottom vanes;

Together with a fellow student seven mobile bed experiments have been carried out in the outdoor facility of Bangladesh University of Engineering and Technology in Dhaka (Bangladesh). Both angle of attack and vane height were varied in order to determine the influence of the configuration on the effects.

From a theoretical analysis and analysis of the results of the experiments, four physical processes that cause the bed level changes around and behind the bottom vane, were identified.

These processes are:

- Vane-induced spiral flow;
- Vortex growth and deformation;
- Influenced sediment transport in longitudinal direction;
- Horseshoe vortex in front of the vane;

The vane induced spiral flow causes sediment transport in transverse direction and is the main effect of the vane. For both low and high angles of attack the spiral flow is present. The vane-induced spiral flow is carried downstream with the main flow. This spiral motion is also called, the main vortex. Changes in local depth significantly influence the development of the vortex and have to be taken into account. The vane height appeared to influence the affected area significantly, since the vortex grows in downstream direction. At the same time the strength of the vortex decays by bottom friction and fluid shear-stresses.

Besides transverse sediment transport, the bottom vane causes a change in the longitudinal sediment transport. The spiral flow changes the structure of the vertical longitudinal velocity distribution and causes more sediment transport on the lee-side of the vane. This effect grows with an increasing angle of attack, and is of importance for angles of attack above 20 degrees.

Finally, a significant scour hole is present for angles of attack above about 20 degrees. The final depth of the scour hole is dependent on both the vane height and the angle of attack. The experiments resulted in some rough estimates for the dimension of the scour hole. The presence of the scour hole did not prevent the vane from working as expected.

With aid of the mathematical model Delft3D-MOR simulations were made of the experiments. The results of the calculations were compared to the results of the experiments. Two modelling options were tested. The investigation focussed on how to model bottom vanes at a high angle of attack.

The bottom vane model in Delft3D-MOR is based on the theory of Odgaard. As not all relevant processes are modelled (correctly), the results were generally not in good agreement with the measurement from the experiments. The used model calculates a depth averaged flow field. As the effect of a bottom vane is dominated by 3D flow phenomena it is difficult to simulate these effects in a 2D flow model, especially on a local small scale.

It was advised to collect more data from the experimental set up in Bangladesh to get more information on the effect of the angle of attack and the vane height. For future modelling it was advised to improve the mathematical model by including more vane-induced physical processes, starting with the ones described in this report. The use of a 3D flow model probably improves the results of the simulations as 3D flow phenomena are simulated directly and not by artificial relations.

Table of contents

The morphological effect of bottom vanes

Appendices

List of figures

List of tables

List of symbols

The list displays only the major symbols that are used throughout this document. All symbols are also specified below the specific formulae.

Symbol	Explanation	
α	Vane or screen angle to mean flow direction	[°]
Δ	relative density sediment	[-]
ε	eddy viscosity	[m^2/s]
θ	Shields parameter	[-]
ϕ	vortex damping	[-]
Γ	vortex intensity	[m/s]
d	local water depth	[m]
$\overline{d}$	average water depth	[m]
g	gravitational acceleration	[m/s^2]
r	distance from the core of the vortex	[m]
s	distance downstream of trailing edge along vortex line	[m]
u	flow velocity in x-direction	[m/s]
v	flow velocity in y-direction	[m/s]
w	flow velocity in z-direction	[m/s]
x	coordinate x-direction	[m]
y	coordinate y-direction	[m]
z	coordinate z-direction	[m]
B_v	effective vane width	[m]
B_{vor}	vortex width	[m]
C	Chézy roughness coefficient	[$m^{1/2}/s$]
H_v	Vane or screen height	[m]
L_v	Vane or screen length	[m]

1 Introduction

1.1 River engineering and vanes

In the Netherlands and Bangladesh, people started influencing their river systems already long ago. Although both countries have totally different river systems and totally different demands on the river, the common goal of river training is to minimize risks and to maximize benefits from the system.

On the river Waal in the Netherlands navigability is a very important issue. The River Waal is one of the most important inland waterways in Europe, and therefore the Dutch authorities are constantly trying to improve the river. One type of bottleneck is the navigable width in bends. The natural curved flow in bends decreases the depth in the inner bend.

At the moment these shallow parts are deepened by dredging, a flexible and therefore cost-efficient option. However, this maintenance dredging is necessary repeatedly. Bottom vanes are intelligent submerged structures that influence flow, and consequently morphology, and are supposed to last for a long time. Although initial construction costs are high, their low maintenance and long lasting effectiveness can make them a favourable alternative for dredging. Recently, also for the river IJssel in the Netherlands, attention is given to bottom vanes, as other river training options appear to be ineffective or too expensive.

In Bangladesh river problems are of a different class. Huge rivers, amongst others river Ganges and Jamuna river, divide the country in parts and pose a constant threat to the people. Examples of large scale problems are several locations of severe bank erosion and the silting-up of the off take of Gorai River, causing multiple problems along this river in the dry season. The bank erosion forces people to move even more than once a year, causing large social problems.

Figure 1.1: Bank erosion and bottom vane in Bangladesh

In Bangladesh bottom vanes could help controlling the behaviour of these large river systems, and reducing the threats they pose. In recent history also prototype vanes have been placed in the Meghna River (Figure 1.1 right).

1.2 The principle of vanes

In literature, many different names appear for the concept of influencing river flow and sediment transport by influencing part of the cross-section by means of foil-like hydraulic structures. Some examples: bottom vane, bed vane, surface screen, guide vane, silt vane, bottom groyne or submerged vane. In principle, there are two concepts.

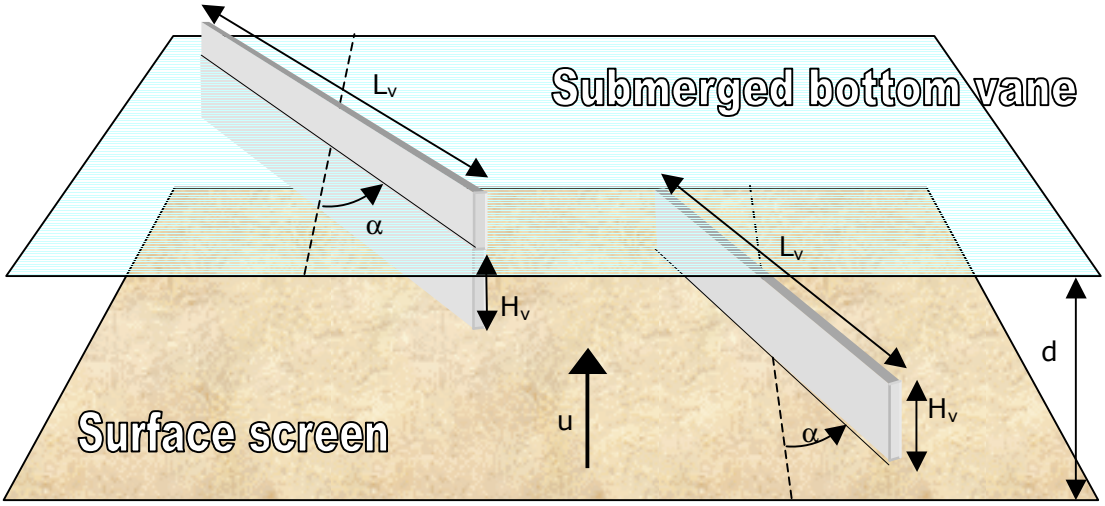

Figure 1.2: Surface screen and submerged bottom vane

The surface screen changes the direction of the near-surface flow, whilst the submerged bottom vane changes the direction of the near-bottom flow. Normally the surface flow will transport less sediment than the bottom flow and therefore the sediment transport direction changes. Furthermore, the vane can induce a secondary flow. Odgaard and co-workers [Odgaard & Spoljaric, 1986, Odgaard & Wang, 1991] derived a theory describing the origin and effects of this vortex for submerged bottom vanes. The vortex resembles the spiral motion that is known from bend flow. Also for surface screens such a vortex has been reported. Of course, the presence, form and strength of the vortex are dependent on the geometry of the vane. The geometry of the vane or screen is characterized by two dimensionless parameters; H_v / L_v and H_v / d. The specification of the symbols can be read from Figure 1.2.

The first parameter is often referred to as the aspect ratio. In aerospace engineering the aspect ratio is also known, but for a wing the value is usually large whilst for vanes and screens it is quite small. The second parameter, vane height divided by water depth, indicates along with the angle of attack, to what extend the main flow is blocked.

The effects caused by a surface screen or submerged bottom vane can be used to influence the behaviour of a morphodynamic system. In order to influence such a system, normally a field of several vanes or screens has to be used to obtain a significant large-scale effect.

1.3 BUET – DUT linkage project

In 2001 CICAT started the Bangladesh University of Engineering & Technology – Delft University of Technology (BUET-DUT) linkage project, titled "Capacity building in the field of Water Resource Engineering and Management in Bangladesh". CICAT is the central liaison office of Delft University of Technology

(DUT) providing its faculties and departments with management support in the field of development cooperation activities.

In December 2002, the author and fellow student J.A. van Zwol had the opportunity to join the Bangladesh research team within the project "The experimental research on the effect of bottom vanes on river flow and morphology". At that time the main goal of the project was to set up experiments to determine the magnitude of local scour around bottom vanes for 20 different configurations. The research was adapted in such a way that two separate M.Sc. theses could be written by the author and the fellow student. The extensions included far field bed measurements and flow velocity measurements. Further information about the research in Bangladesh, and results, can be found in the measuring report [Zijlstra & van Zwol, 2003].

1.4 Mathematical modelling

In river engineering, mathematical modelling is a tool that is used very often. Representing reality in a model makes it possible to make predictions. The problem with modelling is always how to simplify reality without loosing the system behaviour that you are looking for. For bottom vanes this problem is quite complex as the flow phenomena around a vane are fully three-dimensional, and therefore hard to simplify.

Delft3D-MOR is a state-of-the-art modelling package for 2D and 3D free-surface flow. At the moment two modelling options for bottom vanes are implemented in a version that is not commercially available yet. Basically, in this report answers are sought to the question "How to model bottom vanes?"

1.5 Reading this report

This report describes the results of the research on the effect of a single submerged bottom vane. In contrast to much other research also high angles of attack are taken into consideration.

After the introduction in this chapter, Chapter two discusses the most relevant literature. The theory of Odgaard is explained and also the experimental and mathematical research of Marelius and Sinha is mentioned. Also some attention is given to relevant literature on mathematical modelling. Chapter three explains the goals, and Chapter four how these goals are reached.

In Chapter five a short summary of the experimental research in Bangladesh is given. The reader must note that there is also an accompanying measuring report with extensive background information on these experiments. For reading this report however, the measuring report does not have to be read.

Chapter six is the core of the report as it treats the morphological effect of a bottom vane. First the physical processes around and behind the vane are investigated. Then the results of the experiments are presented. Finally, based on the experimental research, the influence of the vane geometry on the physical processes is discussed. Chapter seven analyses the water level set up caused by the vane.

Then in Chapter eight the mathematical modelling of vanes comes up. The current modelling options and experiences are given. It is discussed how vanes at high angles of attack can be modelled.

Finally in Chapters nine and ten the conclusions and recommendations are presented.

2 Literature

2.1 Introduction

The use of hydraulic structures to guide flow in a river is not a new invention. In South-Asian regions like Bangladesh and India "bandalling" was applied already some time ago and still is [Joglekar, 1971]. Also in de former Soviet-Union research was done just past the 2nd world war on how to control flow with artificial secondary flow [Potapov, 1950]. Furthermore, WL|Delft Hydraulics was involved in research on surface screens [Filarski, 1966] and Remillieux [Remillieux, 1972] explored the possibility of using bottom vanes already 30 years ago.

In most of this early research, physics were not deeply explored. Mainly the practical application of bottom vanes and surface screens was investigated. Also quite some field tests were conducted, resulting in some practical considerations on how to use vanes or screens to influence river morphology.

2.2 Theory of Odgaard

In 1986, Odgaard and Spoljaric [1986] presented, and tested, a first basis for the well-known description of bottom vanes. The theory is derived for so-called small-aspect submerged bottom vanes at an angle of attack of 10-15 degrees with the flow. In 1991 Odgaard and Wang [1991a, 1991b] published the full theory. They derived this theory from aerodynamics by considering the vane as an aircraft wing. On the high-pressure side, the water moves up along the vane and on the low-pressure side, it moves down. At the end of the vane the two flows meet and create a spiral motion (Figure 2.1, left). This vortex grows or expands until it is bounded by the bottom or the water surface. On the bottom the direction and magnitude of the shear stress is changed, causing a change in velocity distribution and sediment transport.

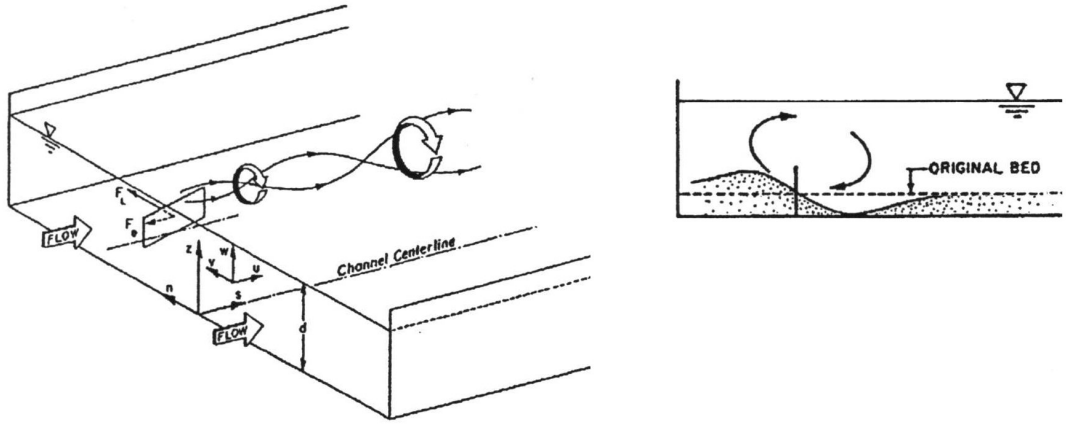

Figure 2.1: Effect of a single vane on flow and bed [Odgaard & Wang, 1991a]

In aerodynamics, this vortex is called the wing-tip vortex. In order to understand what happens two pictures from aerodynamics have been added below.

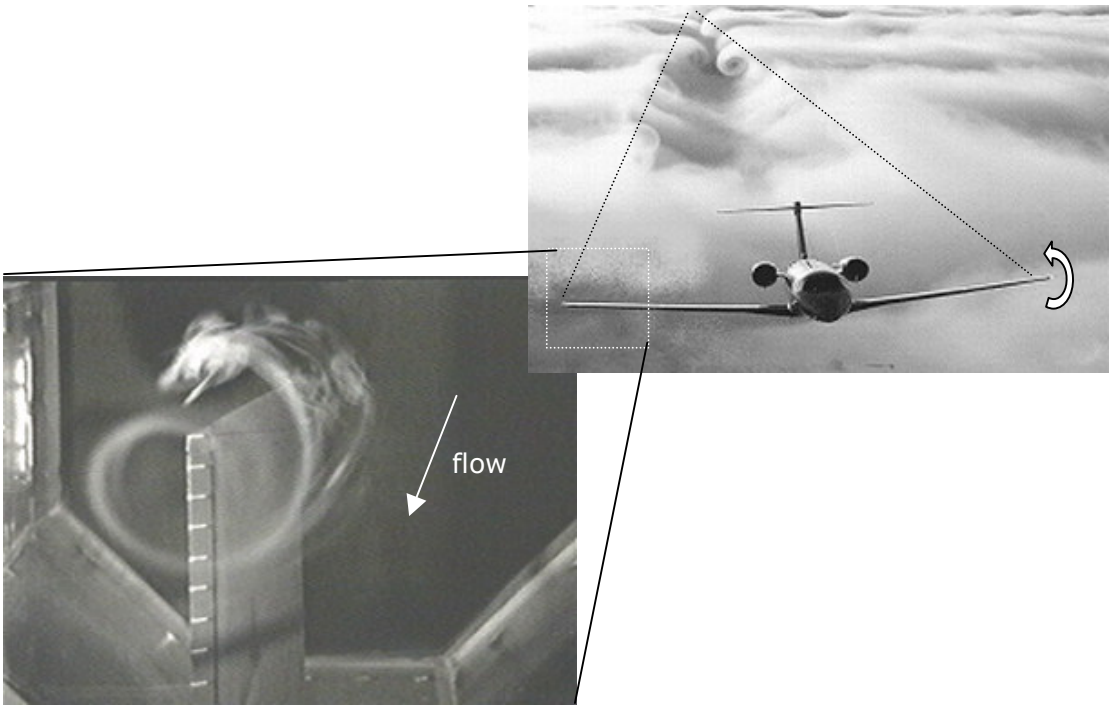

Figure 2.2: Wing tip vortex in aerodynamics

The picture on the right shows an aircraft in flight. "Downstream" of the plane, rotating airflow can be distinguished in the clouds. This vortex originates from the tip of the wing, as can be seen in the left picture taken in a wind tunnel. In principle, the left picture also shows what happens for a bottom vane.

According to Lamb [1932], the tangential velocity caused by such a vortex in water, can be described by:

$$v_\theta = \frac{\Gamma}{2\pi r}\left[1 - e^{-\frac{u}{4\varepsilon s}r^2}\right] \tag{2.1}$$

in which:

Γ	vortex intensity at s= 0 $[m^2/s]$
r	distance from core $[m]$
u	flow velocity x-direction $[m/s]$
ε	eddy viscosity $[m^2/s]$
s	downstream distance along streamline $[m]$
v_θ	tangential velocity $[m/s]$

Figure 2.3 below shows what this so called "Rankine" vortex looks like in an unbounded flow field (input parameters are based on the characteristics of the flume used in the experiments, Section 5.2). The x-axis coincides with the vortex core-axis.

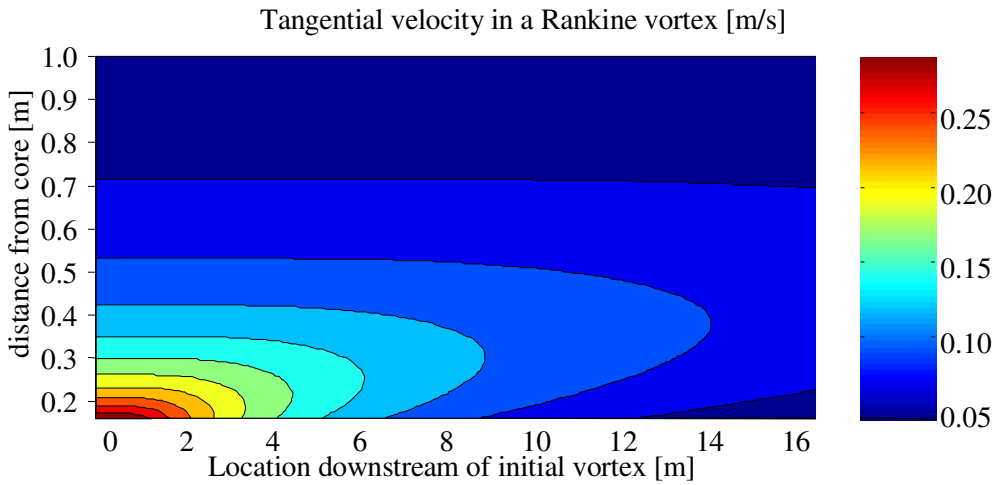

Figure 2.3: Tangential velocity in a Rankine vortex

The initial vortex decays in downstream direction, whilst the point of maximum tangential velocity shifts away from the core-axis. This description is valid only for an unbounded flow field. In a river or flume, the river bed or the water level bounds the development of the vortex.

By using the method of images the effect of the bed and water level can be derived. Adding up the effect of imaginary sources below the bed and above the water level give the total effect. Furthermore, the vortex intensity is derived from the lift force. Then Odgaard obtains the following description for the near-bed velocity. In this description, he assumes that the image from the water level is so small that it can be neglected.

$$v_{s|z=0} = \frac{F_L}{\pi\rho u H_v}\sum_{j=1}^{\infty}\frac{(-1)^{j+1}}{r_j}\left[1-e^{-\frac{u}{4\varepsilon s}r_j^2}\right]\frac{z_j}{r_j} \qquad (2.2)$$

with

$$F_L = \frac{\rho\pi\alpha}{1+\frac{L_v}{H_v}} L_v \int_0^{H_v} u^2 dz$$

in which:

$v_{s\|z=0}$	near-bed transverse velocity $[m/s]$
F_L	lift force on vane $[N]$
z_j	vertical distance from stream bed to core $[m]$
r_j	distance from core $[m]$

The remaining parameters are defined in Figure 1.2.

The solution of the summation describes the transverse velocity field caused by the vane. In practice, however, usually not this full equation is used or solved. With aid of experiments more simple equations are derived, and Odgaard's theory is only used to calculate the maximum transverse velocity at $s = 0$. The far field description then becomes:

$$v_{z=0}(s, y) = v_{s=0|z=0} \cdot \phi(s) \cdot \phi(y) \tag{2.3}$$

The longitudinal damping ($\phi(s)$) is described by a simple logarithmic damping:

$$\phi(s) = 1 - e^{\frac{-\lambda_d}{s}} \tag{2.4}$$

with

$$\lambda_d = \frac{3}{2\kappa}\frac{Ch}{\sqrt{g}}\left(\frac{H_v}{h}\right)^2 [m]$$

in which:

g	gravitational acceleration $[m^2/s]$
C	Chézy roughness coefficient $[m^{1/2}/s]$
κ	von Karman coefficient $[-]$

In this formula λ_d represents the characteristic damping length. The Figure below shows how the damping develops.

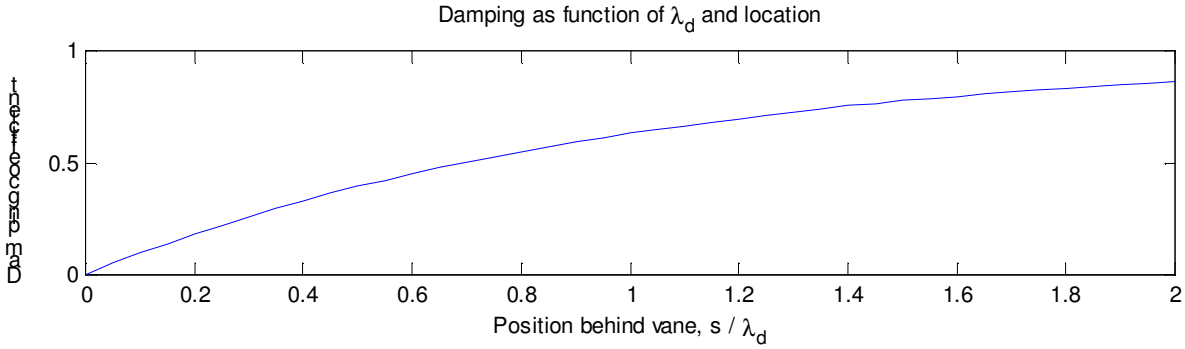

Figure 2.4: Damping of transverse near-bed velocity in longitudinal direction

According to the theory of Odgaard & Spoljaric [1986] the vortex spreads as a cosine in transverse direction.

$$\phi(y) = \cos\left(\pi\frac{y}{d}\right) \tag{2.5}$$

valid from:

$$-\frac{\overline{d}}{2} \le y \le \frac{\overline{d}}{2}$$

Later, Wang [1991] described the transverse velocity distribution as:

$$\phi(y) = \frac{1}{1 + \left(\frac{y - \mu}{\delta_H H_v} \right)^2} \tag{2.6}$$

with

$\phi(y)$	vortex damping in transverse direction $[-]$
$\bar{d}$	average initial bed level $[m]$
μ	location of maximum transverse velocity (usually core axis) $[m]$
δ_H	coefficient for height core centre relative to vane height (experimentally found at 0.8) $[-]$

Figure 2.5 shows the difference between the cosine and the function Wang suggested for an arbitrary numerical example.

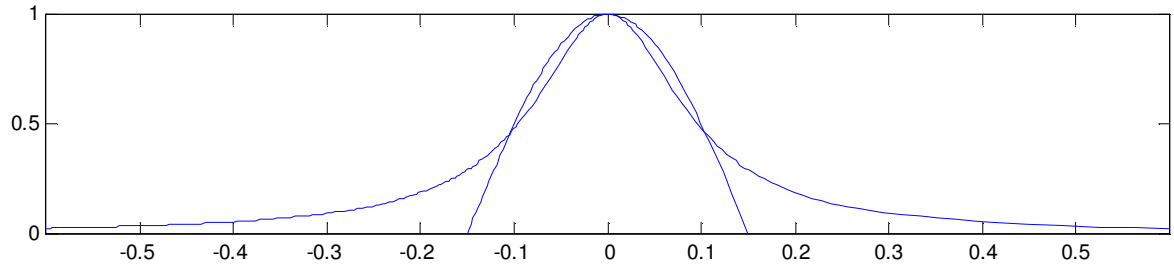

Figure 2.5: Distribution of transverse velocity

The theory of Wang fits much better on experimental data. Note that the theory of Wang resembles the Lamb vortex description as the decay in width (for Lamb vortex also height) depends on the square of the distance to the core of the vortex.

Odgaard & Spoljaric [1986] included the following formula for the bed level change in a cross-section in case of a single vane based on the cosine distribution of transverse velocity:

$$\frac{d - \bar{d}}{\bar{d}} = \frac{K}{\pi} \sin\left(\pi \frac{y}{\bar{d}} \right) \tag{2.7}$$

valid from:

$$-\frac{\bar{d}}{2} \le y \le \frac{\bar{d}}{2}$$

with

$$K = a v_{sc} = \frac{3\alpha\sqrt{\theta}}{2k} \frac{v_{sc}}{\sqrt{gD\Delta}}$$

in which:

v_{sc}	transverse flow velocity in cross-section $[m/s]$
α	ratio of projected surface area to volume of a particle, divided by that for a sphere of the same volume (river sand 1.27) $[-]$
$k\ (\approx 1)$	ratio of critical near bed velocity [Odgaard & Spoljaric, 1986] $[-]$
θ	Shields parameter $[-]$

Obviously, this formula only predicts bed level change in the range $-\frac{\overline{d}}{2} \le y \le \frac{\overline{d}}{2}$ and is just a simple approximation of the reality.

2.3 Experiments for high angles of attack

Since Odgaard restricted his theory to low angles of attack, Marelius and Sinha [1998] explored the possibilities for applying higher angles of attack. Odgaard states that vanes at high angles of attack cause extra flow resistance and cause formation of large scour holes. Marelius and Sinha [1998] suggest that higher angles of attack cause a stronger circulation and that the formation of a scour hole may even improve the effectiveness of the vane or vane system. Furthermore, they questioned the design equations for vane systems of Odgaard:

"First and foremost, continuously evolving flow field and topographical features in the field may result in vanes at higher angles of attack than originally intended. Secondly, the highly idealized analysis of flow through fix-bed straight rectangular channel presents an overly simplified picture of the situation in the field".

Marelius and Sinha set up a series of experiments in which they determined which angle of attack induces the largest circulation, and for that angle they extensively measured the flow field to reveal the complex 3D-flow around the vane. Figure 2.6 shows the results of the experiments. Marelius and Sinha concluded that the intensity of the vortex rotation is at a maximum for an angle of about 40 degrees. The first figure shows this. The second and third figures show that not only the wing-tip vortex is present but also two counter rotating vortices originating from the horseshoe vortex. They also conclude that due to the scour hole the vortex is effective over a larger width, but acknowledge the practical problems for such large scour holes.

Sinha and Marelius [2000] undertook a numerical study of flow around a submerged vane. They were capable of reproducing the measured velocity field with good general agreement.

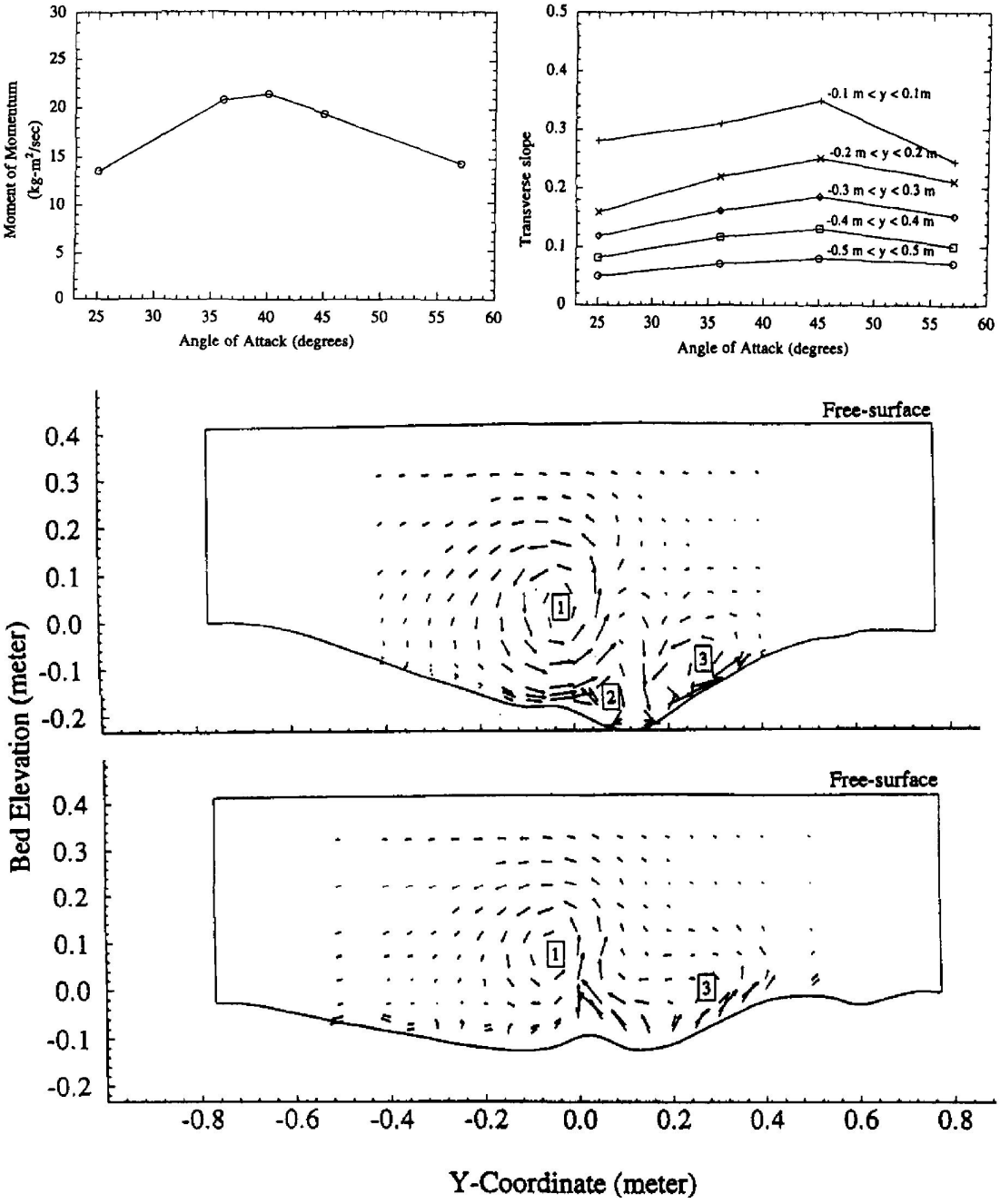

Figure 2.6: Results experiments [Marelius & Sinha, 1998]

Although Marelius and Sinha did show the shortcomings of Odgaard's theory, no improved theory was derived. For high angles of attack, so far, no theoretical description is available.

2.4 Delft Cluster project "Vanes and screens"

In the period 2000-2002 WL|Delft Hydraulics executed the Delft Cluster Project "Vanes and screens". The main objective was to implement and test the modelling of bottom vanes and surface screens in the mathematical modelling environment Delft3D-MOR. More in general, the research intended to obtain more insight in the

physical mechanisms that determine the hydraulic and morphological effects of bottom vanes.

The research consisted among other things of a series of experiments. In these experiments the lift and drag forces exerted on the vane by the flow were measured and compared to the theory of Odgaard [Jongeling & Flokstra, 2001].

Some important conclusions and recommendations for this study are:

- Higher vanes cause a relatively larger effect on the flow and the effect can be noticed further downstream but lower vanes can cause more changes directly downstream of the vane;
- The theory of Odgaard generally underestimates the maximum transverse flow velocity directly behind the vane. At more distance behind the vane, the effects of higher vanes are over-estimated and those of lower vanes under-estimated. In general, the prediction for higher vanes is better than for lower vanes;
- The function of Wang (2.6) [Wang, 1991] describes the distribution of transverse velocity in transverse direction fairly well;
- The experiments are conducted with only one angle of attack (17.5°). Therefore, it is advised to further investigate the effects of different (higher) angles of attack since this parameter mainly determines the characteristics of the flow field behind the vane;
- Some attention can be paid to the effect of local sedimentation or erosion on the effect of a vane;

Finally, two ways of modelling vanes were implemented in the Delft3D-MOR modelling environment. [Flokstra et al., 2002]

Type 1 vane modelling is based on the theory of Odgaard. A vane is modelled within one grid cell, and a mathematical sub-model calculates the vane-induced transverse bed shear stress. With aid of damping formulas, the transverse bed shear stress in grid cells downstream of the grid cell containing the vane, is calculated. In this modelling only the sediment transport direction is influenced. Besides some extra resistance, no effects on the flow field are included.

In type 2 vane modelling a vane is modelled by placing submerged weirs on grid cell boundaries. The effect of the vane on the far field follows from the changed flow field. The sediment transport is not directly influenced like for type 1 vanes.

For the modelling of vanes some recommendations have been made that are relevant for this study.

- For type 1 modelling:
  - The vanes are switched off if the angle of attack is larger than 22 degrees. At least the vane resistance should be taken into consideration. Furthermore, it is stated that Marelius and Sinha showed that vanes at higher angles of attack have larger effect;
  - More test cases;
- For type 2 modelling:
  - Making model tests to judge the performance of the modelling;
  - Making a simulation in Delft3D for a flume of which the model results are known;

2.5 Design study bottom vanes for river Waal

Besides participating in the Delft Cluster project, WL|Delft Hydraulics has performed more experimental research on bottom vanes in the recent past. The reports are summarised, and important conclusions are repeated below.

- Q2418, Optimaliseren lengte bodemschermen, 1998;
- Q2322, Waalbocht Hulhuizen: flankerend onderzoek schermen, 1997;
- Q1779, Fairway improvement of the Bovenwaal; Scale model test with bottom vanes, 1995;
- Q2264/Q2291, Waalbocht Hulhuizen, schermenonderzoek in de Zandgoot, 1996, 1997;

All research was conducted in a fixed-bed flume. Important conclusions were:

- In general the theory of Odgaard underestimates the maximum transverse flow velocity directly behind the submerged vane;
- Further downstream of the vane, the effects of low vanes are under-estimated and those of high vanes over-estimated;
- Directly downstream of the vane the width of the vortex is about $\delta_H (\approx 0.8) H_V$. Further downstream it is better to take the vortex width equal to the water depth. For relatively high vanes the value $\delta_H (\approx 0.8) H_V$ for the initial vortex width is also not very accurate;
- The deviation of the vortex-line from a straight line from the centre of the vane is very small;
- High vanes are more effective further downstream, whilst low vanes are more effective directly behind the vane;
- For high vanes the vortex core axis shift towards the bottom, whilst for low vanes the vortex core axis shift towards the water level;

3 Problem description and objectives

The problem description is split in three parts. The main part of the study is the investigation of the morphologic behaviour in a flume caused by a single vane. Secondly, the water level set up caused by the vane, is investigated. And finally, it is investigated whether current bottom vane modelling is capable of predicting the behaviour of a single vane.

3.1 Morphology

In literature, almost no information is available on vanes and morphology. Most done research focuses on the flow phenomena, and not on the transport mechanisms. Of course, in principle, morphology can be determined from the flow field, but the interaction between them is often too complex. But even the flow phenomena itself are not exactly known. Many authors questioned the theory of Odgaard describing the vane-induced spiral flow by means of the wing-tip vortex theory from aerodynamics. Based on experimental research, others [Flokstra et al., 1998] concluded that the theory was not complete since theory and measurements of lift forces on the screen did not correspond well. Besides that, their theory is not valid for high angles of attack, whilst Marelius and Sinha [1998] showed in their experiments that for high angles of attack similar results can be obtained.

The main restrictions in the theory of Odgaard are:

- Not valid for high angles of attack, due to flow separation (lift coefficient);
- Neglect of complex 3D-flow around vane (horseshoe vortex);
- Effect of scour holes on the near-vane flow field is not included;
- Simplified description for morphological development behind screen;

Since Marelius and Sinha proved that also for high angles of attack the desirable effect can be obtained, similar processes like Odgaard and co-workers showed for low angles of attack, must exist also for high angles of attack.

It is expected that high angles of attack cause scour like around bridge piers or other constrictions in rivers. Local scour is a phenomenon that is best predicted from empirical relations. For vanes, such a relation is unknown and it is also not known how this scour influences the functioning of the vane.

The theory of Odgaard, and much other research, was restricted to small angles of attack, as vanes at high angles of attack would have large scour holes and too much water level set up.

This leads to the following goals:

- Identify the main processes that cause the morphologic development behind a bottom vane in a straight channel, for both low and high angles of attack;
- Determine the influence of vane height and angle of attack on these mechanisms;

3.2 Water level set up

A vane or screen introduces extra flow resistance. This flow resistance decelerates the water movement and results in water level set up. Water level set up is an important factor in river management as it raises flood levels. The complex flow around vanes and the scour hole make it difficult to analytically predict the amount of water level set up.

Goal:

- Determine the magnitude of water level set up;

3.3 Modelling

The current knowledge on the physics on vanes is not complete. In the computational models Rivcom and Delft3D the theory of Odgaard and Wang [1991] containing an idealized description of flow past submerged vanes is used. Odgaard's theory is not valid for high angles of attack since the flow phenomena are not described correctly anymore. Marelius and Sinha [1998] did investigate the flow around high angle of attack vanes, but they did not present any theoretical expression to describe it. It should be investigated whether Odgaard's model also makes reasonable predictions for higher angles of attack.

As described in Section 2.4, Delft3D-MOR supports two bottom vane modelling options; type 1 and type 2 modelling. For the modelling of vanes, the following recommendations were made in the recent Delft Cluster report [Flokstra et al., 2003, p.42]:

- Extension of the type 1 vane model with respect to large angles of flow attack;
- Extension of the vane type 2 model with a vortex line model;
- Execution of additional type 2 morphological simulations for cases for which a datasets with measurements is available;

The first recommendation can only be fulfilled if knowledge is available on how vanes at large angles of attack work. So far, only experimental data are available for fixed-bed experiments, except for one dataset by Marelius and Sinha.

Goals:

- Obtain experimental data to test the modelling of bottom vanes;
- Determine whether the Delft3D-MOR bottom vane model can calculate the effect of a single vane, and determine whether it is possible to model vanes at high angle of attack for type 1 modelling without adaptations to the model;
- Determine the performance of the Delft3D-MOR type 1 bottom vane model for modelling high-angle-of-attack vanes (only in case it is possible to model high angles of attack);
- Determine whether the type 2 modelling is suitable to simulate the behaviour of vanes at high angles of attack;
- Investigate how modelling can help understanding the complex flow around bottom vanes. Investigate which modelling options are best for near-future vane modelling in order to further investigate the complex behaviour of flow and transport in vane influenced areas;

4 Research method

In order to reach the goals set in Chapter 3, a research plan was set up. The chapter is divided in three parts, morphology, water level set up and mathematical modelling.

4.1 Morphology

To investigate morphology and water level set-up, an experimental research was set up at BUET, Bangladesh. In the flume, bottom vanes were tested with several heights and angles of attack on a movable bed under controlled conditions. The results have been analysed, and together with data from previous research, the underlying physical processes are investigated.

In order to understand the morphology, first the main processes around a bottom vane are identified. Then it was chosen to set up an experimental model and see how the results vary for different single vane configurations. By varying the angle of attack and vane height, the significant processes can be recognised from the changes in the results of the experiments. It was decided to test both low and high angles of attack, as this had not been done before. Also the vane height was investigated.

By analysing the bed level and also the flow velocity measurements, the influence of the angle of attack and vane height are investigated.

In the following sections it is described how the different measurements have been obtained, processed and visualised.

4.1.1 Bed level measurements

From the experiments seven series of bed level measurements were obtained. These were processed and presented graphically. In this section is explained how this was done.

4.1.1.1 Data post processing

The data obtained from the experiments were first processed before they were analyzed. The bottom was measured on an irregular grid and therefore it was difficult to simply plot pictures. The measuring points slightly varied for the different experiments but in general the following area was measured.

Bed level measuring points	Grid size in x-direction	Grid size in y-direction on intervals -0.5m > y > 0.5m	Grid size in y-direction on interval -0.5 m < y < 0.5 m
x = 14.50 – 15.30 m	5 cm	10 cm	5 cm / 2.5 cm
x = 15.30 – 16.00 m	10 cm	10 cm	5 cm / 2.5 cm
x = 16.00 – 18.00 m	20 cm	10 cm	5 cm / 2.5 cm
x = 18.00 – 20.00 m	50 cm	10 cm	5 cm

Table 4.1: Bed level measuring points

The measurement points were interpolated on a fine grid of 2 x 1 cm^2 with the aid of the mathematical program Matlab. Near the vane, this generated errors since no distinction was made between measuring points in front and behind the vane. Since this was not the area of interest, no solution was necessary. Besides that, the errors are rather small due to the fine grid.

Besides plain measurement errors the original data set contains disturbances caused by ripples. In order to reduce these effects, the interpolated data set was spatially averaged on an area of 8 x 3 cm^2. This averaging only influences the data that was obtained from a finer grid in the first place. The dataset thus obtained contains the bed level in cm above the reference level. By subtracting the average of the dataset from the actual data the bed level change is obtained. By using this method, it is assumed that all erosion is exactly counterbalanced by sedimentation in the area x = 14.50 – 20.00 m from y = -1.25 – 1.25 m.

The following table compares the different average bottom levels. It has to be borne in mind that the accuracy of a single bed level measurement is estimated at seven mm. Note that A3c stands for the second dataset obtained during a check. The moment of measuring (hours of flow) is given between brackets.

Average bottom level [cm + REF]	A3 (8h)	A3c (42h)	A1 (17h)	A4 (34h)	A2 (16h)	B2 (35h)	C2 (35h)	B3 (49h)
Used for installation vane	50.7	N.A.	52.3[1]	51.2	51.2	51.2	51.2	51.2
From bed level measurements	N.A.	51.0	51.4	50.9	51.4	51.7	51.3	51.5
- before processing	51.3	50.9	51.5	50.6	51.6	51.6	51.4	50.9
- after processing								

Table 4.2: Average bottom levels

Since the calculated average bed level after processing is assumed to be the best representation of the true value of the bed level, and since this value is not equal to the bed level used to install the vane, the actual vane height and water depth are not exactly equal to the intended value (compare first and third row).

The new properties are summarized in Table 4.3 below.

[cm] or [cm + REF]	A3	A1	A4	A2	B2	C2	B3
Top of vane (bed for installation + H_v)	50.7 +12	52.3 +12	51.2 +12	51.2 +12	51.2 +6	51.2 +18	51.2 +6
Measured average water level (PG2)	80.9	82.2	81.1	81.1	81.3	81.4	81.3
Average bed level	50.9	51.5	50.6	51.6	51.6	51.4	50.9
Actual vane height	11.8	12.8	12.6	11.6	11.6	11.8	12.3
Water depth	30.0	30.7	30.5	29.5	29.7	30.0	30.4
H_v / d	0.393	0.417	0.413	0.393	0.391	0.393	0.405

Table 4.3: Corrected water depth and vane height

During the first four experiments the bed was not reconditioned systematically. Only the visually observed deviations from the average bed level were levelled before starting a new experiment. From the results (preliminary contour plots), it appeared that the resulting bed levels from experiment A2, subsequent to experiment A4, were clearly influenced by the results of experiment A4. The longitudinal profiles in Appendix B show that especially on the section x = 15.50 up to 16.50 m, the bed of experiment A2 is about 1 cm below the average.

[1] A measuring error was made in experiment A1. This value is too high.

For experiments A3, A4, C2 and B3 this is also the case, but this is clearly caused by the scour hole around the vane. Since experiment A2 did not have a significant scour hole, influences up to x = 16.50 m are not expected, and are therefore probably originating from the previous experiment A4. Also further behind the vane (x = 18.00 – 20.00 m), the bed measurements indicate patterns that contain remains from the sedimentation pattern in experiment A4. It was decided to correct for these effects in experiments A1, A2 and B2. The correction applied is subtracting the average of each single cross-section from the measured data on the section x = 15.40 – 20.00 m. These experiments did not have large scour holes and are therefore not expected to show change in the longitudinal direction as in experiments A4, A3, B3 and C2. So, after the correction, the longitudinal profile for these experiments is perfectly flat, except for the section x = 14.50 – 15.40 m where the correction was not applied because the scour hole influences the cross-sectional average.

In Figure 4.1, the modifications to the dataset have been presented graphically.

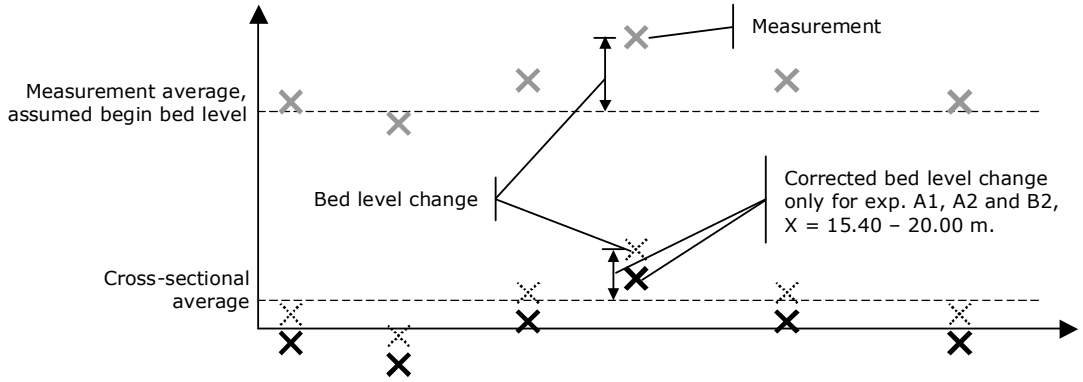

Figure 4.1: Corrections to dataset

4.1.1.2 Output

A contour plot was generated for each experiment. Whilst the contours suggest a continuous record, it has to be realized that the result is obtained from an irregular grid of which the data density is much higher near the vane, and in the centre line behind the vane. The contour plots are displayed in Appendix C. For experiment A3 two contour plots are included, the original measurements after 8 hours, and the check after 42 hours.

Furthermore, cross-sectional plots have been generated. These cross-sectional plots provide better insight in the bottom profile. The cross-sectional plots are the result of averaging the cross-sectional profile over a certain distance. The resulting plots are displayed in Appendix D.

In Appendix E the difference between the check measurements and original measurements for experiment A2 are displayed. In the following analysis however, the original data is used.

Finally, in Appendix F photographs of the resulting bed are included.

4.1.2 Flow velocity measurements

During the experiment flow velocities were measured near the vane and in the far field. For the morphological development mainly the far field data has been used. In Appendix A the measuring locations, x = 15.20, 15.80 and 16.60 m have been indicated. The locations are at respectively 0.0, 1.5 and 3.5 vane lengths, or 0.0, 2.0 and 4.33 times the water depth behind the trailing edge of the vane.

During the experiments a Labview environment stored the measurements in overview files containing the time, coordinates and average u and v velocities. These files were imported in Matlab and plots were produced. No further operations were applied to improve the dataset.

Two types of plots are made of the data. First, the transverse flow velocity in the cross-sections x = 15.20, 15.80 and 16.60 m is plotted. In these plots (Appendix G) the transverse velocity is vector plotted in a y-z plane and the magnitude of the transverse velocity is plotted as a function of the y coordinate. With coloured lines and markers the z-coordinate is indicated.

The second series of plots (Appendix H) indicate the longitudinal or stream wise velocity at cross-section x = 15.80 m. The magnitude of the velocity is plotted against the Y coordinate. For the different z coordinates again the coloured lines and markers are used.

4.2 Water level set up

The water level set up is investigated in the experimental model too. Water level measurements have been taken at three locations, one and eleven meters in front of the vane (PG1 and PG2), and nine meters behind the vane (PG3). So, the water level slope can be calculated by dividing the water level elevation difference, by ten.

The accuracy of the measurements is limited. Due to wave action in the flume, it was difficult to estimate the water level. The accuracy is expected to be about 1 mm.

On a regular basis all three point gauges were read. For every experiment approximately 50 measurements were taken. These were analysed, corrected and averaged. The measuring report [Zijlstra & van Zwol, 2003] describes this more extensively.

In order to obtain more data also the three-dimensional flow model Delft3D has been used to investigate the water level set up.

4.3 Modelling

In this research an experiment – model approach was chosen. So, first experimental data was collected, and then a morphological model was used to reproduce the results and evaluate the model.

The current modelling is evaluated and compared to the found physical processes around vanes. It is investigated how high angle of attack vanes can be modelled within the current Delft3D-MOR bottom vane model.

Numerical simulations are made for an initial flat bottom to see how the bed level develops. Then runs are made with initial bed levels equal to the experimental results and the bed level development is evaluated.

Both type 1 and type 2 modelling have been tried in order to judge the modelling possibilities.

5 Experiments in Bangladesh

5.1 Summary

In the period from March to June 2003 experimental research was done at Bangladesh University of Engineering and Technology (BUET) in Dhaka, Bangladesh. Before beginning the experiments several preparations had to be made since the facility was not ready at arrival. More or less one month was needed to complete preparations and test runs.

Figure 5.1: Outdoor facility BUET, Bangladesh

In the remaining two months, seven experiments were executed. The experiments were conducted in a straight flume with a movable bed. During the experiments scour development around the vane was monitored. After several hours also velocity measurements were taken. The main goal was to map the local flow field around the vane, but also some measurements were taken in the far field behind the vane. After the experiment, the bed level change was measured.

Main goals of the experiments were to investigate, for both low and high angles of attack:

- the dimensions of scour holes around vanes;
- the near-vane flow field;
- the effect of a single vane on the bed level behind the vane;

These goals differ from the goals in Chapter 3 as these are the goals of the experiments in Bangladesh only. These goals are only slightly modified compared to the original BUET-DUT linkage project goals for the experiments.

5.2 Experimental conditions

In the measuring report [Zijlstra & van Zwol, 2003] the design of the experiments is described in detail. Here, a brief summary is given.

The flume at BUET has a fixed width of 2.5 m and a length of 45 m. Since 3D-flow phenomena near the bottom vane were of main importance scaling was applied according to the Froude-scale. No prototype is available, but reasonable velocities in reality (River Waal and general conditions Bangladesh) are 1-3 m/s. The vane length was chosen 40 cm, from which typical length scales of 20-60 resulted. The velocity in the flume was bounded by the practical capacity of the pumps, and was 0.272 m/s along with a water depth of 30 cm. The sediment transport rate in the flume was relatively low, resulting in large time scales for morphological development.

An experimental programme consisting of twelve experiments was proposed, but finally only the following seven experiments could be finished within the available time. Table 5.1 shows the seven experiments.

Experiment	Vane height [cm]	Angle of attack [°]	H_v / d
A1	12	10	0.4
A2	12	20	0.4
A3	12	30	0.4
A4	12	40	0.4
B2	6	20	0.2
B3	6	30	0.2
C2	18	20	0.6

Table 5.1: Experimental programme

The rationale of selecting these experiments was to have at least one series of equal height for multiple angles of attack (A1-A2-A3-A4) and one series of equal angle of attack for different heights (A2-B2-C2).

5.3 Preparations Bangladesh

During the first month in Bangladesh much effort was needed to set-up the experiments. Since this was part of the graduation project, some attention is given to the activities here.

At arrival in Dhaka the flume had just been finished and the Bangladeshi researchers had executed only a few test runs. In the first week, an inventory was made of all materials and equipment required. Finally, during this first month the following list of actions was fulfilled:

- Permission to take equipment from the indoor laboratory and permission to store equipment on location:
  - EMS and related equipments;
  - Point-gauges;
- Obtaining equipment:
  - Construction of a bed level measurement device (made design and ordered at the university's metal work shop);
  - Shopping of required materials (e.g. measuring line, tape, tubes, rake);
  - Design of a system to hold (clams), and to determine the location of the EMS;
  - Installing and calibrating point gauges and accompanying reference plates;
- Cleaning of facility (polluted by debris, clay and organic materials)
- Arrangements to hire workers
- Finishing the upstream part of the flume:
  - The upstream part of the flume had not yet been fixed at arrival. The bottom has been levelled and fixed with brick and cement;
  - The accompanying guide walls did not result in a satisfactory equal distribution of the discharge, this was adjusted;

- Arranging the data acquisition system:
  - Connection laptop and EMS by RS232 port;
  - Programming the Lab view-environment;
- Measurements of the flume:
  - Arranging a water level instrument;
  - Measuring of needed elevations of all object in the research;
- Test runs:
  - Sediment transport, ripple development, scour duration;
  - Velocity measurements and calibration of the Rehbock weir(s);

5.4 General model parameters

All details about the set-up are described extensively in the measuring report [Zijlstra & van Zwol, 2003]. Here a summary of the main parameters is given.

Parameter	Symbol	Magnitude	Dimensions
Flow velocity	u	0.272	[m/s]
Water depth	$\overline{d}$	0.30	[m]
Estimated alluvial roughness	C	35	[$m^{1/2}$/s]
Ripple height	Δ_r	0.05 – 0.07	[m]
Estimated total sediment transport rate	s	2.0 x 10^{-7}	[m^2/s/m']
Rouse parameter	u_* / w_s	1 – 2 (transition bed-suspended load)	[-]
Median grain size	D_{50}	130 – 170 x 10^{-6}	[m]

Table 5.2: Model parameters

5.5 Value of the experiments

The experimental model tests in Bangladesh have been executed with restricted means. Therefore the reliability of the experiments reduces. Concerning the morphological development of the model, the following restrictions must be mentioned:

- Varying grain size's in the model. It is uncertain how this has developed during the experiments. Grain sorting might have influenced the results as the model bed was not replaced every experiment;
- During the experiments, besides the expected ripples, larger bed forms developed. In the last experiment a flat bed developed. This behaviour is, so far, inexplicable. Fine particles (silt) might account for this. Obviously, this effects the alluvial roughness, and with that, the water level slope;
- The longitudinal bed slope of the model was not constant during the experiments causing deviations from the intended equilibrium water slope;

- Despite the consequent control of discharge and water depth fluctuations in the water depth up to 5 mm have been reported. This was mainly caused by discharge variations. Due to power fluctuations and pump problems, the discharge sometimes dropped to 95%;
- The sediment transport mechanism could not be fully identified. The water was not transparent, so suspended transport is expected. However, this effect might also be caused by wash load;
- The ripple migration in the model was slow. Also the adaptation of the longitudinal profile was slow. Furthermore the sediment transport rate was also quite low. Together this leads to the conclusion that the flow velocity was relatively close to the critical velocity for sediment transport. Despite the fact that this was noticed already during the experiments, nothing could be done as the pump capacity was already reached;

Despite the limitations, the results of the experiments can be considered valuable, as the obtained dataset is unique. Previous research has not led to a consistent dataset with results of multiple single vane tests for both high and low angles of attack in a movable bed flume. Therefore, this dataset is a useful starting-point for a study concerning the morphological behaviour of bottom vanes.

5.6 Results

For all measuring results, background information on set-up and execution, accuracies, design and scaling, the reader is referred to the measuring report [Zijlstra & van Zwol, 2003].

6 Morphological behaviour of a single vane

6.1 Introduction

In this chapter the goals for the morphological behaviour of a single bottom vane are treated. They are repeated from Chapter 3:

- Identify the main processes that cause the morphologic development behind a bottom vane in a straight channel, for both low and high angles of attack;
- Determine the influence of vane height and angle of attack on these mechanisms;

This research is restricted to a single bottom vane in a straight flume. The above-mentioned goals are treated by means of a theoretical analysis (Section 6.2), the results of the experiments, and comparison to previous research.

Before drawing conclusions, the uncertainties of mainly the experiments are taken into consideration.

6.2 Physical processes

The morphological behaviour of vanes is analysed based on the physical processes. The complex behaviour of vanes is the result of interaction between various processes that are mutually influencing one another.

The identified processes that will be treated are:

- Vane-induced spiral flow;
- Vortex growth and deformation;
- Influenced transport in longitudinal direction;
- Horseshoe vortex in front of the vane;

The processes mentioned are all water movements; of course these processes are again influenced by the bed level change that they cause. In the analyses the influence of the processes on the near-bed velocity are most important.

6.2.1 Vane-induced spiral flow

The main bed level change is caused by the vane-induced spiral flow (or main vortex). In principle, this is the mechanism of the wing tip vortex as described by Odgaard and Wang [1991] (Section 2.2). As discussed, this theory is not valid for high angles of attack. Nevertheless, Marelius and Sinha [1998] showed that spiral flow is still present for high angles of attack. But other research has shown that the theory of Odgaard is not correct. How the vane exactly raises the spiral flow will not be treated here. The reader is referred to the M.Sc. thesis of van Zwol [2004] which will treat this subject in more detail.

Here, it is assumed that a certain spiral flow is present, and causes a certain near-bed transverse flow velocity resulting in transverse bed shear stress. Finally, sediment will rearrange in such a way that either a cross-sectional slope or the increased water depth results in a new equilibrium state.

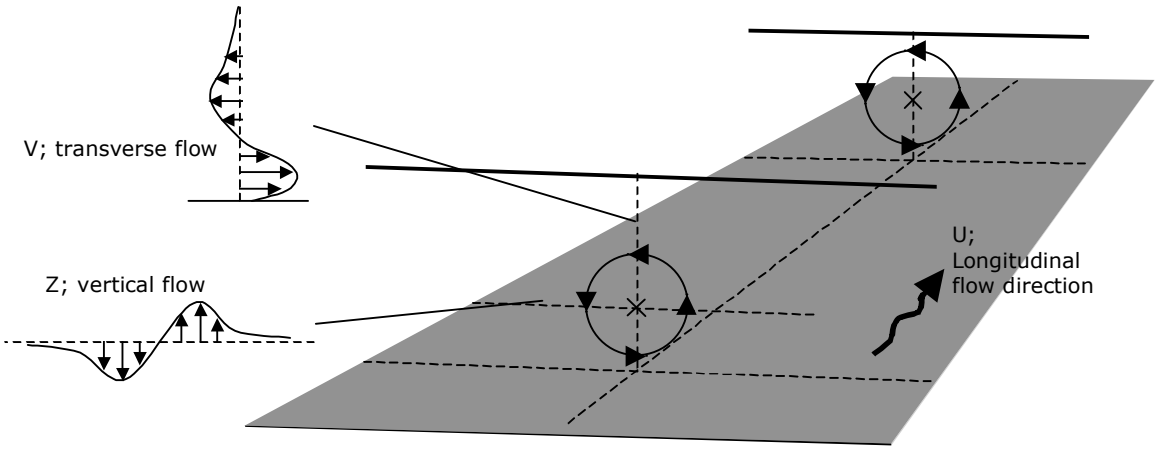

Figure 6.1: Vortex spiral flow v and z velocity components

6.2.2 Vortex growth and development

A vortex, or spiral flow, is a rotational movement in the cross-section of a river or channel. As mentioned in Section 2.2, this process can be described by the Rankine vortex model. The vortex can be considered as rotation that is transported downstream with the longitudinal flow.

The growth of the vortex is established by shear stresses between the water particles. If a certain group of particles is moving faster than the surrounding particles, they will pass on momentum to the slower particles. Figure 6.2 shows this. From left to right the process develops in time, logically the shear stresses become zero when the velocity gradient becomes zero.

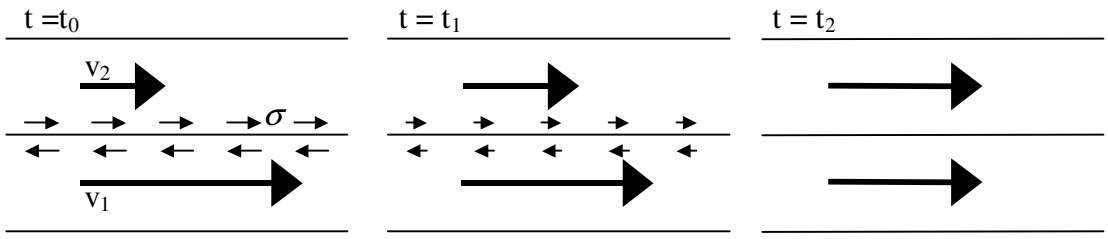

Figure 6.2: Shear stress due to velocity gradient

According to Odgaard and Wang [1991] the wing tip vortex core at s=0 (trailing edge) is situated at $z = 0.8H_v$. The Rankine vortex will grow until it is bounded by water level and bed level (Figure 2.3). Logically the equilibrium vortex axis is at $0.5d$. In Figure 6.3 the development of a vortex in downstream direction is schematically shown. The circles indicate the path of maximum transverse velocity of the rotation in the cross-section (magnitude is not considered in the figure!).

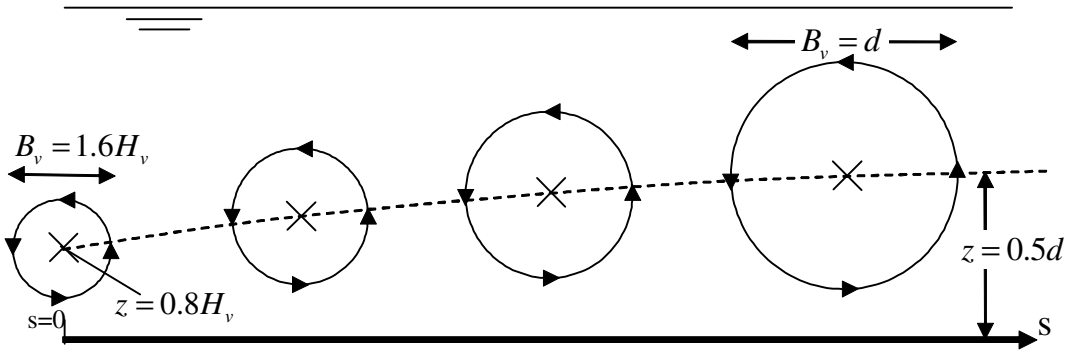

Figure 6.3: Vortex growth in downstream direction

While growing, the vortex looses energy due to friction forces as it moves downstream. The fully developed state with a vortex axis at $0.5d$ and $B_v = d$ is not always reached as the vortex can already have been damped out before it reaches this state.

In most cases the vortex development is not this simple. The top of a bottom vane is usually relatively close to the bottom, so the vortex core will also be close to the bottom. The vortex will quickly grow towards the bottom and not be able to grow further. This is shown in Figure 6.4.

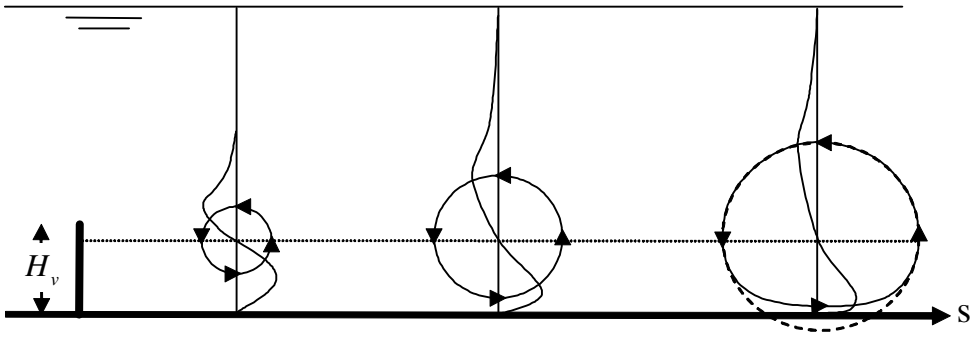

Figure 6.4: Bounded vortex growth

When the vortex cannot grow further, the flow is basically trapped near the bottom, causing higher near-bed velocities. Of course, also the resistance increases, and the vortex will loose more energy. If the vortex cannot grow, also the displacement of the vortex core in upward direction is stimulated, as the velocity gradients below the core, are higher than above the core (spreading does continue in the upper part of the vertical, Figure 6.3).

The maximum transverse near-bed velocity in a cross-section is a function of damping of the original vortex intensity, the vortex growth and the elevation of the initial core axis ($0.8H_v$).

Besides the above-mentioned growth, also the depth influences the vortex. Initially in a flume the depth is constant, but later, and also in reality, the depth is not constant. Such a depth variation can be a vortex leaving an outer bend or its own scour hole. When depth increases or decreases, the spiral motion does not disappear, since the movement has inertia. Consider the situation in Figure 6.5.

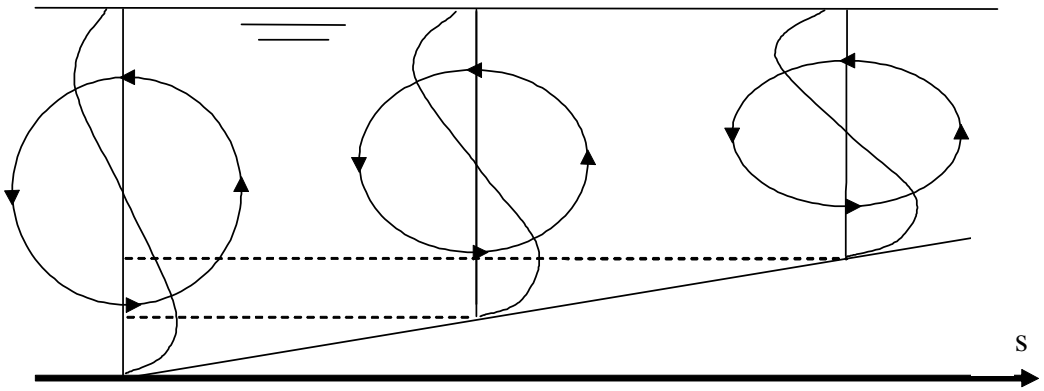

Figure 6.5: Vortex deformation by decreasing depth

What happens is dependent of the 3D flow structure. In this case it is assumed that the change in depth is gradual, and that the longitudinal flow structure in the cross-section stays uniform. In that case the longitudinal flow simply accelerates and the vortex is transported with it. As the same amount of water has to rotate through a small water depth, the transverse flow velocities have to increase. The vertical flow velocities will stay more or less the same.

In this section, several aspects of vortex growth and deformation have been treated. In reality these process cannot be seen separate from each other as they interact. However, splitting up the processes can make the complex behaviour better understandable.

6.2.3 Influenced longitudinal transport

The longitudinal transport is influenced by change in velocity distribution. X-impulse is transported in the vertical by the vane-induced circulation. The result is a changed vertical velocity distribution, with an increased longitudinal velocity near the bottom on the lee side of the vane, and a decreased value on the pressure side.

In experiments this influence has been measured, but only Wang [1991] noted the effect on the sediment transport. In aerodynamic-research the effect has also been reported by means of direct skin friction measurements [Pauley & Eaton, 1987]. Also various experiments showed significant velocity profile differences between the lee side and the pressure side. Figure 6.6 shows an example from Struiksma & de Groot [1996]. The left side of the figure is the lee side. The centre of the vane was located at y = -0.1 m. These measurements are taken at s = 0.5 m.

In this figure it is clearly visible that the flow velocity at z = 0.02 m is significantly higher behind the lee side (negative y-coordinate). Note that these measurements have been taken above a fixed bottom (z=0 m)

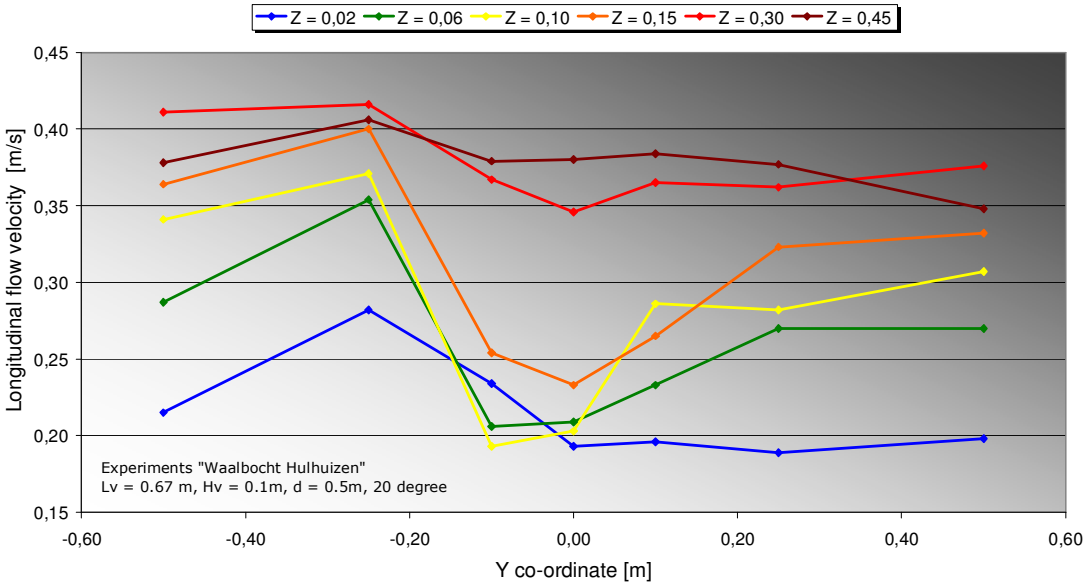

Figure 6.6: Increase longitudinal bed shear stress due to spiral flow

Besides an experimental proof, also a simple theoretical explanation is easy to find. The transverse and vertical flow in a cross-section can be considered as transporters of u-momentum in a cross-section (Figure 6.1). Figure 6.7 explains how an equilibrium logarithmic vertical velocity profile changes when a rotating flow is superimposed.

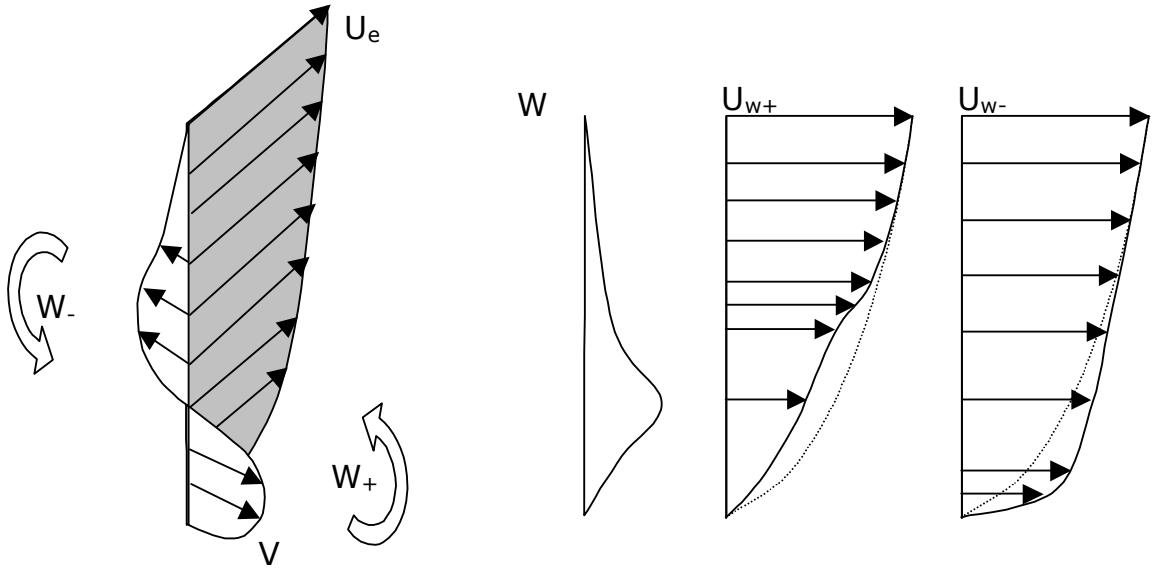

Figure 6.7: Longitudinal velocity profile changed by vertical flow

On the left side the vane-induced transverse (v) and equilibrium longitudinal flow (U_e) are schematically displayed. The arrows left and right of the profile indicate the up flow and down flow. The vertical flow velocity profile (w) that is displayed is in reality somewhere right and left of the vortex axis. The profiles indicated by U_{w+} and U_{w-} show the vertical longitudinal flow distribution influenced by up or down flow. Figure 6.7 shows only the influence of vertical flow (w). The influence of transverse flow (v) is marginal as the difference of longitudinal flow velocity at the

same elevation in transverse direction is usually small. For the vertical direction the difference can be significant.

The changed longitudinal velocity profile can only persist if u-momentum is being supplied. If not, the longitudinal velocity profile will return to the equilibrium logarithmic profile due to the bottom friction. If the vertical velocities are relatively small, the bed resistance will dominate, and the deviation from the equilibrium profile will not be significant.

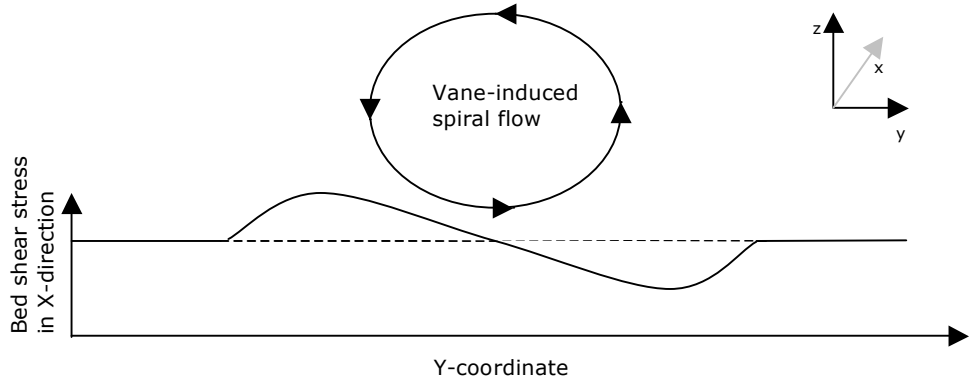

Figure 6.8: Increase longitudinal bed shear stress due to spiral flow

Important to the morphological development is the change in bed shear stress. As near-bed velocity increases or decreases, the sediment transport in longitudinal direction also changes. This is indicated in Figure 6.8. It is clear that this effect will increase when the vane-induced circulation is larger. It is important to remember that the sediment transport is not linear to the flow velocity (power three to five). So, a small increase of near-bed flow velocity can result in a larger increase of sediment transport.

6.2.4 Horseshoe vortex

In front of the vane a horseshoe vortex can develop, like observed for cylindrical bridge piers [Breusers & Raudkivi, 1991]. The strength of this vortex is strongly dependent on vane height and angle of attack. Along with the angle of attack the ratio effective blocking-depth is expected to play a key role.

The horse-shoe-vortex is responsible for the scour hole in front of a bottom vane. As the vane height and angle of attack increase, the volume of the scour hole increases too, since the horseshoe vortex is stronger. The horseshoe vortex is guided along the vane up to the trailing edge. From there the forcing is gone, but the vortex is still present. It is carried with the flow downstream and damps out. The magnitude can still be significant and can also cause bed level changes behind the vane. Note that the fact that the spiral flow is leaving the vane is different than for bridge piers, where the vortex is fixed in front of the bridge pier. Figure 6.9 shows a principle sketch of a horseshoe vortex on the pressure side of the vane.

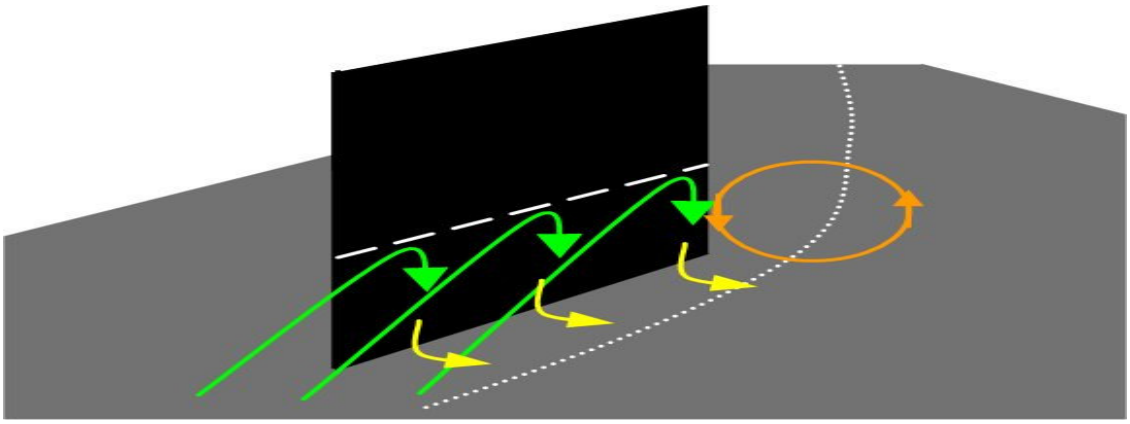

Figure 6.9: Initial trailing edge horseshoe vortex

The development of a horseshoe vortex is a cyclic process. When the initial bed is flat a small horseshoe vortex initiates, but mainly the downward flow starts to erode sediments. As this hole grows, more space is available for the horseshoe vortex and the process grows stronger. This process ends when the hole is at such a depth that the velocities have reduced in such a way that no more sediment is transported outside. This cyclic process can results in large scour holes.

The sediment that originates from the scour hole is deposited somewhere behind the screen. The horseshoe vortex carries the sediment near the vane but dampens out relatively quickly behind the vane. The main flow is not capable of transporting all this sediment so depending on the transport mechanism (bed or suspended load) these sediments are deposited closely or somewhat further behind the vane.

The vane-induced spiral flow also influences where these sediments are deposited. At the trailing edge the horseshoe vortex meets the main vortex. The upward flow of the main vortex can transport the sediments offered by the horseshoe vortex high into the vertical. In case of fine sediments deposition of these sediments will be significantly further downstream of the vane. Of course for bed load this is not the case. For bed load the near-bed flow velocity is dominant. In case of the horseshoe vortex the near-bed velocity is directed away from the vane (yellow arrow in Figure 6.9), and so, the sediments will be transported in that direction and form a bar downstream of the pressure side of the vane.

6.2.5 Resulting bed transport direction

The direction and magnitude of the bed load is directly dependent on the near-bed flow. If the above-mentioned processes are regarded, already an idea is present of how the morphologic development caused by a single vane is characterised.

- The main vortex will cause a transverse bed shear stress downstream of the vane. This bed shear stress has a maximum in the centre line behind the vane and is distributed in transverse direction according to the formula of Wang [Wang, 1991] (Section 2.2);
- Depending on the magnitude of the main vortex, the longitudinal velocity profile will be changed. On the lee side of the vane the near-bed longitudinal flow velocity will increase and cause more sediment transport. On the pressure side the opposite will occur;
- Depending on the vane geometry a horseshoe vortex develops and causes a scour hole. Somewhere behind the vane the sediment from the scour hole is deposited;

When the first two effects are added up, Figure 6.10 is obtained. The effects are not real magnitudes. The magnitude of the effects is dependent on the vane height and angles of attack, and will be quantified later in this chapter.

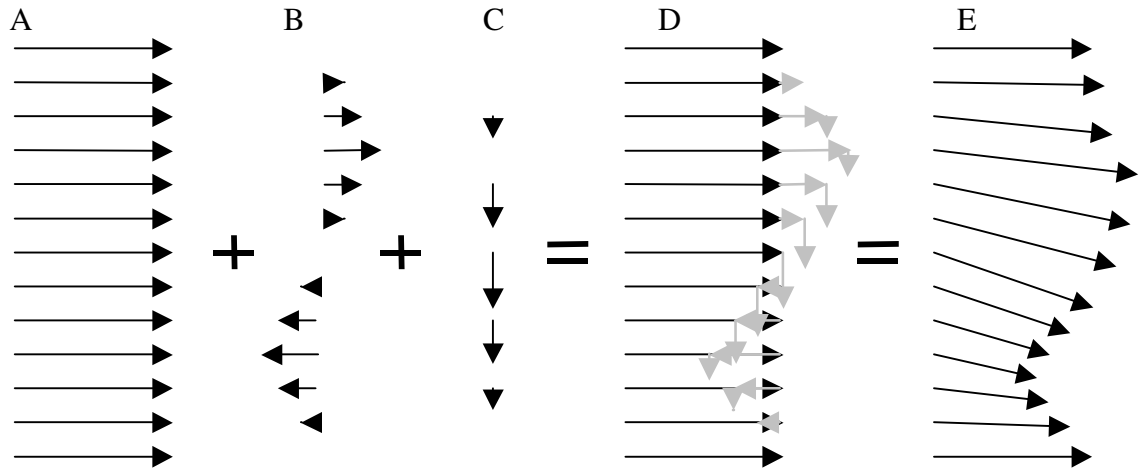

Legend

A	undisturbed uniform near-bed flow
B	change in longitudinal near-bed flow velocity by main vortex
C	vane-induced transverse near-bed flow velocity
D	adding up vectors
E	resulting near-bed flow velocity

Figure 6.10: Theoretical flow field by vane

6.3 Results of the bed level measurements

The results presented in this chapter are all based on the results of the experiments. In this chapter many references are made to the figures in appendix C (contour plots) and appendix D (cross sectional plots). Also the experiments will be compared based on their number. To be perfectly clear, the experiment numbers are repeated. The letter represent the vane height and the number the angle of attack.

Experiment	A3	A1	A4	A2	B2	C2	B3
angle of attack [°]	30	10	40	20	20	20	30
vane height [m]	0.12	0.12	0.12	0.12	0.06	0.18	0.06

Table 6.1: Experiment numbering

6.3.1 Vortex width

The main vortex caused by the vane, causes the bed behind the vane to change. This is caused by a change in transverse transport. In general, an erosion channel develops, together with a deposition area. The position of the sedimentation-erosion is described by reporting the zero crossing. This is the point at which the bed level is zero, on the transition between sedimentation and erosion. If a zero crossing is not present, N.A. is reported. N.A. is also reported when no significant sedimentation-erosion pattern is present as the found zero crossing is unreliable.

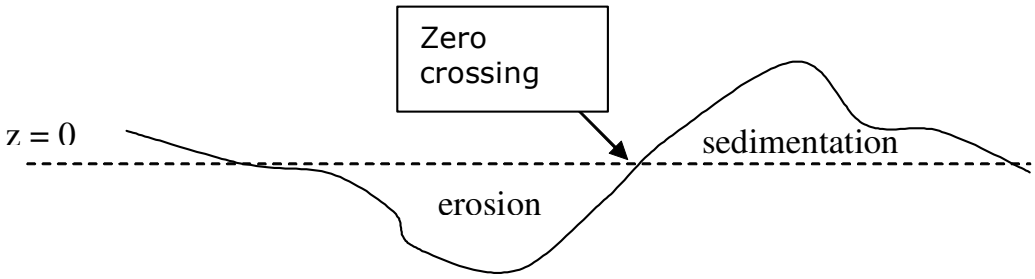

Figure 6.11: Example zero crossing

Zero crossings directly behind the vane cannot be reported, as due to the scour around the vane the bed level directly behind the vane is below the zero line. From appendix B it can be seen that from x = 16.00 m and onward, the bed level change is more or less zero on average.

In Table 6.2 the y-coordinate at which the cross-sectional bed level plots crosses the z = 0 line.

y-coordinate [m]	A3c (42h)	A1 (17h)	A4 (34h)	A2 (16h)	B2 (35h)	C2 (35h)	B3 (49h)
x = 16.00 m	0.16	0.03	0.05	0.02	0.02	-0.04	0.32
x = 16.50 m	0.08	0.00	0.07	0.05	0.07	0.00	0.13
x = 17.00 m	0.02	0.12	-0.03	0.01	-0.07	-0.05	-0.02
x = 18.00 m	-0.15	N.A.	-0.27	0.08	N.A.	-0.08	N.A.
$x = \overline{16.20 - 17.20}$ m	-0.70	-0.42	-0.70	-0.40	-0.43	-0.42	-0.60
	0.02	0.02	0.03	0.02	0.05	-0.04	0.06
	0.74	0.46	N.A.	0.58	0.27	0.60	0.80

Table 6.2: Zero crossings based on cross-sectional plots

In Table 6.3 the same is done, but then based on the contour plots. Further, also the zero crossing to the side of sedimentation erosion pattern is indicated. The result is different from the previous table as the green area ($0.05m \geq z \geq -0.05m$) in the contour plots is kept as criterion, which is slightly different from an absolute zero crossing.

y-coordinate [m]	A3c (42h)	A1 (17h)	A4 (34h)	A2 (16h)	A2c (42h)	B2 (35h)	C2 (35h)	B3 (49h)
x = 16.00 m	-0.50	-0.35	-0.45	-0.25	-0.30	-0.30	N.A.	-0.45
	0.15	0.05	0.10	0.05	0.10	0.05	0.05	0.30
	0.65	0.50	0.60	0.40	0.30	0.35	0.40	0.70
x = 17.00 m	-0.70	-0.40	-0.55	-0.75	-0.30	-0.45	-0.45	-0.60
	0.05	0.00	0.00	0.00	0.00	0.00	-0.05	0.00
	0.70	N.A.	N.A.	0.25	0.35	0.25	0.65	0.75
x = 18.00 m	-0.70	N.A.	N.A.	-0.35	N.A.	N.A.	N.A.	-0.70
	-0.15	N.A.	-0.25	0.10	N.A.	N.A.	-0.10	N.A.
	0.80	N.A.	N.A.	0.45	N.A.	N.A.	N.A.	0.70

Table 6.3: Zero crossings and edges sedimentation erosion pattern based on contour plots

From this data something can be said about the vortex width. Subtracting the left and right zero crossing results in the width over which the vane has had influence. For now it is assumed that this is the vortex width. In Table 6.4 the width of the sedimentation-erosion pattern is compared to depth, depth at the trailing edge (the point of origination of the vortex) and to the effective width of the vane.

The width on vision is the width determined straight from the contour plots on the area x = 16.00 – 17.00 m. At the spot at which the sedimentation-erosion pattern was most visible, the width was determined. Note that this was a subjective approach.

	A3c (42h)	A1 (17h)	A4 (34h)	A2 (16h)	A2c (42h)	B2 (35h)	C2 (35h)	B3 (49h)
Vortex width x = 16 m [m]	1.15	0.85	1.05	0.65	0.60	0.65	N.A.	1.15
x = 17 m [m]	1.40	N.A.	N.A.	1.00	0.65	0.70	1.10	1.35
Vortex width $\overline{x = 16.20 - 17.20}$ m	1.44	0.88	1.40	0.98	N.A.	0.70	1.02	1.40
Width on vision [m]	1.10	0.60	1.20	0.65	N.A.	0.65	0.80	1.15

Table 6.4: Width sedimentation-erosion pattern

	A3c (42h)	A1 (17h)	A4 (34h)	A2 (16h)	A2c (42h)	B2 (35h)	C2 (35h)	B3 (49h)
Average depth at trailing edge [m]	0.36	0.31	0.42	0.31	0.30	0.31	0.34	0.40
Depth at trailing edge [m]	0.40	0.32	0.45	0.33	N.A.	0.30	0.38	0.43
$B_{vor} / \overline{d}$ [-]	3.7	2.0	4.0	2.2	N.A.	2.2	2.7	3.8
$B_{vor} / \overline{d}_{x=15.20m}$ [-]	3.1	1.9	2.9	2.1	N.A.	2.1	2.4	2.9
$B_{vor} / d_{x=15.20m}$ [-]	2.8	1.9	2.7	2.0	N.A.	2.2	2.1	2.7
B_{vor} / B_v [-]	5.3	8.6	4.4	4.7	N.A.	4.7	5.7	5.5

Table 6.5: Dimensionless vortex width

in which

B_{vor}	Width over which vortex has effect
$d_{x=15.20}$	Local depth at trailing edge
$\overline{d}_{x=15.20}$	Average depth at trailing edge on the interval y = -0.20 – 0.20m
B_v	Effective vane width ($B_v = L_v \sin(\alpha_v)$)

In Table 6.5 the vortex width on vision has been made dimensionless by dividing it by the depth (0.3m), the depth at point of origination (trailing edge of the vane) and by the effective width of the vane.

For an ideal fully developed circular vortex, the vortex width would be equal to the depth. Odgaard also suggested this (Section 2.2). From all results above, it is obvious that this is a too small distance. Even for the small low angle of attack vanes, A1, A2, and B2 the width over which the effect of the vortex is noticeable, is about two times the depth. For the higher angles of attack this increases to four times the depth. But when dividing by the local depth at the trailing edge, the values reduce to two for experiments A1, A2, B2 and C2 and about 2.7 for experiment B3, A3 and A4.

6.3.2 Erosion channel

In Table 6.6 the magnitude of the erosion channel is indicated by reporting the deepest point (thalweg) in the cross-section. Also the y-coordinate is reported. Near the vane the reported deepest point must be on the lee side of the vane, as the primary deepest point on the other side of the vane is caused by the horseshoe vortex. These two different deepest points can be clearly distinguished in Appendix D.2.

y-coordinate [m] elevation [cm]	A3c (42h)	A1 (17h)	A4 (34h)	A2 (16h)	B2 (35h)	C2 (35h)	B3 (49h)
x = 15.20 m	-0.16 -4.2	-0.16 -1.2	-0.09 -9.2	-0.18 -1.7	-0.08 -2.8	-0.21 -2.7	-0.11 -5.7
x = 15.60 m	-0.01 -5.9	-0.14 -1.4	-0.05 -6.6	-0.25 -0.5	-0.15 -4.3	-0.36 -2.5	-0.02 -8.9
x = 16.00 m	-0.20 -7.9	-0.24 -1.0	-0.17 -5.8	-0.08 -1.9	-0.14 -3.2	-0.10 -0.5	-0.12 -8.5
x = 16.50 m	-0.20 -6.3	-0.12 -2.4	-0.25 -4.4	-0.12 -1.2	-0.20 -2.2	-0.11 -1.9	-0.15 -5.4
x = 17.00 m	-0.16 -3.6	-0.30 -1.6	-0.30 -3.5	-0.10 -1.7	-0.36 -1.7	-0.21 -4.3	-0.15 -2.1
x = 17.50 m	-0.28 -2.1	-0.24 -1.2	-0.58 -2.3	-0.17 -1.2	N.A.	-0.15 -2.5	N.A.
$x=\overline{15.60-16.20}$ m	-0.19 -6.6	-0.17 -1.0	-0.14 -6.0	-0.09 -1.8	-0.15 -3.2	-0.10 -0.5	-0.11 -8.2
$x=\overline{16.20-17.20}$ m	-0.19 -4.9	-0.15 -1.6	-0.26 -4.0	-0.11 -1.1	-0.24 -1.2	-0.23 -2.1	-0.15 -3.9

Table 6.6: Depth and y-coordinate of thalweg from the erosion channel

The y-coordinates of the thalweg tell something about the direction in which the vortex develops. The values of these y-coordinates in Table 6.4 vary greatly. It is sometimes difficult to determine a deepest point since in some experiments the erosion channel is not always clearly present at a certain location (e.g. Appendix C.7, experiment C2 at x = 16.00 m).

In general the y-coordinates of the thalweg of the erosion channel tend to shift further outward in downstream direction. However, the zero crossings in Table 6.2 and Table 6.3 do shift outward, but not always very convincing. Nevertheless, the conclusion is supported by the general impression of the contour plots where the erosion channel is also shifting to the left, especially for the higher angles of attack (see Appendix C, the erosion channel, blue parts, tend to shift to the left in downstream direction).

Figure 6.12 presents the depth of the thalweg as a function of the x-coordinate. In general the vortex effect damps out in downstream direction.

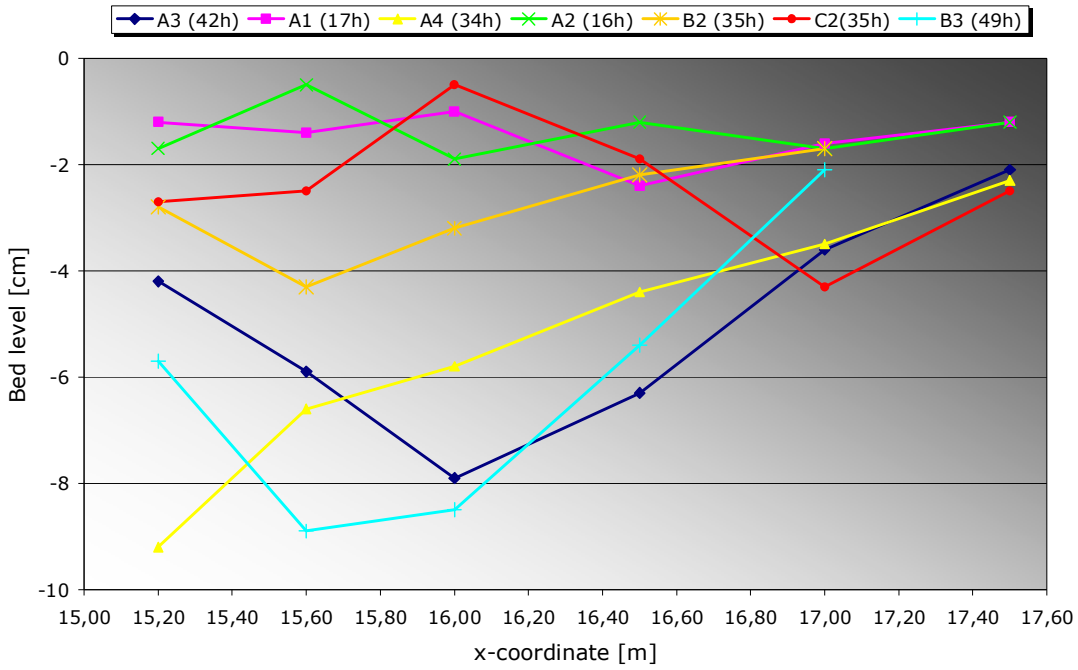

Figure 6.12: Depth thalweg erosion channel

Figure 6.12 shows that experiment A4 does not have the deepest erosion channel. Experiment B3 has a larger effect. This might be due to the fact that experiment A4 was less far developed (measurement experiment A4 after 34 hours, and B3 after 49 hours). When comparing experiment A3 and B3, it can be seen that initially experiment B3 has the second deepest channel, but further downstream the effect of the vane in experiment A3 is larger. Probably the vane height is responsible for this difference. Experiment A1 and A2 have a more or less constant deepest point. It has to be noted that these effects are doubtful since the deepest point is of the same order of magnitude as the ripple effects. It is striking that experiments C2 has its largest deepest point at x = 17.00 m whilst in the other experiments this is much closer to the vane. Striking is the relatively large depth of the erosion channel in experiment B2, despite the low vane and the small angle of attack.

6.3.3 Sedimentation pattern

The sedimentation pattern is difficult to characterise. Its form differs per experiment. The sedimentation pattern is a combination of sedimentation by the main vortex and sedimentation by the horseshoe vortex, and also sedimentation of sediments originating from the scour hole that are transported by the main flow.

The contour plots provide a helpful tool to get insight in the sedimentation pattern. In Appendix C.1 a difference is visible. Downstream of the pressure side of the vane, a sedimentation bar is visible; whilst further downstream a larger pattern is visible. The sedimentation bar is the result of the horseshoe vortex. The larger pattern is a combination of the main vortex and some sediment originating from the scour hole. In Appendix C.2 the sedimentation pattern cannot be divided as the different sedimentation patterns have grown together. For experiment B3 (Appendix C.2) the bulb of the sedimentation pattern is shifted more towards the vane than for experiment A4 (Appendix C.1)

Here the highest point in the cross section (Table 6.7), and the highest point in longitudinal direction (Table 6.8) are reported without determining its origin (horseshoe vortex, main vortex or both). Again N.A. is reported if the highest point is not present, or improbable.

y-coordinate [m] elevation [cm]	A3c (42h)	A1 (17h)	A4 (34h)	A2 (16h)	B2 (35h)	C2 (35h)	B3 (49h)
$x=\overline{15.60-16.20}$	0.45 1.2	0.10 1.1	0.55 1.3	0.10 1.1	0.17 2.4	0.14 0.5	0.47 3.0
$x=\overline{16.20-17.20}$	0.45 3.3	0.11 1.1	0.55 2.9	0.11 1.4	0.16 1.5	0.34 2.3	0.49 4.1
$x=\overline{17.20-18.50}$	0.13 3.3	N.A.	0.07 3.8	N.A.	N.A.	0.60 1.6	0.09 4.3

Table 6.7: Elevation and y-coordinate of the highest point in a cross section

	A3c (42h)	A1 (17h)	A4 (34h)	A2 (16h)	B2 (35h)	C2 (35h)	B3 (49h)
x-coordinate [m]	19.00 3.2	N.A.	19.00 3.8	N.A.	N.A.	19.50 2.3	18.00 4.2

Table 6.8: Elevation and x-coordinate of the highest point in longitudinal direction

For high angle of attack vanes, a highest point is present relatively far downstream of the vane and close to the flume axis (so straight behind the vane). If this point would have been formed by the vane-induced transverse flow only, the effect should have been further away from the flume axis. Presumably the sedimentation is also caused by the increased longitudinal transport as described in Section 6.2.3. This will be discussed in more detail in Section 6.6.

6.3.4 Horseshoe vortex

On the pressure side of the vane, a horseshoe vortex is present. A spiral flow is generated and guided along the vane and leaves the vane at the trailing edge. The intensity is however not reduced to zero yet, and therefore influences the bottom behind the vane (Section 6.2.4).

In front of the vane, the horseshoe vortex digs a scour hole. Table 6.9 shows the location, and value of the maximum scour, as found in the processed dataset.

	A3c (42h)	A1 (17h)	A4 (34h)	A2 (16h)	B2 (35h)	C2 (35h)	B3 (49h)
Scour [cm]	-11.6	-5.8	-20.3	-6.8	-2.9	-13.7	-16.5
x-coordinate [m]	15.02	14.84	15.20	14.86	14.88	14.88	15.18
y-coordinate [m]	0.08	-0.01	0.17	-0.01	-0.01	-0.01	0.17

Table 6.9: Location and magnitude of maximum scour

The size of the scour hole has been defined as the begin bed level minus 2 cm contour. In Table 6.10 the average location of this contour at section, x = 14.80 – 15.20 m, is given (value follow from Appendix D.2). From the y-coordinates the width of the scour hole has been calculated, and has been divided by the effective width of the vane ($=L_v \sin(\alpha)$). N.A. was reported for experiment B2 as no scour hole was present.

	A3c (42h)	A1 (17h)	A4 (34h)	A2 (16h)	B2 (35h)	C2 (35h)	B3 (49h)
y-coordinate -2 cm crossing, left and right side [m]	-0.43 0.35	0.01 0.08	-0.39 0.44	0.03 0.09	N.A.	-0.26 0.29	-0.30 0.38
Width scour hole [m]	0.78	0.07	0.83	0.06	N.A.	0.55	0.68
Width scour / effective vane width	3.8	1.0	3.2	0.6	N.A.	4.1	3.4

Table 6.10: Width scour hole centre vane

The horseshoe vortex leaves the vane at the trailing edge and damps out in downstream direction. The influence of this vortex can be seen in the geometry of the bottom.

In Table 6.11 the effect of the horseshoe vortex downstream of the vane is described by means of the thalweg. The deepest point and its y-location are reported below. N.A. is reported if the horseshoe vortex is no longer discernible. Also the dimensionless distance downstream of s=0 (trailing edge) is given.

y-coordinate [m] elevation [cm]	A3c (42h)	A1 (17h)	A4 (34h)	A2 (16h)	B2 (35h)	C2 (35h)	B3 (49h)
x =14.90 m	0.01 -13.6	0.01 -5.0	-0.02 -19.6	0.01 -6.2	-0.01 -2.7	0.01 -13.3	-0.02 -16.4
x =15.00 m	0.07 -14.3	0.04 -2.7	0.06 -19.5	0.04 -2.7	0.04 -1.0	0.04 -10.2	0.08 -15.4
x =15.10 m	0.11 -14.2	0.06 -2.5	0.14 -19.1	0.09 -1.7	0.05 -0.05	0.08 -7.4	0.17 -15.8
x =15.20 m (s = 0.0 m)	0.16 -12.5	0.06 -2.4	0.17 -20.2	0.11 -2.6	N.A.	0.16 -8.4	0.17 -16.5
x =15.40 m (0.5 L_v)	0.19 -10.0	0.02 -0.5	0.21 -15.6	0.10 -1.5	N.A.	0.16 -8.5	0.19 -13.4
x =15.60 (1.0 L_v)	0.20 -6.8	N.A.	0.25 -10.8	N.A.	N.A.	0.18 -6.5	0.17 -7.8
x =15.80 (1.5 L_v)	0.25 -4.3	N.A.	0.29 -6.9	N.A.	N.A.	0.31 -4.3	0.18 -2.5
x =16.20 (2,5 L_v)	N.A.	N.A.	0.34 -1.1	N.A.	N.A.	0.29 0.4	0.34 -0.4

Table 6.11: Depth and y-coordinate of the thalweg from the channel formed by the horseshoe vortex

Figure 6.13 graphically presents the data. Like for the erosion channel, the effect of the horseshoe vortex damps out in downstream direction too. Only the effect of the horseshoe vortex damps out much quicker, as the intensity of the spiral motion is much smaller.

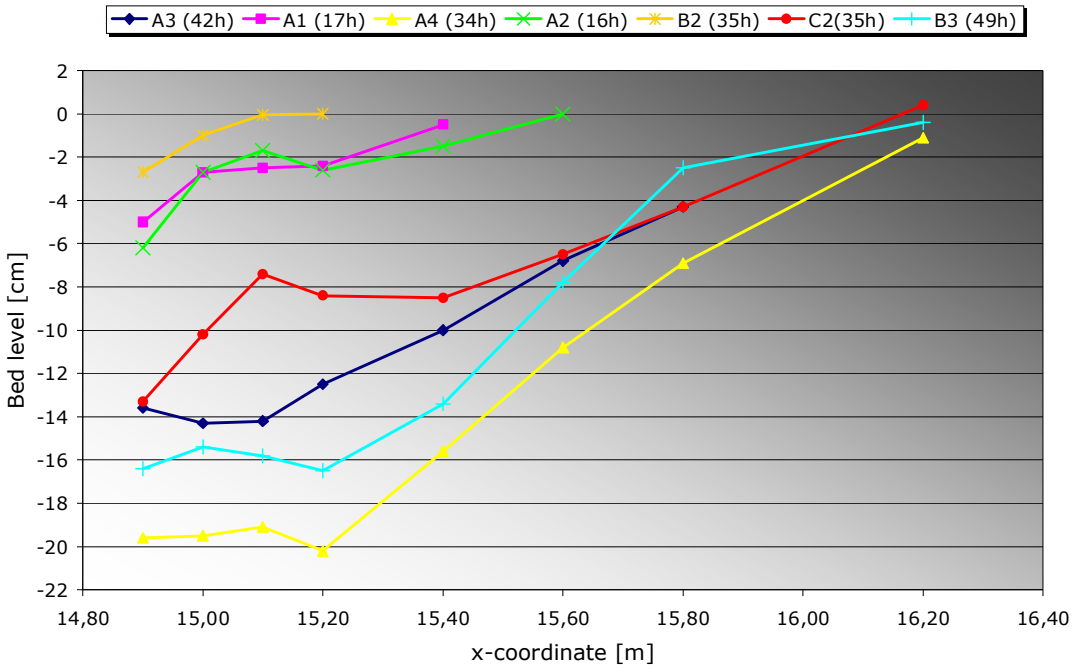

Figure 6.13: Depth and y-coordinate of thalweg of horseshoe vortex channel

If experiment B3 and A3 are compared, it is peculiar that the bed level is lower for experiment B3 that for A3, whilst opposite is expected since a higher vane (respectively 6 cm vs. 12 cm) should cause a larger horseshoe vortex. As can be seen from experiment C2 the depth at x = 15.20 is not only dependent on the horseshoe vortex. This can be derived since the initial horseshoe vortex for experiment C2 causes the same scour as for experiment A3 at x = 14.90 m, but the bed level at x = 15.20 is much smaller. The main vortex causing the erosion channel on the other side of the vane also determines the depth at the trailing edge, and interacts with the horseshoe vortex. In the contour plot of experiment B3 (Appendix C.2), it is visible that in this case the main vortex and the horseshoe vortex interact, but for experiment A3 (Appendix C.3) the effects are more separated. Since the near vane effect of the main vortex on the bed level is higher in experiment B3 than for A3, the bed level is eroded more.

Figure 6.13 also shows that the vane height is an important parameter for local scour. While experiments A2 and B2 have only little scour in front of the vane, the higher vane in experiment C2 causes much larger scour.

6.4 Results of the flow velocity measurements

Flow velocities have been measured at four locations behind the vane, x = 15.20 m, x = 15.80 m, x = 16.60 m and x = 18.80 m. The number of flow velocity measurements at x = 18.80 m was very small and provided no useful data, so these have been discarded.

The grid of far field flow velocity is much smaller than the grid of the bed levels, so it cannot be used to describe the flow field in detail. The flow velocity data will be used to support the conclusions drawn from the bed levels and from the theoretical analysis. The flow velocities measurements are presented in Appendix G (transverse, v) and Appendix H (longitudinal, x).

6.4.1 Vane-induced spiral flow

In Table 6.12 the maximum measured transverse velocity is at an elevation of 2 cm above the initial bed is presented. These values are read from the figures in Appendix G. For a few locations the measurement at z = 2 cm was not possible (due to sedimentation) and therefore z = 4 cm is used. The table shows the Y-coordinate at which the maximum velocity was measured, and the value of the velocity.

y-coordinate [cm] V_{max}[m/s]	A3	A1	A4	A2	B2	C2	B3
x = 15.20 m	-5.0 0.13	-3.4 0.06	-6.5 0.12	-3.4 0.05	3.4 0.08	-3.4 0.08	5.0 0.12
x = 15.80 m	5.0 0.08	6.5 0.05	N.A.	0.0 0.05	3.4 0.04	-3.4 0.04	2.5 0.07
x = 16.60 m	-2.5 0.07	-3.5 0.06	0.0 0.08	6.8 0.07	1.7 0.03	6.8 0.07	10.0 0.07

Table 6.12: Maximum transverse flow velocities at x = 15.20, 15.80, 16.60 and 18.20 m

The near-bed at x = 15.20 m is highest for experiment A4 with almost $0.5\overline{u}$. For experiment C2 the maximum near-bed velocity increases in downstream direction. Note that this is the near-bed velocity and not the maximum velocity in the whole cross section. Experiments A3, A4, B2 and B3 show a 'normal' decline. In experiment A1 and A2 the near-bed maximum velocity stays more or less constant.

The y-coordinates tell something about the direction of the vortex development. The y-coordinates vary quite a lot. In general, at x = 15.20 m, the maximum velocity is at the lee side of the vane, except for experiment B3. The values further downstream do not show regularity. This might be due to measuring errors. This will also be treated in Section 6.5.

From the figures in Appendix G the points at which the transverse velocity becomes zero have been estimated and reported in Table 6.13. From these zero points the theoretical vortex width can be calculated. The coordinates have been rounded at 0.05 cm.

	A3	A1	A4	A2	B2	C2	B3
x = 15.20 m	-0.25 0.25	-0.20 0.15	-0.35 0.25	-0.25 0.15	-0.25 0.20	-0.25 0.25	-0.35 0.25
Vortex width at x = 15.20 m	0.50	0.35	0.60	0.40	0.45	0.50	0.60
x = 15.80 m	-0.20 0.20	-0.15 0.10	-0.25 0.10[1]	-0.15 0.15	-0.10 0.20	-0.20 0.15	-0.25 0.20
Vortex width at x = 15.80 m	0.40	0.25	0.35	0.30	0.30	0.35	0.45

Table 6.13: Estimate vortex width based on velocity measurements at x = 15.20 and 15.80 m

According to these transverse velocity measurements, the vortex width at x = 15.80 m appears to be more or less equal to the water depth, with exception of experiment B3 and A3. If taking the scour at x = 15.20 m into consideration, the vortex width is still more than the local water depth.

[1] Measurements at x = 16.60 m as measurement at x = 15.80 m was not available.

Figure 6.14 on the next page displays the transverse velocity profiles at two cross-sections in the centre of the flume (y=0). The results of the flow three experiments with an angle of attack of 20 degrees are compared (dashed line, x = 1580 cm, line, x = 1521 cm).

The figure reveals the difference in the vertical structure. For the highest vane, experiment C2, the vortex core is at z = 16 cm for both x-coordinates. For experiment A2, the middle vane height, this is at z = 11 cm, and finally for experiment B2 the values vary and are respectively z = 5 cm and z = 10. Obviously, the vane has grown upward in this case. This is logical as for the low vane the initial vortex is close to the bottom. The figure also shows that the near bed velocity at x = 1520 cm is the highest for experiment B2, the low vane. For the higher vanes the maximum transverse velocity is located further up in the vertical due to the fact that the vortex is generated near the vane top and has to grow towards the bottom. The maximum transverse velocity at x = 1520 cm (trailing edge) is located more or less at halve a vane height. The second negative maximum is logically located at 1.5 vane heights.

6.4.2 Increased longitudinal transport

In Section 6.2.3 was indicated that by the vane-induced spiral motion the longitudinal near-bed flow velocities increase. This is checked on basis of the measured stream wise (or longitudinal) flow velocity measurements. In Appendix H the measurements are presented. It can be seen that the near-bed flow velocity at x = 15.80 m ($1.5L_v$ downstream of s = 0 m) indicated by the green lines (squares z = 2 cm, circles z = 4 cm) is in general higher on the lee side.

For experiment C2 however, the difference is not present near the bed, but the plot does indicate that the difference is present at a slightly higher elevation. Presumably this is due to the fact that the vortex has not yet grown towards the bottom. In Appendix G.6 the transverse velocity measurement for experiment C2 do also indicated that the vortex is not grown to the bottom because the maximum transverse velocities appear at z = 12 cm.

Figure 6.15 on the next page presents the measured longitudinal flow velocities for experiment A1, A2 and A3 (same vane height). Experiment A4 is missing as no measurements are available at x = 15.80 m. The lowest marker for each line indicates the bed level.

The figure shows that in all cases the flow velocities are higher on the lee side (open markers). For experiment A3 the difference is maximal. As indicated in Section 6.2.3 the difference increases with the vane-induced spiral flow intensity. However, for experiment A1 the difference is larger than for experiment A2. The figure for experiment A2 in Appendix H also shows a somewhat different course than the figures for experiment A1 and A3, as the maximum velocity is already reached at y = -0.10 m.

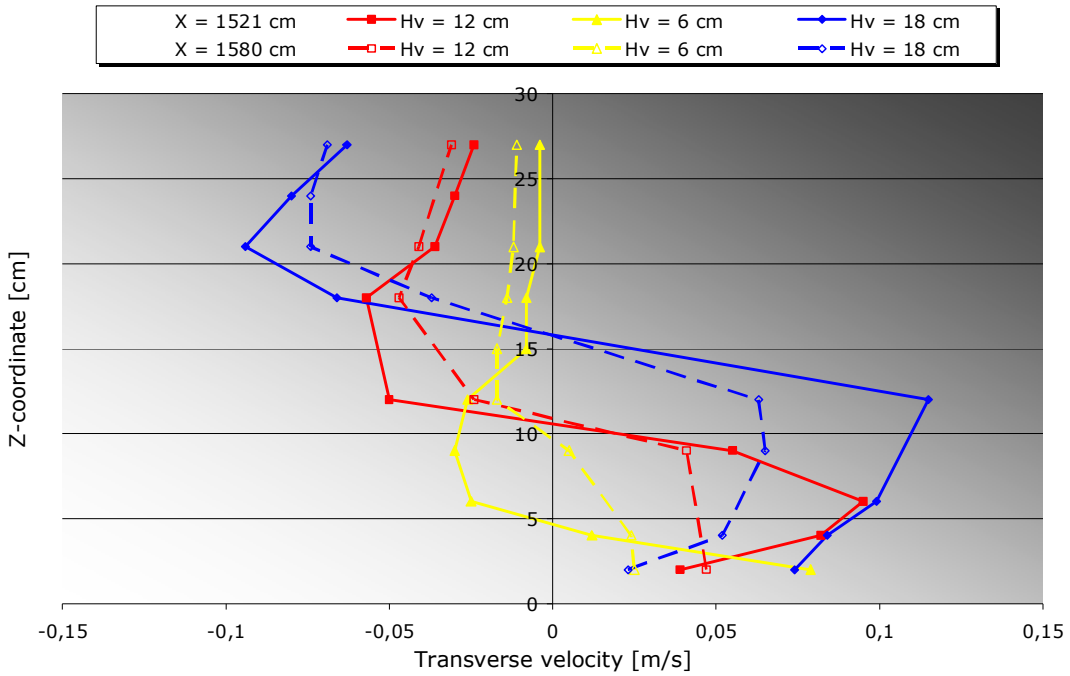

Figure 6.14: Measured transverse flow velocities 20 degree angle of attack

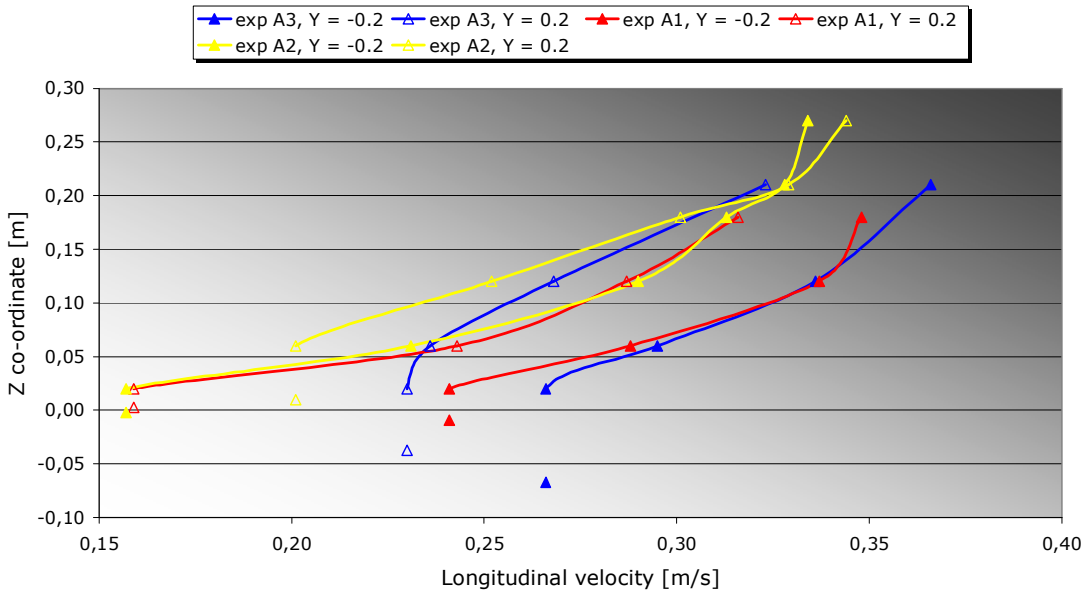

Figure 6.15: Measured vertical distribution of longitudinal velocity at x = 15.80 m

6.5 Uncertainties in the experimental measurements

Before drawing conclusions from this chapter, the uncertainties in the data from both bed and velocity measurements is discussed.

6.5.1 Measuring accuracy

In the measuring report [Zijlstra, van Zwol, 2003] the accuracy of the acquired data was treated. The accuracy of a single bed level measurement was estimated at seven mm. As a movable bed model was used, ripples were present. These ripples influence the bed level measurements. By spatially averaging, the effect of this noise can be reduced, but it can still influence results.

The theoretical accuracy of a P-EMS (used for the flow velocity measurements) according to the supplier (WL|Delft Hydraulics) equals "+/- 0.01 m/s or +/- 1% of measured value", for "Clean liquids and suspensions, including slurries". Practical knowledge however, indicates larger errors for movable bed experiments, especially for the near-bed measurements. During these experiments zero-shifts were reported. This means that all measurement values were in- or decreased with a certain value. This error was found up to values of several cm/s, but can be recognised in the results by a systematic shift of the results. For the transverse velocity measurements an accuracy of 0.01 m/s is the maximum, but presumably larger. So, since the measured velocities are only a few cm/s the effect can be large. For the longitudinal velocity measurements this error is less serious.

6.5.2 Large scale flume conditions

During the experiments, much was learned about the flume behaviour. The morphological time scale appeared to be in the order of days instead of hours. This was mainly due to the low sediment transport rate. In the measuring report it was estimated that this adaptation time equals about 1000 hours.

After analyses of the longitudinal bed slopes, it was discovered that the overall average bed slope was not in equilibrium. During the experiments the average slope gradually reduced, as the initial state was too steep. This probably caused erosion and/or sedimentation fronts that walked through the model. These have been visually observed.

Each experiment took about 30-50 hours. After an experiment, the bed was measured. The large-scale adaptation mainly took place in the upstream and downstream area of the vane, since the water level and depth in the vane area were controlled. Because of this and the fact that the duration of a single experiment was rather small compared to the adaptation time of the flume, it is expected that the results will be only marginally influenced.

6.5.3 Equilibrium state?

In morphology, it is important to know whether the results are equilibrium state conditions or just a transient state. For finding relations, or comparing results, the development in time has to be taken in consideration. In these experiments, two main processes determine the bed development, the scour process around the vane and the erosion-sedimentation process caused by the vane-induced spiral flow.

At the time the experiments were designed, it was estimated that the equilibrium state of the model could be reached within 8 hours. When the first experiment was executed, it was discovered that at least two days were needed to reach equilibrium scour. Of course, this duration is also dependent on the angle of attack

and the vane height. The main reason for this slow development is probably a low flow velocity.

During the subsequent experiments, the scour measurements were analysed to determine whether an acceptable approximation of the equilibrium was reached. It was accepted that the equilibrium state for the erosion-sedimentation process was not reached when measuring the bed. As this saved time, more different configurations could be tested within the available time at the facility. At that time it was believed that this would result in a more valuable dataset.

For experiment A3, two datasets are available; bed level measurements after 8 hours and after 42 hours of flow. The measurements after 42 hours were a check, as it was suspected that the bed had changed a lot. After analysis the changes appeared to be very large, but at that time it was not possible anymore to make a full bed level measurement series. Despite the lower measuring density of the check, the dataset has been used. The amount of data appeared to be sufficient to generate a reliable image of the bed level.

For experiment A1 and A2 the bed level measurements were also taken in an early stage of development. Unfortunately, the checks performed later were not of high density and did not provide enough information to be used for analyses. For experiment A2 there was sufficient data to make a comparison to the full bed level measurements. This has been done in Appendix E. For experiment A1 however, this was not possible since only 3 cross-sections were measured during the check.

Before making flow velocity measurements a certain time was allowed to elapse to eliminate the strong change in flow field by the scour process. Nevertheless, during the velocity measurements the far field was still developing and also the scour hole appeared to be not fully developed. This means that when comparing different flow velocity measurements, it is not sure whether the difference between them is caused by spatial variations or change in time.

Experiment (duration)	A3 (44h)	A1 (39h)	A4 (51h)	A2 (41h)	B2 (35h)	C2 (35h)	B3 (49h)
Elapsed time [hours]	28	26	36	25	21	23	29

Table 6.14: Hours elapsed before taking far field flow velocity measurements

When these elapsed hours are compared to the scour development figures from the measuring report [Zijlstra & van Zwol, 2003], it can be concluded that the near-vane bed is almost stable. As the measurements are used for a qualitative purpose, these effects are not expected to have serious influence on the conclusions.

6.5.4 Approach flow velocity profiles

In Appendix H longitudinal flow velocity records have been presented. The figures show a difference between left and right side of the flume. It has to be reported that these difference can of course also be caused by a non-equally distributed discharge. During the experiments a lot of attention was paid to get an equal distribution but this was hard to reach.

Figure 6.16 on the next page shows the longitudinal velocity as measured in front of the vane. There are left-right differences. However, the differences are small and not consequent. For experiment A1 the flow velocity is higher on the right side (positive y-coordinate) whilst for experiment A2 it is opposite. Finally experiment B2 shows an almost similar profile left and right. The errors are not considered systematic, and are expected not to influence the results in such a way that the conclusions drawn are wrong.

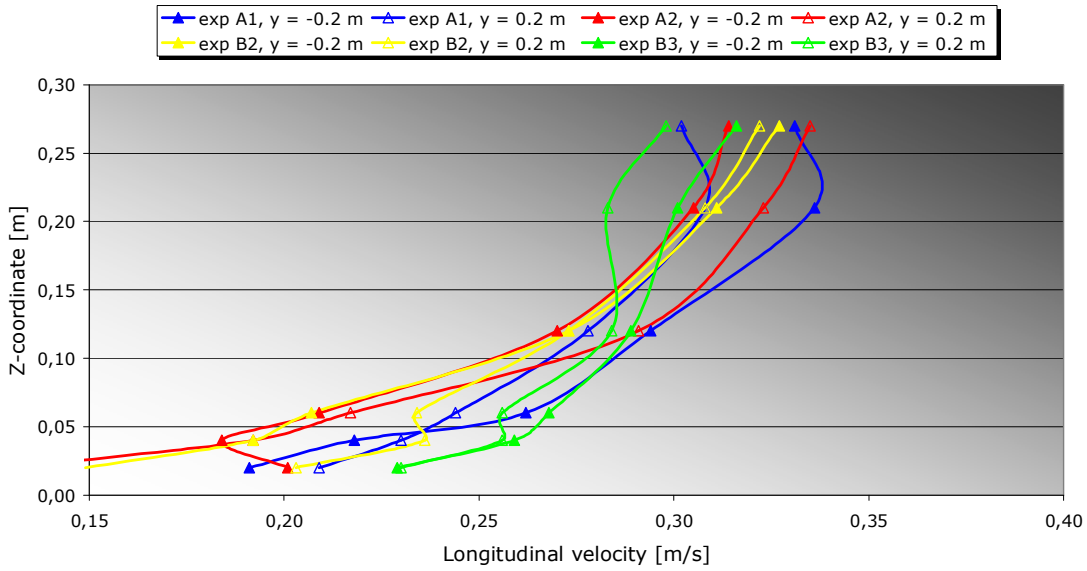

Figure 6.16 Longitudinal flow profiles x = 13.60 m

6.5.5 Alternate bars

A cause for disturbances in the model bed can be alternate bars. These bars are caused by free or forced oscillations between model bed and flow. The measured longitudinal profiles do not directly indicate the presence of alternate bars but contain some behaviour that might be explained by alternate bars. In Appendix J it is checked whether alternate bars could be present in the used set-up. This was not the case.

6.6 Discussion on the influence of the vane geometry

In this section the results of the experiments, both bed measurements and far field velocity measurements will be related to physical processes to account for the system behaviour. Furthermore, the influence of the vane height and angle of attack will be discussed in relation to the processes that are identified in Section 6.2.

6.6.1 Vane-induced spiral flow

As stated by Marelius and Sinha [1998] the vortex strength increases with the angle of attack, also above 20-degree angles of attack. In these experiments it is also shown that the intensity of the spiral flow increases as the angle of attack increases. This can be derived from e.g. the erosion channel depth (Figure 6.12) but also from the measured transverse flow velocity (Table 6.12).

In this study no quantification is given. More details on how the spiral flow is generated can be found in the M.Sc. Thesis of J.A. van Zwol [2004].

For increasing vane height, the vortex strength also increases, as can be seen in the above-mentioned table and figure. Of course there is a limitation to the height. A vane with a height equal to the water does obviously cause no spiral flow. The optimal vane height (optimal: maximum vane-induced spiral flow) is estimated at half the water depth.

6.6.2 Vortex growth and development

The width of the influenced area increases with the angle of attack. Odgaard suggested a vortex width equal to the depth, but this is appears to be too small. . From the bed level measurements (Table 6.5) it appeared that the vortex width in the area 2-4 L_v downstream of the trailing edge (x = 16.00 – 17.00 m) equals two to four times the average water depth. For high angles of attack this reported vortex width is slightly too high as the horseshoe vortex effect is also included in this width. Nevertheless, like for the low angle of attack, a width of at least two times the water depth is influenced.

The flow velocity measurements indicate a smaller width. At 1.5 L_v downstream of the trailing edge the vortex width equals one to 1.5 times the depth, with increasing angle of attack. Note that this is smaller than found in the bed level measurements. This indicates that the changes in the bed level are not only caused by the transverse flow, but that other effects, like the increased longitudinal transport, play a role. Of course stability also plays a role. If the bed level decreases somewhere, the neighbouring points can also go down without actually being influenced by the effect self, but on basis of stability.

The above-reported vortex width is for both bed and velocity measurements based on the near-bed. So, at a higher elevation the vortex can be even wider.

For increasing vane height the vortex development changes. The initial vortex core for a relatively high vane is not near the bottom and so the influence on the sediment transport direction will be smaller than for a low vane. When comparing the contour plots in Appendices E.1, C.6 and C.7 (experiments A2, B2 and C2), it can be seen that the deepest point of the erosion channel shifts from x = 15.50 m for a vane height of 6 cm, towards x = 17.20 m for a vane height of 18 cm. These observations support the hypothesis that the vortex grows larger in downstream direction (Section 6.2.2) and that for a higher vane the vortex "touches" the bottom further behind the screen. In Figure 6.14 this growth is also identified.

Figure 6.17 is taken from aerodynamics, but shows perfectly what is meant above.

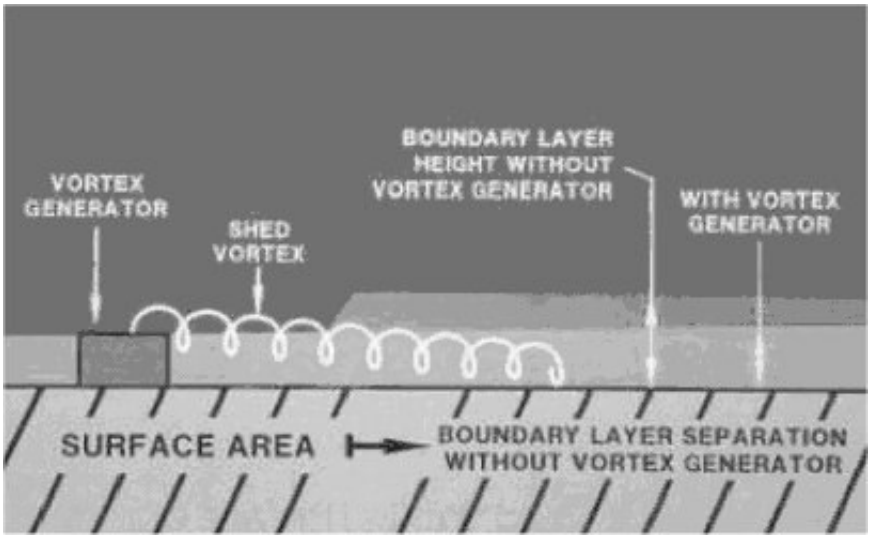

Figure 6.17: Vortex generator on a wing [http://www.smartcockpit.com/]

This vortex growth evidently influences morphology. A low vane will have more effect on the transverse sediment transport near the vane, and a high vane has more effect further downstream of the vane.

6.6.3 Increased longitudinal transport

From the theoretical analysis it follows that the longitudinal transport (near-bed flow velocity) is changed more for stronger vane-induced spiral flow. The measured longitudinal velocities (e.g. Figure 6.15) do also indicate that. So, it can be concluded that this effect increases with the angle of attack, but also with the vane height (since the vane-induced spiral flow increases).

For an increasing vane height, the vortex core will be higher above the bed and also the vertical flow velocities that transport the x-impulse downward are located higher in the vertical. Then the effect on the near-bed flow velocity will be, compared to a lower vane, smaller. Based on the plot in Appendix H it can be estimated for experiment C2, that the longitudinal flow velocity difference between pressure and lee side is higher at an elevation of z = 9 cm or z = 12 cm than for an elevation of z = 2 cm or z = 4 cm.

If the longitudinal transport changes, also the longitudinal slope should change. Appendix B shows the longitudinal slope. It is clear that for the higher angles of attack and the high vane (experiment C2) the longitudinal slope has changed significantly indicating transport in longitudinal direction. Also for experiment B2 a slight decrease in the average bed level from x = 15.50 – 16.50 m is visible. Based on the fact that the cross-sectional plot in Appendix D.4 is almost symmetrical for experiment B2, the near bed longitudinal velocity on the lee side is probably not increased, as this would have caused a deeper erosion channel (asymmetric development of sedimentation-erosion pattern). For experiment A2 the change of the longitudinal profile is not reliable, as described in Section 4.1.1.

The influence of the height is visible when comparing experiment B3 and A3 in Appendix B. For the low vane (B3) the effects are stronger closer to the vane and also the sedimentation is closer to the vane. For experiment A3 the effects are somewhat less directly downstream of the vane and the sedimentation bulb is located further downstream. In principle this is also valid for experiment A4. Only, due to the higher initial vane-induced spiral flow, the total amount of sediment moved is larger.

The increase of longitudinal transport on the lee side of the vane, clarifies the deeper erosion channel. The channel is not only eroded by the transverse vane-induced spiral flow, but also sediment is transported downstream.

6.6.4 Horseshoe vortex

A horseshoe vortex has been reported in front of the vane by Marelius and Sinha [1998]. They tested a vane at a 40-degree angle of attack. From the bed level contours in this research also such a process is been identified. The magnitude of the horseshoe vortex is dependent on the vane height and the angle of attack. For angles below 20 degrees almost no significant scour appeared, but for higher angles of attack the scour quickly increases. The influence of the height is large. For experiment B2 no scour was reported, whilst for experiment C2 a local maximum depth of 1.4 times the average depth was found.

The local scour process will start when the flow velocities exceed some critical value and sediment is scoured away. As the scour hole grows, the horseshoe vortex will get more space to develop and magnify the scour process. So, the initial condition is determining whether a scour hole will develop or not. From these experiments it can be derived that a significant scour hole will develop if the angle of attack is larger that 20 degrees, but this is of course also dependent on the vane height.

From the scour monitoring during the experiments, something can be said about the scour development in time. Also Appendix C.3 provides some information. The scour process appeared to close to the leading edge of the vane. In time, the scour hole grew towards the trailing edge, and in case of a strong horseshoe vortex (e.g. experiment A4), also a channel was formed downstream of the vane. The small figure on the right schematically indicates the scour development in time.

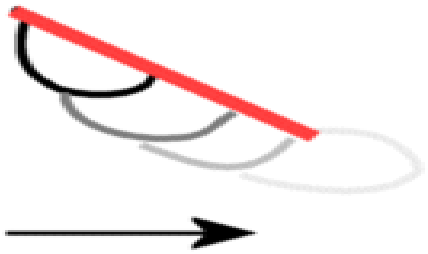

6.6.5 Total morphological behaviour

The main processes determining the morphological behaviour in the far field are the main vortex and the changed longitudinal transport by this vortex. The transverse flow causes the sedimentation-erosion pattern behind the vane. The increased longitudinal transport on the lee side of the vane causes the erosion channel to erode more than it would do for only transverse flow. This effect grows larger for higher angles of attack, and shifts downward for higher vanes.

If these effects are added up (Section 6.2.5) the resulting bed can be understood. The centre line of the morphological change (zero crossing) tends to shift towards the lee side in downstream direction for higher angles of attack as sediments transported by the increased longitudinal flow are deposited again.

Marelius and Sinha found this in their experiments too (Figure 6.18). The shift of the zero line stops at a certain distance downstream of the vane as the change in longitudinal flow is no longer present. Appendix C.2 (experiment B3) indicates that the normal symmetrical erosion-sedimentation pattern (only caused by transverse flow) might return further downstream (x = 18.50 – 20.00 m).

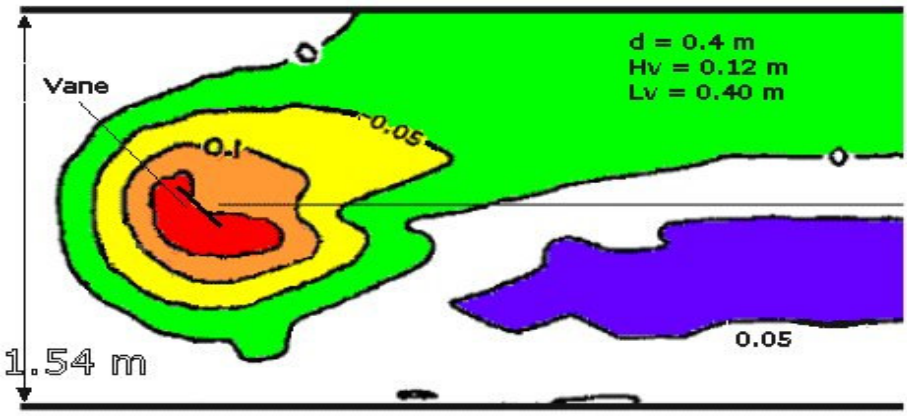

Figure 6.18: Bed levels from experiment [Marelius & Sinha, 1998]

Appendix C.3 shows that this asymmetry is not present in an early stage. The sediment originating from the scour hole can be found in the area x = 16.00 – 17.50 m at about y = 0.4 m. This means that the sedimentation further downstream is mainly caused by the vane influenced transverse and longitudinal velocities. The fact that the sedimentation blocks the flow might again increase the flow through the erosion channel causing more erosion at its turn.

The horseshoe vortex does not seem to have a direct influence on the far field morphology itself. However, sediments are deposited in the far field that originate from the scour hole which the vortex digs. These deposition patterns might influence the development of the erosion channel. From the current study no clear answer can be given to this question. The horseshoe vortex leaves the vane at the trailing edge and digs a relatively small channel straight downward, moving the sedimentation of the main vortex further outward. The horseshoe vortex transports sediments along the vane to a downstream location and therefore contributes to the formation of a longitudinal slope.

6.7 Conclusions

- The vane-induced spiral flow is found for angles of attack up to 40 degree and also for a 20-degree angle of attack vane with a height of 0.6 H_v / d ;
- Besides the familiar vane-induced transverse flow velocities, an influence of the vane on the longitudinal near-bed flow is recognised. With that also the sediment transport changes. Downstream of the lee side the transport capacity increases whilst on the pressure side this decreases. This influence is stronger if the vane-induced spiral flow is larger, so for higher angles of attack or higher vanes;
- The vane-induced spiral flow has to develop in downstream direction. The initial height of the vortex core determines the course of the morphological changes. For a higher vane the effects are somewhat more spread in downstream direction, and for low vanes the effect is strong directly downstream of the vane;
- The affected area is much wider than suggested by Odgaard and Wang [1991a, 1991b]. For all experiments the influenced area was at least twice the water depth and for high angles of attack this was increasing to 4 times the water depth. So, the spiral flow in a cross-section is not circular but elliptical;
- In the sedimentation-erosion pattern, the erosion channel is locally deeper than the sedimentation pattern is high. This is presumably caused by the increased longitudinal transport;
- In front of the vane a horseshoe vortex has been recognised causing local scour. This horseshoe vortex can develop from angles of attack of about 20-degrees. For increasing vane height the process becomes stronger. The horseshoe vortex deposits the sediment downstream of the pressure side of the vane.

7 Water level set up

7.1 Introduction

During the experiments, the water level was measured at three locations along the sidewall of the flume. By means of the measurements, an analysis is made to estimate the water level set up caused by the vane. The goal is to find the magnitude of the water level set up caused by the bottom vane.

7.2 Measurements

The water levels were measured by means of three point gauges that were mounted on the sidewall of the flume. The point gauges were located at x = 4, 14 and 24 m. The vane was installed at x = 15 m.

The measuring gave the following results [Zijlstra & van Zwol, 2003]:

Experiment	A3	A1	A4	A2	B2	C2	B3
PG1 [cm]	81.00	82.26	81.18	81.26	81.51	81.56	81.43
PG2 [cm]	80.90	82.20	81.09	81.06	81.33	81.41	81.31
PG3 [cm]	80.58	81.95	80.78	80.84	81.07	81.16	81.13
ΔPG1-PG2	0.10	0.06	0.09	0.20	0.18	0.15	0.12
ΔPG2-PG3	0.32	0.25	0.31	0.22	0.26	0.25	0.18
ΔPG1-PG3	0.42	0.31	0.40	0.42	0.44	0.40	0.30

Table 7.1: Water level measurements

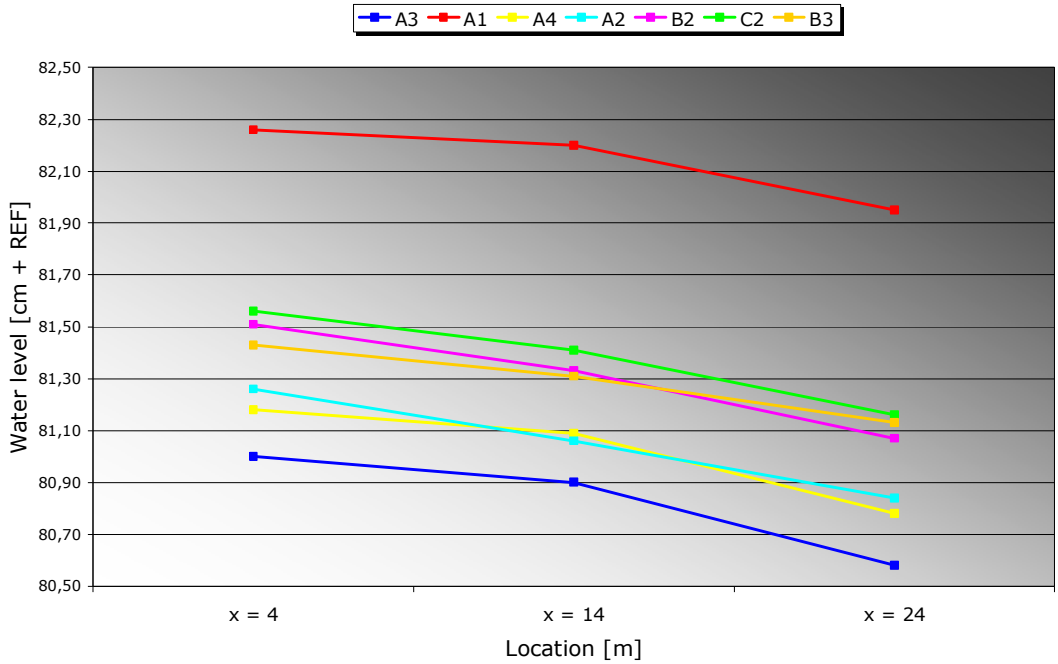

Figure 7.1: Water level measurements

The results show that the water level gradient on PG1-PG2 is always smaller than PG2-PG3. The gradient PG1-PG3 is almost constant, except for experiment A1 and B3, but the values are still within the accuracy range.

7.3 Delft3D-FLOW simulation

In the mathematical model Delft3D-FLOW a full 3D water movement model was made to obtain more insight in the water level set up, and also whether the local effects influence the flow in the far field. The model has an option to close grid cells partly over depth at the boundary of grid cells, "rigid sheets". The grid was refined in the area were the vane was modelled in order to make positioning at a more accurate angle possible. In Figure 7.2 on the next page an example is given (in grey dots the modelled vane).

As can be seen, many alternatives for the vane modelling are available. Which one to choose? In this case the symmetric alternative feels like the best, but in case of a less favourable situation the decision may not be this easy, as a symmetric solution is not possible. At the right side of the figure, two examples are given. The problems are clear, for the top-right figure an appropriate solution has been found, but it is the same as the schematisation on the left. So, whilst the vane is in reality positioned differently, the model will generate the same results. Due to this schematic representation, and the use of a simple eddy-viscosity approach for turbulence, the near-field conditions are supposed to be poorly reproduced. So, the results of these calculations are indicative. Modelling of the complex flow by more complex turbulence models (and non-hydrostatic flow) is simply not (yet) possible in Delft3D.

The results of the calculations are given in Figure 7.4 and Figure 7.3 on the next page. The first figure shows results in longitudinal direction and the second figure shows the water level in three cross-sections in front of the vane.

Although the results seem acceptable, some remarks have to be made:

- The results are not sensitive to the angle of attack. The set up is dominated by the vane height. This is not realistic, but can be explained since Delft3D only calculates the set up from the oblique rigid sheets;
- The model does not 'feel' the guidance by the vane. Therefore, the solution is totally symmetric to the flume axis. The parallel rigid sheets hardly influence the result. Basically the set up in this model is the same as for an oblique wall;
- The water level set up predicted by the model is much higher than measured in the experimental model;

Despite the remarks, it can be concluded that PG2 is clearly not fully influenced by water level set up according to this model. At x = 14 m, the set up is not fully developed to the sidewall. In reality, this distribution is probably different for all configurations, since the angle of attack will also have influence on this.

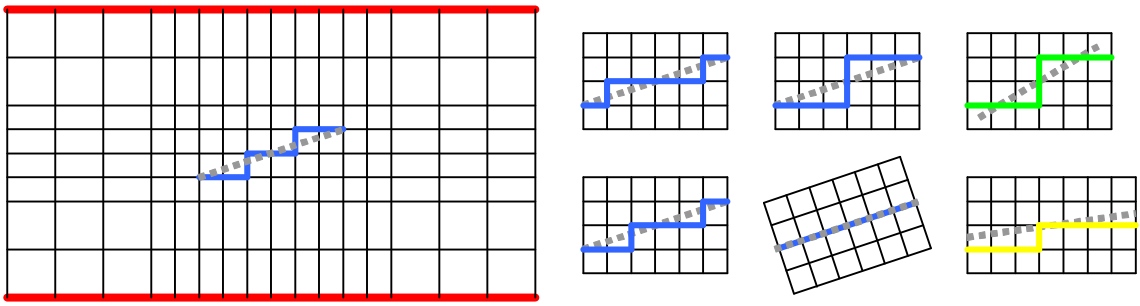

Figure 7.2: Grid 3D water level set-up simulation

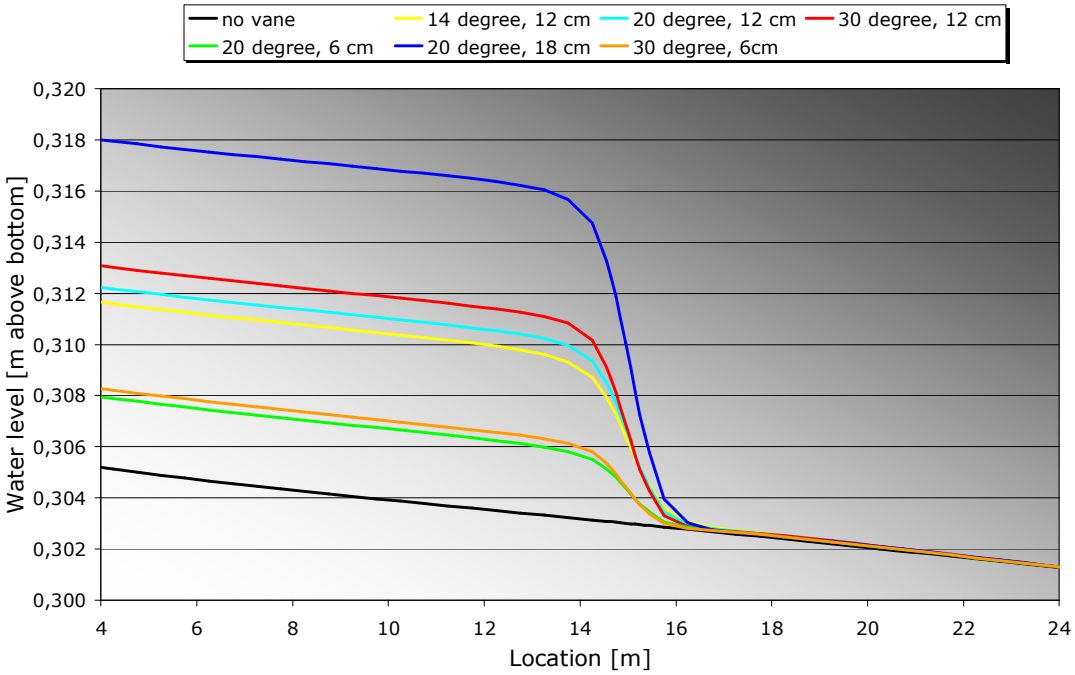

Figure 7.3: Water levels according to Delft3D simulation at 40 cm from wall

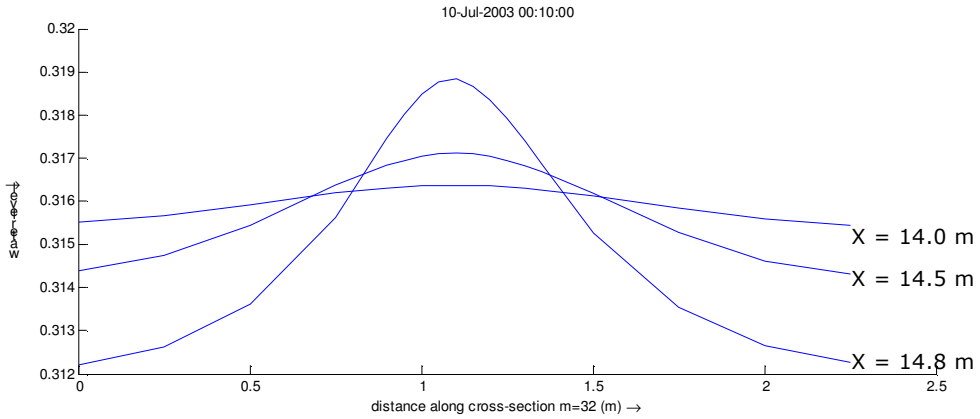

Figure 7.4: Water levels in front of vane according to Delft3D-FLOW

7.4 Effect of scour hole

Decelerating flow and loss of impulse in the cross-section causes the water level set-up in front of the vane. However for some vane configurations a scour hole forms. This scour hole increases the effective cross-section again and might be able to compensate water level set-up to a certain extend. In Appendix D.2 the average cross-section from x = 14.80-15.20 m is shown. The average increase of the cross-section at x = 15.00 m is calculated in the table below.

x = 15.00 m y = -0.5 – 0.5 m	A3c (42 h)	A1 (17 h)	A4 (34 h)	A2 (16 h)	B2 (35 h)	C2 (35 h)	B3 (49 h)
Average elevation above zero-bed [cm]	-3.2	-0.9	-8.9	-0.8	-0.1	-4.1	-5.4
Relative cross-sectional area [%]	+11	+3	+30	+3	0	+14	+18

Table 7.2: Increase net flow area by scour

The effect of this scour hole on the water level set up is difficult to determine. On the one hand the cross-section is widened, but on the other hand the flow decelerates causing a higher water level. Since the flow around the vane is strongly determined by a 3D flow pattern, hydrostatic pressure is not necessarily present, making simple approaches impossible.

7.5 Discussion

From the Delft3D calculation it follows that PG2 is no reliable source to determine water level set up. According to the model, PG1 (x = 4m) is fully influenced and PG3 (x = 24 m) is not influenced.

Normally, water level set up disappears in upstream direction, as the water level tends to return to the equilibrium depth. The model does not show this. With the theory of Bresse an estimate of the length over which the effect reduces, is made:

$$L_{1/2} = \frac{0.24 h_e}{i_b}\left(\frac{h_0}{h_e}\right)^{4/3} \approx 350m \tag{5.1}$$

From this, it follows that in the model area no reduction of the set up is noticeable as the flume length is only 30 m. So, PG1 is fully influenced by the set-up and PG2 is also influenced but in an unknown proportion since the propagation of set up in transverse direction is unknown. PG3 is not influenced, as it lies behind the vane. This can also be seen in the Delft3D results (Figure 7.3).

So, for analysis in theory the difference between PG1 and PG3 can be used to estimate the water level set up. In the measuring report [Zijlstra & van Zwol, 2003] was concluded that the average roughness was estimated at 35 $m^{1/2}/s$. The only problem for using this value is that it is based on the same water level measurements, so no information can be deduced on which part originates from water level set up.

More uncertainty is introduced by the fact that the bottom level is not exactly known. Besides that, the bed was not in equilibrium condition, causing backwater effects. The non-flat bed also introduced depth variations and with that flow accelerations and decelerations. These effects are all in the order of a few tenths of a millimetre, but as set-up is also expected to be very small these influences cannot be neglected.

When looking at the measured water levels, it can be noticed that the differences between the gradient PG1-PG3 is more or less equal for five out of seven experiments. If water level set-up was significant, the results of experiments C2 (very high vane) and A4 (high angle) that are likely to have a large water level set up, would have been different. But instead, experiment B2 shows the largest gradient whereas a very small gradient was expected as the vane is low and has a small angle of attack. More contradictory results are obtained for experiment A1. The gradient PG1-PG3 is relatively small (as expected) but the difference between PG1-PG2 and PG2-PG3 is very large, whilst, if no, or very little, set-up is expected, these slopes should have been more or less equal, like for experiment A2.

Although for high vanes and vanes at high angles of attack, some water level set up is expected, this does not have to happen. Since the vanes at high angles of attack and high vanes caused quite large scour holes, the constriction for the flow reduces significantly, and therefore the set-up might have reduced.

7.6 Conclusions

- The water level set up is most likely very small (order 10^{-4} m);
- The physical model errors (measurements and bed level) are too large to obtain reliable results for quantitative results on the water level set up;
- The schematised Delft3D model overestimates the water level (set up) as the flow is not guided around the vane like in reality. The model only 'sees' the perpendicular structures and calculates the set up according to these oblique constrictions. Note that in reality the constriction is almost zero as the vane's thickness is negligible;

8 Mathematical modelling of bottom vanes

8.1 Introduction

With bottom vanes being believed an effective way of river training, also the desire to model the effects of vanes arises. In this chapter the Delft3D-MOR model with bottom vane module will be discussed and tested. The tests are limited to a vane at a high angle of attack. First it is investigated how a vane at a high angle of attack can be modelled and then Delft3D-MOR is tested on reproducing the measured morphological changes in the model. Furthermore the restrictions of the model are discussed. Finally, in short, the nearby-future possibilities of full 3D modelling are discussed.

8.2 Introduction to Delft3D-MOR

Delft3D is an extensive modelling environment for 2D and 3D free-surface flow. It is capable of solving many problems with water, varying from waves, current and tides in combination with sediment transport, contaminants, heat and many more. The heart of the model is the flow module. This module is capable of solving three dimensional flow, but not (yet) capable of taking into consideration vertical accelerations and non-hydrostatic pressure.

In river engineering practice, use is made of Delft3D-MOR, a version of Delft3D for morphological development. At the moment the modelling environment is usually applied in 2D mode. The flow module is solved with one layer, what comes down to a depth-averaged approach. From the result of the flow calculations the sediment transport module calculates a sediment transport rate. Finally the bottom module calculates the bottom change.

To save precious calculation time, the flow module is not necessarily solved continuously, but only if the bottom has changed and the change to the flow field and the corresponding sediment transport significant.

8.3 Modelling vanes and screens in Delft3D-MOR

As the Delft3D-MOR model does not solve a 3D flow but a 2D depth-averaged flow, problems arise when modelling vanes. The flow around vanes cannot be easily simplified to depth-averaged flow, as the processes are fully three-dimensional. Even if the model would be three-dimensional, the flow module would still not (yet) be capable of solving near-vane flow because neglecting vertical accelerations and assuming hydrostatic pressure results in inadmissible errors. Besides that, a very fine grid is needed to correctly implement vane geometry in the model (see also Figure 7.2). Of course also a curvilinear grid can be used instead, but this is not always practical when modelling a river. But even more important, small grid cells are needed to simulate the near-vane flow. For a common practice model such small cells cause excessive calculation times

So, for modelling vanes in a 2D modelling environment like Delft3D-MOR a different approach is needed. In principle there are two solutions:

- A mathematical model that calculates the effect of a vane for one or several grid cells;
- A sub-model that solves the fully 3D flow and transport around a vane (nesting a 3D model)

Both options have their strong and weak points. The mathematical model must produce a result that can be used in the 2D model. This can be a change of the depth averaged velocity, the depth averaged transport or (theoretically) a bed level change. This means a simplification of reality. The advantage is the relative short calculation time compared to a sub-model.

A sub-model overcomes the simplification of reality of a mathematical model, but still depth averaged quantities have to be fed back to the 2D model on the boundaries of the sub-model. A fully 3D sub-model will take quite some calculation time. It is also the question how big a sub model must be. Only the near-vane area, or also the whole area that the vane influences ?

In the current implementation of vanes and screens in Delft3D-MOR, two modelling solutions are available, type 1 and type 2 modelling. One of the main differences between these options is the relative size of the vane to the grid. Figure 8.1 shows this.

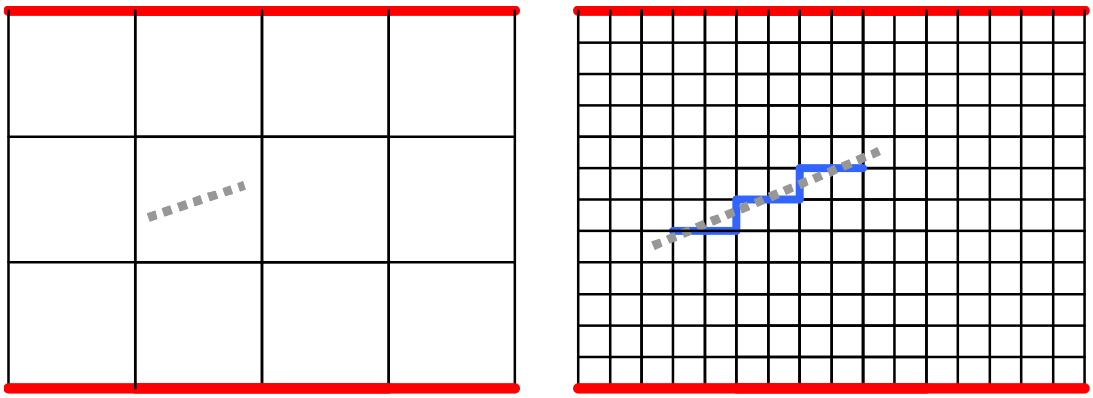

Figure 8.1: Sub-grid level and grid level vane modelling (type 1 and 2)

Furthermore, type 1 vanes are supposed to be relatively small ($L_v \approx d$) and type 2 vanes have the dimensions of flow guiders ($L_v >> d$).

8.3.1 Type 1 bottom vanes

Type 1 modelling is a sub-grid solution. The flow module does not see the vane, except for some artificial resistance. A mathematical model calculates the intensity of the vane-induced spiral flow of the bottom vane in the grid cell concerned. Two mathematical models are available. The first is based on the theory of Odgaard and Wang (Section 2.2) and the second one is a relation based on experimental measurements. After that, the model will calculate the net vane-induced transverse bed shear stress for the surrounding cells.

In summary the model calculates the vane influence as follows:

- Calculate initial vortex strength

  ⇒ For the Odgaard model

$$j_b = \frac{d}{2} v_{\max} \tag{9.1}$$

with

$$v_{\max} = \left(\frac{\Gamma \delta_s}{\pi 0.8 H_v} \right)_{s=0} \varphi_D(s) + \frac{\Gamma}{2\pi(0.5 L_v + s)}$$

  ⇒ For the experimental model

$$j_b = \alpha_{initialvortexstrength} \frac{1.58}{2} U \tan(\alpha) H_v^{0.8} L_v^{0.3} d^{-0.1} \varphi_D(s) \tag{9.2}$$

in which:

j_b	integral transverse velocity
$\alpha_{initialvortexstrength}$	tuning coefficient for initial vortex strength
$\varphi_D(s)$	damping function
Γ	vortex intensity according to theory of Odgaard

- Calculate damping in longitudinal direction (included in above mentioned formulae);
- Calculate vortex-line (along which the centre of the vortex moves downstream);
- Calculate average transverse bed velocity to determine shear stress for the grid cell vane and surrounding cells (integral over each cell);

$$v_{z=0} = \frac{1}{A_{cell}} \iint \frac{j_b}{B_{vor}} dxdy \tag{9.3}$$

in which:

A_{cell}	Area of grid cell
B_{vor}	Water depth for Odgaard model (d)
	$1.6 H_v$ for empirical model

- Finally the model calculates the directional change of the sediment transport;

The main characteristics of this type 1 model are:

- Near-vane flow velocities are not calculated. The local flow causing scour is absent;
- The influence on the far field flow is artificially introduced by the mathematical model by means of a changed sediment transport direction;
- Since the theory of Odgaard is valid for small angles of attack only, the model only works for angles of attack below 22 degrees. If the angle of attack is larger, the simulation ignores the vane;
- The equal distribution of transverse velocity over the influenced width is a simplification of reality. In reality the vortex intensity damps out to the side;
- The vortex is assumed to be a perfect circular rotation at all time. Time, location and bathymetry dependencies are not taken into consideration. In the Odgaard model the vane width is equal to the depth, and in the experimental model $1.6H_v$. In reality the vortex deforms and grows, which obviously also influences the near-bed velocities.

8.3.2 Type 2 bottom vanes

For the second method of modelling, the vane is modelled at a grid scale level. The vane is modelled by submerged weirs, which are located on the grid boundaries (thick line in Figure 8.1 right). As the flow module can handle these overflow structures (weirs), no adaptations in the model code like for type 1 vanes, are necessary. Due to the limitation of modelling the vane on grid cell boundaries, problems with modelling a sufficiently accurate geometry, as described in Figure 7.2, play a role.

Again the complex 3D flow near the vane is not calculated, as only the depth averaged flow is used. However, in contradiction to type 1 modelling the vane is modelled in the flow module and some 2D flow effects are taken into consideration. As the vanes are implemented in the flow-module every angle of attack is possible.

The modelling does include an adaptation to the sediment transport module. The user has to specify a coefficient to control the amount of sediment passing the vane. Logically, the other fraction is blocked.

The model includes:

- Vanes are modelled as weirs so energy loss is included in the model;
- The weirs (vane) do (partially) block the sediment transport;

The restrictions of the model are:

- Near-vane complex 3D flow is not taken into consideration, no local scour effects are included in the simulation;
- As vertical accelerations are neglected, the flow module does not calculate the correct effect of the vane in the far field. The vane-induced spiral flow is not simulated;

8.4 Modelling of the vane-induced physical processes

To correctly model the morphological behaviour of the vane, it is necessary to model all relevant vane-induced processes. In Section 6.2 these processes were presented. For all these processes it is indicated to what extent they are modelled.

- Vane-induced spiral flow:
  - Type 1

    ⇒ Modelled by a mathematical model that calculates the changed sediment transport direction downstream of the vane;
  - Type 2

    ⇒ The vane is modelled in the flow module, and the changed flow field causes the sediment transport to change;
- Vortex growth and deformation:
  - Type 1

    ⇒ The transverse bed shear stress is calculated by dividing the spiral flow intensity by the vortex width that is chosen equal to the depth or to $1.6H_v$ depending on the model (Odgaard or experimental). The mathematical model uses an exponential damping formula to calculate the vortex intensity downstream of the vane;
  - Type 2

    ⇒ Not modelled;
- Influenced transport in longitudinal direction:
  - Type 1

    ⇒ The effect of an increasing longitudinal sediment transport caused by the vane-induced circulation is not included in the mathematical model;
  - Type 2

    ⇒ Also not modelled;
- Horseshoe vortex in front of the vane:
  - Type 1

    ⇒ The vane is not present in the flow module and no model is included for the horseshoe vortex;
  - Type 2

    ⇒ Except for the scour and erosion caused by the change in the depth averaged flow, no local scour is modelled;

From this it can be concluded that the expectations of the model should not be too high as most (local) processes are not included in both type 1 and type 2 vane modelling. However, it is still interesting to what extent the results do look like the experimental results. By doing this, the importance of the neglected processes can be estimated and the reliability of the predictions of the model can be evaluated.

8.5 Simulations with Delft3D-MOR

The Delft3D-MOR model was used to make morphological simulations for the experiments executed in Bangladesh to see whether the results of the model correspond to the experiments. Use has been made of both type 1 and type 2 modelling. The main question was whether Delft3D could produce acceptable results for vanes at high angles of attack without having the effect of scour holes and influenced longitudinal transport modelled.

Also an answer is sought to the question how to model high angle of attack vanes. It has been suggested to use the type 2 modelling, but the question is whether this is acceptable without modelling the vortex.

The sediment transport in the model was adjusted until it was more or less the same as the estimated value from the experiments. The time scale in the mathematical model is therefore to be expected in the same order of magnitude as in the experiments.

Several experimental runs with the model have been made. An initial flat bed has been used, and simulations were made with an initial bed equal to the most extreme experimental outcome, experiment A4. Also one calculation was made with an initial bed level equal to experiment B3.

8.5.1 Type 1 simulations

For type 1 vanes it is not possible to model a 40-degree angle of attack vane as the model automatically switches of vanes at an angle of attack larger than 22 degrees. In the simulations use has been made of the experimental vane model.

It was decided to use an 18-degree angle of attack vane and mathematically increase the vortex strength by means of a calibration coefficient in the model. Basically this is the same as increasing the angle of attack as can be seen from Equation (9.2). The actual value of the calibration coefficient was determined by trial and error, in such a way that the depth of the erosion channel, more or less equalled the measured value in the experiments.

First, simulations with an initial flat bed were made to see how the model responded without the bed topography found in the experiments. The tuning coefficient was changed in order to see how this affected morphology. For the calculation of the vane influence in the far field use is made of a vortex line. From the separation point of the vane, an imaginary line is calculated along which the maximum vane-induced spiral motion moves downstream. This vortex-line can be calculated in two ways; straight backward along the grid lines or as a function of the streamlines. For the streamline option four sub-options are available to chose the flow field used for a streamline computation; (1) depth averaged flow field, (2) velocity field at vane height derived of depth averaged flow, (3) same as option 2 but including spiral motion or (4) same as option 3 but also including upstream vane-induced flow. It was investigated how option (1) and (4) changed the results. Note that spiral flow was switched off in all the computations. This is possible as the vane induced spiral motion is calculated in a different way then the spiral flow in the normal model.

From these tests it was decided to use an initial vortex strength coefficient of 2 and vortex-line option 4 to make simulations with an initial bed equal to the results of experiment A4 and B3. Furthermore the influence of the scour hole was investigated for experiment A4 by keeping the scour hole fixed by dredging. Note that the sediment balance in the model is disturbed, as sediment is artificially subtracted. It was not possible to re-supply the sediment behind the vane as this option is not implemented in the vane version of Delft3D-MOR.

8.5.2 Type 2 simulations

For the type 2 vane modelling fewer computations have been made, as it was almost directly clear that this type of modelling was not very suitable for the current purpose. In the first calculation already, it appeared that the influence of the vane on the far field morphology was very small.

A fine grid was defined in order to accurately model a vane at 40-degree angle of attack. The height and length of the vane were respectively 12 and 40 cm, and the initial bed was equal to the results of experiment A4. The vane was schematised as follows:

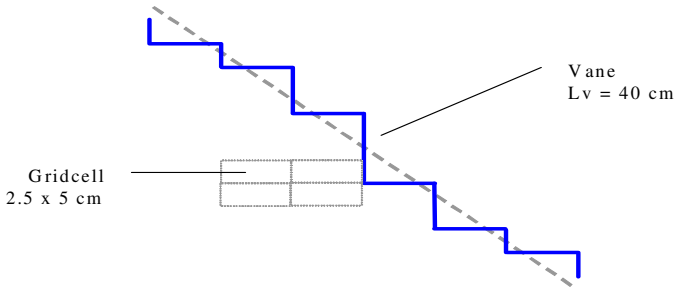

Figure 8.2: Type 2 vane schematisation

8.5.3 Overview simulations

An overview of all simulations and the appendix in which the results can be found. In the appendices the development of the bed level is presented. Between the successive pictures always a difference of one day is present.

- Reference simulation, no vane, begin bed levels equal to experiment A4, fine grid (5x2 cm^2) (Appendix I.1);
- Vane type 1 simulations initial flat bed, grid (10x10 cm^2):
  - Lift coefficient x2, vortex strength x2, Vortex-line option 4 (Appendix I.2) (Reference case);
  - Lift coefficient x2, vortex strength x2, Vortex-line option 1 (Appendix I.2);
  - Lift coefficient x1, vortex strength x1, Vortex-line option 4 (Appendix I.3);
  - Lift coefficient x2, vortex strength x4, Vortex-line option 4 (Appendix I.3);
- Vane type 1 simulations, grid (10x10 cm^2):
  - Initial bed exp. A4, vane type 1, reference vane (Appendix I.4);
  - Initial bed exp. B3, vane type 1, reference vane except vane height 6 cm (Appendix I.5);
  - Initial bed exp. A4, vane type 1, reference vane, with sediment withdrawal (Appendix I.6);
- Vane type 2 simulations, fine grid (5x2 cm^2):
  - Initial bed exp. A4, vane type 2 (Appendix I.7);
  - Initial bed exp. A4, vane type 2, with sediment withdrawal (Appendix I.7);

8.6 Simulation results

The simulation results are displayed in Appendix I. In order to make an orderly picture, the subsequent figures have not all been given legends. In all cases the interval between the figures is 24 hours and the subsequent pictures are ordered top-down.

8.6.1 Reference simulation

The reference calculation is made to see whether the model behaves as expected. Flow velocity, water depth and sediment transport were checked. The behaviour of the simulation is as expected. The scour hole slowly moves downstream and fills up. Also the initial disturbances disappear. After 8 days however, the scour hole has not totally disappeared yet. Furthermore the bed is not yet in equilibrium. So, also the timescale of the model is, like the flume, quite large. The sediment transport in the model is at average about $3 \cdot 10^{-7} m^2 / s$ (in the experiments $2 \cdot 10^{-7} m^2 / s$, Table 5.2).

8.6.2 Type 1 initial flat bed

For the initial flat bed four simulations have been made in order to find out how the settings influence the results and to see what settings give the best system behaviour (depth erosion channel, vortex influence). In the appendices no first picture (t=0) has been given, as the bed is totally flat. So, the first picture in the series is after 24 hours, the second after 48 h. etc.

Appendix I.2 and I.3 show the results of the initial flat bed calculations. Comparing the two figure series in Appendix I.2 reveals the influence of the vortex-line type. The calculation with vortex-line type 1 shows that the vortex is carried downstream in a straight line along the flume axis. This is expected as the vortex should follow the depth averaged flow. In this case the depth averaged flow is directed straight downstream, so the vortex also develops in that direction. The other simulation shows a vortex line that starts under a certain angle towards the lee side and then bends back parallel to the flume axis. This is caused by the vane-induced transverse flow that is taken into account when calculating the vortex line. However, measurements in other experiments [Struiksma & de Groot, 1996] point out that the vortex line is deviating from the centre line towards the pressure side instead of towards the lee side. Nevertheless, vortex line option 4 is chosen for the other simulations as for high angles of attack the bed level measurements in the current research showed a zero crossing that is shifted towards the lee side of the vane.

The influence of the initial vortex strength follows from Appendix I.2 left, and I.3. When the vortex is stronger the bed level changes are larger, and therefore the changes are spread more in width. The effects are noticeable further downstream as the vortex is stronger. For the following calculations with type 1 vanes an initial vortex coefficient of 2 is selected.

Normally a coefficient of 0.51 is used for calculations. According to the theory, when changing the angle of attack, the initial vortex strength is proportional to the factor $\tan(\alpha) \approx \alpha$. However, the theory is not valid for angles of attack larger than about 20-25 degrees. However, Marelius and Sinha [1998] showed that even when flow separation becomes relevant, the increase of the vortex strength is still more or less linear to the angle of attack. As in this case a vane at 40-degree angles of attack is intended, but the model cannot handle that, the initial vortex coefficient should be artificially increased.

The ratio $\tan(40^\circ)/\tan(18^\circ)$ is about 2.6, what would signify a vortex coefficient of 0.51*2.6=1.3. From this point of view the coefficient of 2 is somewhat high, but for qualitative analysis this is no problem.

In the simulation the results also grows asymmetric in time. The erosion channel is deeper than the sedimentation pattern is high. Besides that, the area of erosion is much larger than the area of sedimentation. It is not clear why this happens, but most plausible is that the initial erosion channel starts attracting water (channel formation) and that the morphologic change is magnified.

The vortex width for the used mathematical model is fixed at $1.6H_v$ (in the Odgaard vane model the vortex width is taken equal to the local depth). However, the observed changes appear to be wider. This is not strange, as the transition between influenced and non-influenced area becomes a gradual transition. As a bed level slope develops, a transverse sediment transport is caused by the slope. This is also explained in Figure 8.3. This also explains a wider influenced area. Striking in the results is the fact that for all calculations the sedimentation bar starts to disappear after about 100 hours (4th picture in series).

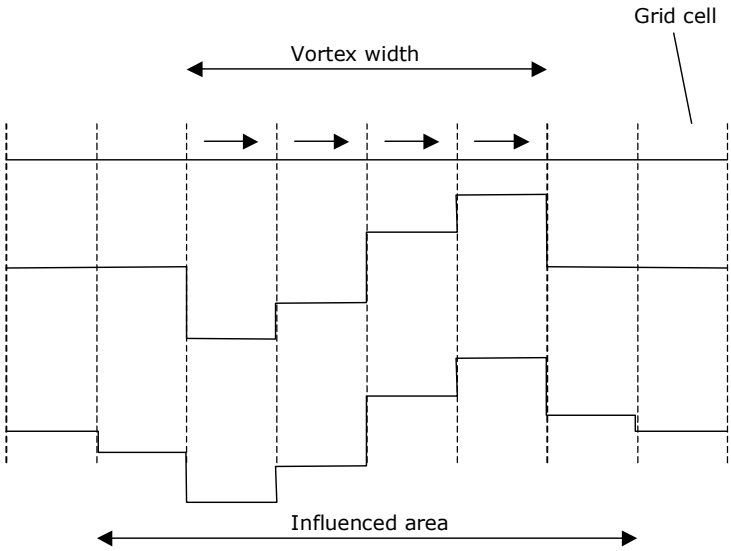

Figure 8.3 Spreading of vane effect on a fine grid

8.6.3 Type 1 simulations

The results of type 1 simulations are displayed in Appendix I.4, I.5 and I.6. For all simulations it can be concluded that the vortex effect is too strong further downstream of the vane. Especially further downstream, x = 18 m and larger, in the experimental results no erosion channel is observed, whilst the model predicts a significant erosion channel up to the downstream model boundary. The damping in the mathematical model is presumably too low, as the initial width and depth of the erosion channel are predicted reasonable.

Furthermore, the sedimentation pattern is totally absent. This was already observed for the flat bed, and cannot be imputed to initial configuration. As expected, the scour hole disappears but this process in clearly influenced by the vane as the scour is transported through the erosion channel. The channel seems to have grown substantially quicker than for a flat bed with vane (Appendix I.2 left), which is logic as the scour hole helps reaching the new equilibrium depth. The influence of the initial bed seems marginal, although the final depth after 8 days is larger for the model with begin bed equal to A4 than for the simulation with the begin bed equal to experiment B3.

The width wise spreading of the vortex for type 1 vanes, is limited to $1.6H_v$. In this case 1.6*12 cm for experiment A4 and 1.6*6 cm for experiment B3. This implies that when simulating a vane on a relatively fine grid no nice sedimentation erosion pattern is obtained, but all grid cells on the influenced width are equally influenced. In the results of the calculations this differences can be seen. The fact that for the simulation of experiment B3 the influenced width is smaller can be seen. But further downstream the difference diminishes, as in both cases the whole bottom on the lee side of the vane is lowered.

For the calculation in Appendix I.7 the scour hole was kept at its position by dredging. In the bottom vane version of Delft3D, it was not possible to re-supply the dredged sediment. As a result, the sediment balance is disturbed causing the whole bed to erode. From the initial scour hole an erosion front moves downstream, resulting in a much deeper erosion channel and also a new channel develops from the scour hole towards the right wall. By keeping the scour hole in place, it is aimed to get the effect of the scour hole on the flow in the model. By artificially introducing a scour hole in the model however, the local depth is increased. This causes the model to use a much bigger depth, and so the calculated vortex properties are different than for the average depth in the model.

8.6.4 Type 2 simulations

The type 2 vane modelling was investigated to see if the effects of vanes under high angle of attack can be predicted with this type of modelling. When looking at Appendix I.7 with the result of the calculations, the answer is unambiguous. The effect of type 2 vanes on the far field is much too small or basically absent. Only in the near vane area an effect is present, but opposite to expected. In front of the vane some sedimentation occurs as bed load is blocked. Keeping the scour hole in place by dredging in the second calculation (right picture series), does not improve the results.

8.7 Discussion

The modelling with Delft3D did not result in reproducing the results from the experiments. It appeared to be possible to simulate vanes at high angle of attack with the type 1 model by artificially increasing the vortex strength.

The calculations with the bottom vane module did not come easily. Stability was a big problem, and when looking at the results of the sediment transport still wiggles are in the model. This might be due to the small scale used in the model. However, the simulations could be kept stable in most cases.

The fixed vortex width in the model is not very realistic. In the experiments it appeared that the vortex width is not equal to $1.6H_v$ but also not equal to the depth, but much wider. When the vortex leaves the scour hole that possibly extends in the far field (or in case of other depth variations), the local depth decreases and according to the mathematical model the vortex spreading decreases linearly with the depth, which is not very realistic as the vortex has a certain inertia to adapt to the new boundary conditions, and might even keep its original width. The fixed value of $1.6H_v$ is therefore more favourable, as in case of depth variation the vortex width will not reduce, but remain the same. Nevertheless, for higher angles of attack this value should be chosen higher.

The deformation of the vortex also influences the damping of the vortex as the deformed water motion is less favourable and causes more turbulence and energy loss. The damping formulae in the mathematical model were validated based on flat bed non-movable bed experiment measurements. Probably for a movable bed model, and especially in an experimental flume with relatively larger ripples the damping is much larger.

The modelling with the type 2 vane model was not successful in reproducing experimental results. The lack of modelled physical processes resulted in poor results, and it can be concluded that the current type 2 vane modelling is not capable of simulating submerged bottom vanes at high angle of attack. It is the questions whether simulating a vane without a mathematical submodel is possible, since the vane-induced spiral flow is a three-dimensional process that cannot be calculated in a depth average flow calculation.

Finally it can be concluded that the results for the vane modelling at high angles of attack are mainly moderate as a result of not modelling the right physical processes that are relevant for the morphology of a single vane.

It is stressed out that the type 1 bottom vane model has been used in river models. The results were reasonable and conform expectations. The simple approach of using only a width average transverse bed shear stress does not work well when details on the local effects like in this study are investigated. Nevertheless the model can work fine on a larger scale were the local processes might not be relevant. This only holds for low angles of attack as for higher angles of attack other processes become significant also on the large scale.

8.8 Recommendations

In the model the effect of a vane is switched of at angles of attack larger than 22 degree. In reality of course, the vane is still present and causes effect. According to the results of current experiments, and also based on the measurements of Marelius and Sinha, it is acceptable keep the vanes active up to 45 degrees. For both the Odgaard and experimental model the increase of the vortex intensity is linear with the angle of attack, what corresponds to the observed transverse near-bed flow velocity in experiments for high angles of attack.

The type 1 vane model can also be extended with the influenced longitudinal transport. It should be possible to make an adaptation to the current modelling that calculates the increased bed shear stress in x-direction.

Both models do not calculate the scour hole. It is expected that in the experiments the influence of the scour hole on the large-scale morphology is relatively small. Therefore for the time being, it is sufficient to include the effect of the scour hole in the calculation of the initial magnitude of the vane-induced spiral flow.

The height of the vane has influence on the morphology of the vane (Section 6.6.2). In the calculation of the transverse bed shear stress an expression should be added that determines the development of the transverse flow velocities in vertical direction. This has to be investigated, but maybe a simple diffusion model already accounts for this effect sufficiently.

8.9 Near future modelling options

During the last decade, computational power has drastically increased. This made it possible to simulate 3D-flow for complex geometries by solving the complete Reynolds Averaged Navier-Stokes (RANS) equations in all three dimensions. As stated before, the use of vanes shows similarity to airfoils. In aerodynamics more

research is executed since the stakes are higher, so knowledge about the behaviour of airfoils, and phenomena like a wing tip vortex, is rapidly increasing.

Since the flow around vanes is completely three-dimensional, an analytical approach always yields simplifications. Therefore, the use of 3D-mathematical models can help understanding the processes around vanes. So far, no thorough research was done on 3D modelling of vanes.

Recently, Spentzos [Spentzos et.al., 2003] presented the preliminary results of 3D stall computations on an airfoil. For high angle of attack vanes, basically also stall occurs, only usually it is referred to as flow separation. The results of these computations show the flow around a stalling airfoil, but can qualitatively also be interpreted as flow around a vane. (Figure 8.4)

After Marelius and Sinha made their experimental set-up, they verified a 3D-model for bottom vanes that was made by Sinha and Marelius [2000]. The model input consisted of the bed levels measured in the experiment. Then the model computed the flow field and the measured flow velocities were compared to the model results. Without going into the details of the results, it was concluded that the model results were in good agreement to the measured flow velocities. This provides faith in the capabilities of 3D mathematical models.

At WL|Delft Hydraulics also calculations were made using the CFX-software package. Only one situation was calculated and no more effort has been done to investigate the functioning of the vane. (Figure 8.5)

In all mentioned calculations the free surface was modelled as a fixed free slip wall. Computation of the free surface takes a lot of computational effort and can lead to stability problems. To solve the stability problems a very fine grid is needed which leads to even more computational effort.

In the near future a new version of the Delft3D model will be released that can calculate flows without neglecting the vertical accelerations and can also handle the free surface. Unfortunately this version was not available in time to be used in this study, but later his model can provide a useful base for further mathematical investigation on the behaviour of bottom vanes. The current Delft3D-flow model was used to see if this model could calculate spiral flow. To some extend this was possible, but the intensity of the spiral motion was much too small.

Besides Delft3D also other software is already available for 3D modelling. At this moment 3D-FLOW and CCHE3D modelling software is available. The CCHE3D model is also capable to handle sediment transport and local scour. An example of the model is given in Figure 8.6.

The enormous increase of computational power allows for very small grids and mathematical models are and will be, available to solve small-scale problems like bottom vanes. However, in river engineering also need exist to model bottom vanes in river systems. The use of a full 3D model to simulate a whole river is not possible as this the modelling of vanes requires a too small grid. At this moment the calculation of bottom vanes is only acceptable for research purpose on one or a few bottom vanes.

However, by studying these models, it might be possible to find an improved method to describe bottom vanes in a 2D morphological model, and to include the effects of scour holes. Another possibility is to nest a full 3D vane model into a larger model. For the research on bottom vanes it is certainly advisable to set-up a 3D model including local scour and sediment transport (like Figure 8.6) to investigate the near-vane flow and the influence of a movable bed in the near-vane area on the affectivity of a vane. The experiments described in this report can be used to validate such a model.

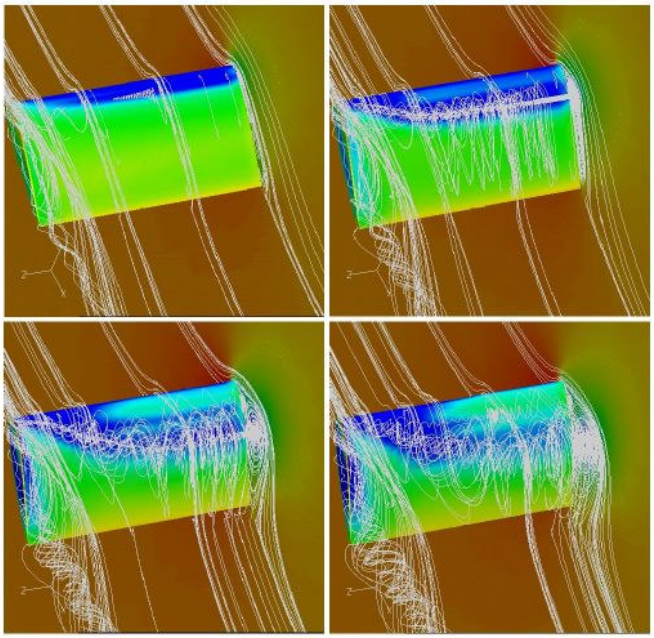

Airfoils at an angle of attack of resp. 13, 20, 25 and 28 degree angle of attack.

The right end of the foil is detached to a fixed wall and the left end is the free surface. The gray lines indicate stream traces. The colored surface indicates the surface pressure.

From the left end of the foil the wing tip vortex develops. The figure series shows the airflow around the airfoils for increasing angle of attack. In the second figure, first flow separation can be observed and in the last figure, the airfoil is seriously stalling. Nevertheless, the wing tip vortex is still present.

Figure 8.4: CFD calculation of airfoils [Spentzos et. al., 2003]

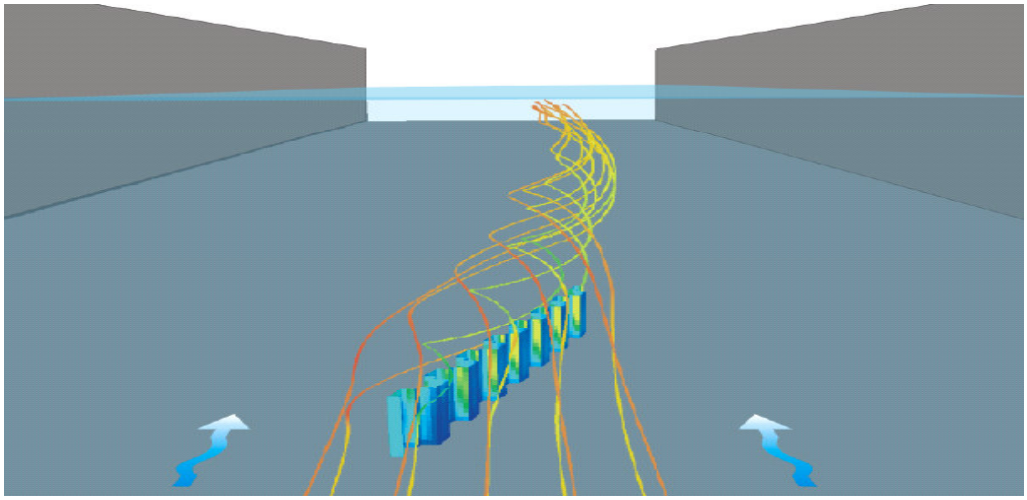

Figure 8.5: CFX calculation of bottom vane

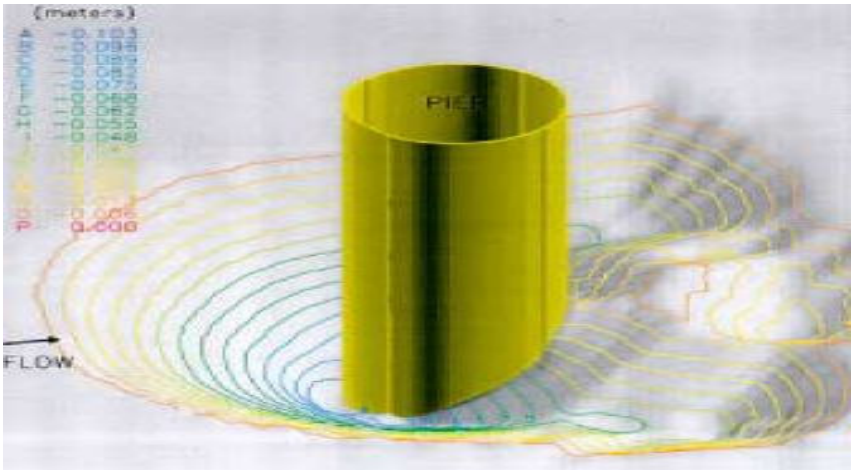

Figure 8.6: Local scour simulation CCHE3D model [http://hydra.cche.olemiss.edu/cche3d]

9 Conclusions

To obtain more insight in the morphological processes caused by bottom vanes a series of movable bed experiments was executed. In most bottom vane research so far, a fixed-bed was used. Seven vane geometries with both low and high angle of attack were tested in a movable bed model. Despite the reduced accuracy due to the possibilities of a model in a developing country, the obtained dataset provides useful insight.

The morphological behaviour has been investigated based on a theoretical analysis and was consequently tested on the experimental data. It was investigated whether current mathematical modelling options are capable of reproducing the results of the experiments.

9.1 Morphological behaviour of a single vane

Four processes were identified and analysed on their influence on the morphology. Per process the conclusions are ordered. The conclusions on the influence of the angle of attack and the vane height are also mentioned.

- Vane-induced spiral flow
  - A vane-induced spiral flow was present in all experiments;
  - The initial vortex strength increases with the angle of attack and vane height. Consequently, the effects on morphology increase also with increasing angle of attack or increasing vane height;

- Vortex growth and development
  - The main vortex resulting from the vane (according to Odgaard a wing tip vortex) has its maximum intensity directly downstream of the vane. The core of the vortex is located, as shown in previous research, on $0.8H_v$. The influence on the morphology, however, is not necessarily maximum at that point as the vortex grows in downstream direction until the bed and/or the water level bounds it. Therefore the maximum influence of the vortex on the bed morphology transport is situated further downstream as the vane height increases;
  - The vortex influenced width in the experiments varied from twice the water depth for low angles of attack to four times the water depth for high angles of attack;

- Influenced longitudinal transport
  - The near-bed longitudinal flow velocity is influenced by the spiral flow. Due to downward directed flow on the lee side of the vane, longitudinal flow from the higher part of the velocity vertical with a relatively large velocity is transported towards the bed causing an increase of the near-bed flow velocity, whilst on the pressure side the opposite happens. As the relation sediment transport - flow is not linear; the increase of transport is larger than the decrease. Note that the effect only persists if the vertical flow keeps supplying momentum towards the near-bed flow, as the bed shear stress causes the vertical velocity profile to adapt to the equilibrium logarithmic profile;
  - The angle of attack influences the vortex intensity. With increasing intensity, the vertical flow velocities that cause the changes in the vertical longitudinal velocity profile also increase. So, the increase in longitudinal transport also increases with the angle of attack;
  - The vane height does not influence the process itself, but has an indirect influence: as the vortex core is located higher above the bed, the maximum vertical velocities that are responsible for the downward transport of longitudinal impulse are also higher in the vertical. This means that the increase of near-bed longitudinal velocity becomes smaller;

- Horseshoe vortex
  - On the pressure side of the vane a horseshoe vortex can develop. This horseshoe vortex is mainly responsible for the local scour around a vane. The critical angle of attack for initiating the scour process caused by this vortex is about 20 degrees, depending on the vane height;
  - The vortex is guided along the vane, and leaves the vane at the trailing edge. The strength of this vortex can be significant but reduces quickly downstream of the vane. For experiment A4 the influence is noticeable up to 5 times the vane length (equals 7 times the water depth). From the experiments it is estimated that a horseshoe vortex can start developing for a vane height larger than 0.4 d or an angle of attack larger than 20 degrees;
  - For the experiments with angles of attack of ten or twenty degrees, the location of maximum scour is situated near the leading edge of the vane. For the experiments with angles of attack of thirty and forty degree angle of attack the location of maximum scour is situated near the trailing edge of the vane;
  - The depth of the scour hole varies from almost zero for experiment A1 and B2 to 0.7 times the average water depth for experiment A4. The vane height is important for the final depth of the scour hole. For the three experiments at an angle of attack of twenty degrees, the vane with 0.2 H_v / d no significant scour was reported, but for the vane with 0.6 H_v / d the scour extended to almost 0.5 d;
  - The sediment eroded by the horseshoe vortex is transported along the vane, and deposited in a bar downstream of the vane. Probably, the supplied sediment is also transported by the main vortex as the horseshoe vortex meets the main vortex at the trailing edge of the

vane. The strong upward flow of main vortex can take sediments up in the vertical (especially the fine sediments);

- Resulting morphological behaviour:
  - The morphological behaviour of a single bottom vane can be accounted for by two processes. For both low and high angle of attack these are: the vane-induced spiral flow causing transverse bed sediment transport and increased longitudinal sediment transport;
  - For small angles of attack the transverse transport of sediment is the most important process. The bed level changes are (almost) symmetrical, and no longitudinal bed slope develops;
  - For higher angles of attack the combination of the two mentioned processes results in an asymmetric bed profile. The erosion channel is deeper than the sedimentation pattern. Most likely this asymmetrical profile disappears further downstream as the effect on the near-bed longitudinal flow velocities damp out quicker that the main vortex. The results of experiment B3 indicate this;
  - The increase of longitudinal transport causes an average longitudinal bed slope as eroded sediment from the lee side is transported in downstream direction. The lowest point is located at the scour hole and the bed level runs up to a maximum at about 7 to 10 vane length downstream of the vane;

9.2 Water level set up

- The measurements in the scale model are not accurate enough to determine the water level set up caused by the tested bottom vanes;
- Despite the uncertainties in the measurements, the average water level difference between the upstream and the downstream measuring location is between 3.0 and 4.4 mm for all experiments. The deviations from the average slope at the vane location are always positive (set up) and between 0.3 and 1.1 mm;

9.3 Mathematical modelling

In the Delft3D-MOR bottom vane model two modelling options are implemented. The type 1 model consist of a sub grid mathematical model that calculates the effect of a bottom vane on the downstream grid cells by means of a change in the depth averaged sediment transport direction. A type 2 vane model consists of submerged weirs on grid cell boundaries. So, in contrast to a type 1 model, a type 2 vane is noticeable in the flow calculation. For a type 1 model the effect of the vane is artificially calculated, whilst for a type 2 model it follows from the changed flow field. In the end only simulations have been made for vanes at high angle of attack.

- Type 1 vane model
  - The influence of initial vortex strength and vortex line model was investigated. It appeared possible to increase the effect of the bottom vane by increasing the initial vortex strength coefficient. It was also concluded that vortex-line option 4 resulted in a asymmetrical bed level change as observed in the result of the high angle of attack experiments;

  - The type 1 bottom vane model was used for simulations for vanes at high angles of attack by increasing the initial vortex strength calibration coefficient to a value of 2 and by choosing vortex-line model 4;
  - The results of the simulations were not in good agreement with the experiments. This is mainly due to the fact that not all physical processes are included in the model;
  - The type 1 vane modelling appeared not to be capable of predicting the bed level changes for a single vane very well. However, there is no reason to believe that the simplified approach is not useful to calculate the effect of a bottom vane field in a large river system. For small angles of attack and relatively low vanes scour is absent and the effect of vanes can be described with the simple model as shown in other research;

- Type 2 vane model
  - The type 2 description appeared not to be capable of reproducing the result from the experiments. The physical processes are not modelled and therefore the result do not show any similarity with the experimental results
  - The model is unsuitable to generate the effect of vanes at high angles of attack as the vane-induced vortex is not included. For the current application, the modelling of a single vane, this resulted in the vane having zero effect on a larger scale as the presence of the vane has only local effects on the flow field;
  - The local effects of the type 2 bottom vane model did not correspond to the observed changes in the model. Where the model predicted sedimentation in front of the vane, the experiment clearly showed a large scour hole;

- Future possibilities:
  - The capabilities of three-dimensional flow models are increasing rapidly and are (almost) capable of handling sediment transport. These models can be used to further investigate the behaviour of vanes;
  - For calculating the flow around bottom vanes sufficiently accurately a very fine grid is needed. This makes application of such calculations in a river model highly unattractive as computational times will be huge (even for nested models);

10 Recommendations

This research has resulted in more insight in the physical processes that cause the morphological effect of bottom vanes. The results from the mathematical model simulations did not match the experimental results well. More research is always desirable, but in this case the research is truly going on in Bangladesh, which makes a further increase on the knowledge on bottom vanes feasible.

10.1 Morphology

- Experimental research:
  - For future experiments more time should be reserved to execute the experiments in order to be sure an equilibrium state is reached. This makes it possible to derive quantitative relations for the morphological processes. At the moment this is impossible as the time-stage of the developments are not known;
  - It is advised to execute a moulded bed experiment (preformed fixed-bed) for a few vane configurations. In a fixed-bed the flow velocities can be measured more accurately and the effect of the scour hole can be quantified by comparing to flat fixed-bed measurements (measurement data available at WL|Delft hydraulics);
  - In the period July – October 2003 researchers at BUET continued the experiments for 13 more configurations varying for 10/20/30 and 40-degree angle of attack and vane heights 0.06/0.09/0.12 and 0.18 m. It is recommended to collect these data and verify the conclusions and findings of this report;

10.2 Water level set up

- Research:
  - A 3D model with free-surface flow might help to get more insight in the water level set up caused by a submerged vane;
  - In the same model also the influence of the scour hole on the water level set up can be investigated by comparing the results for a flat and a non-flat bottom

10.3 Modelling bottom vanes

- As a first approach for high angles of attack, the initial vortex strength can be manually raised in the type 1 vane model. As in reality the vortex is still present for high angles of attack, and the intensity can still be reasonably predicted with the implemented vane models, it is advised to not switch of vanes in the mathematical model when the angle of attack exceeds 22 degrees;
- To improve the type 1 vane model for high angles of attack the increased longitudinal transport can be added in the vane type 1 model;
- With aid of the results of more experimental data and eventual 3D simulations, an effort can be made to formulate a more satisfying vane model that also takes scour and other detailed effects into account;
- It is not advised to add a vortex line model to the type 2 vane model. The type 2 vane model can be used in the soon to be released Delft3D model that can handle non-hydrostatic pressure and the free surface for 3D flow. By applying this model together with a fine grid, the type 2 vane description can be tested again, but now for full 3D flow. It is expected that the results will match reality much better that the 2D approach. This Delft3D will probably also be capable of handling sediment transport for 3D flow so can provide a sound base for vane modelling;
- As the possibilities of 3D modelling have increased and have made it (almost) possible to make reliable simulations with sediment transport, it is advised to make these calculations for several vane configurations and investigate the complex flow and sediment transport mechanisms to better understand what happens around a vane;
- It is expected that a new version of Delft3D that can calculate 3D flow without neglecting the vertical accelerations will be released soon.

Literature

Breusers, H.N.C. and Raudkivi, A.J., 1999,
Scouring, Balkema, Rotterdam.
Colombini, M., Seminara, G. and Tubino M., 1987,
Finite-amplitude alternate bars. Journal of Fluid Mechanics, Vol.181, pp.213-232.
Flokstra, C., de Groot, F. and Struiksma, N., 1998a,
Optimaliseren lengte bodemschermen; Deel 1: Krachtmetingen, WL|Delft Hydraulics, report Q2418. (in dutch)
Flokstra, C., de Groot, F. and Struiksma, N., 1998b,
Optimaliseren lengte bodemschermen; Deel 2: Stroomsnelheidsmetingen, WL|Delft Hydraulics, report Q2418. (in dutch)
Flokstra, C., Jagers, H.R.A. , Wiersma, F.E., Mosselman, E., Jongeling, T.H.G., 2003,
Numerical modelling of vanes and screens, development of vanes and screens in Delft3D-MOR, Delft Cluster Report, DC1-331-3.
Filarski, R., 1966,
Oriënterende proeven oppervlakte schermen, Rapport M777, Waterloopkundig Laboratorium. (in dutch)
Joglekar, D.V., 1971,
Manual on river behaviour control and training, Central Board of Irrigation and Power, Publ. No.60 (revised), New Delhi.
Jongeling, T.H.G. and Flokstra, C., 2001,
Bodemschermen: Stromingskrachten en snelheidsveld bij variatie van de schermhoogte, Delft Cluster Report (in dutch), WL|Delft Hydraulics report Q2677/Q2849.
Lamb, H., 1932,
Hydrodynamics, sixth edition, Cambridge University Press, Cambridge U.K.
Marelius, F. and Sinha, S.K. , 1998,
Experimental investigation of flow past submerged vanes, Journal of Hydraulic Research, IAHR, Vol. 38, No. 1, pp. 65-71.
Mosselman, E. and Wang, Z.B., 1994,
Onderzoek Watersnood Maas; Deelrapport 6: Morfologische aspecten. WL | Delft Hydraulics. (in dutch)
Odgaard, A.J., 1986,
Meander flow model, I: Development, Journal of Hydraulic Engineering, ACSE, Vol. 112, No. 12, pp. 1117-1136.
Odgaard, A.J. and Spoljaric, A., 1986,
Sediment control by submerged vanes, Journal of Hydraulic Engineering, ACSE, Vol. 112, No. 12.
Odgaard, A.J. and Wang, Y., 1991a,
Sediment management with submerged vanes, I: Theory, Journal of Hydraulic Engineering, ACSE, Vol. 117, No. 3, pp. 267-283.
Odgaard, A.J. and Wang, Y., 1991b,
Sediment management with submerged vanes, II: Applications, Journal of Hydraulic Engineering, ACSE, Vol. 117, No. 3, pp. 284-302.

Pauley, W.R. and Eaton, J.K., 1987,
Experiments on the development of longitudinal vortex pairs in a turbulent boundary layer, AIAA Journal, nr. 26(7), pp. 816-823.
Potapov, M.V., 1950,
Regulation of water streams by method of artificial transverse circulation, complete works, Vol. 2, Part 3, pp. 101-onwards, Abbreviated abstracts in translation from Russian by R. Batalin.
Remillieux, M., 1972,
Development of bottom panels in river training, Journal Waterways, Harbours and Coastal Eng. Div., ASCE, Vol. 98, No. WW2, pp. 151-162.
Sinha, S.K. and Marelius, F., 2000,
Analysis of flow past submerged vanes, Journal of Hydraulic Research, IAHR, Vol. 38, No. 1, pp. 65-71.
Spentzos, A., G. Barakos, K. Badcock and S. Schreck., 2003,
CFD Investigation of 2D and 3D dynamic stall, international symposium on integrating CFD and experiments, sept 2003, University of Glasgow. http://www.aero.gla.ac.uk/integration/abstracts/spentzos.pdf
Struiksma, N. and Crosato, A., 1989,
Analysis of a 2-D bed topography model for rivers, in River Meandering, S. Ideka and G. Parker (Eds), Water Resources Monograph, p. 153-180.
Struiksma, N. and de Groot, F., 1996,
Waalbocht Hulhuizen, schermonderzoek in de zandgoot, WL|Delft Hydraulics, report Q2264. (in dutch)
Vriend, H.J. de, Wang, Z.B. and Havinga, H., 2001,
Riverdynamics, Hand-outs CTwa5311, TU Delft, Faculty Civil Engineering and Geosciences.
Wang, Y., 1991,
Sediment control with submerged vanes, thesis presented to University of Iowa in partial fulfilment of the requirements for the degree of Doctor of Philosophy.
Wang, Y and Odgaard, A.J., 1993,
Flow control with vorticity, Journal of Hydraulic Research, Vol. 31, No. 4.
Zijlstra, R and Zwol, J.A. van, 2003,
Measuring report, experimental study of submerged vanes in the outdoor facility at BUET, Delft University of Technology.
Zwol, J.A. van, to be published in 2004,
Working title: "Design aspects of submerged vanes", M.Sc. thesis, Delft University of Technology.

Appendices

A Coordinate system

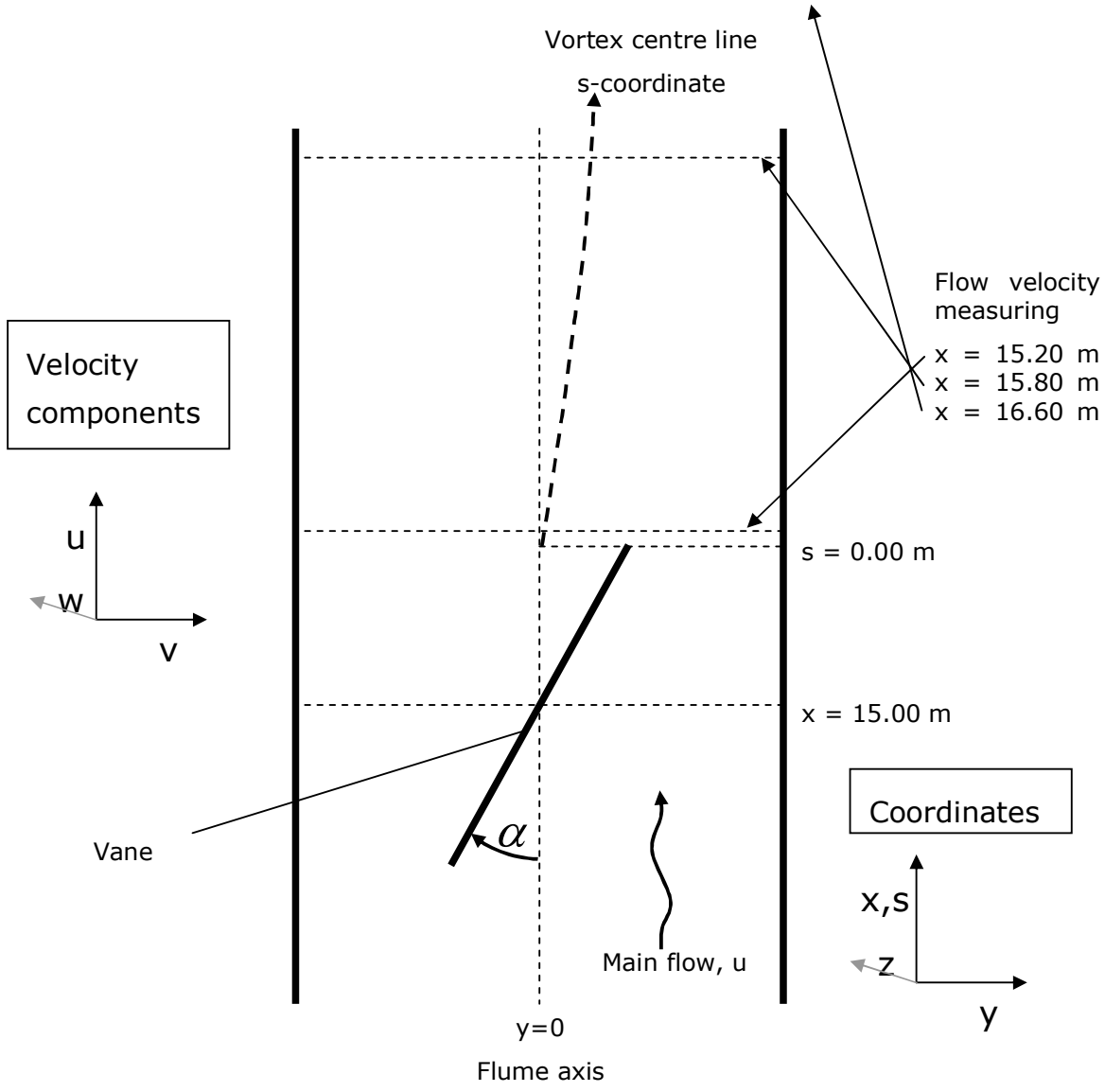

B Longitudinal profiles bed level

Note that the presented longitudinal profile is a width averaged profile.

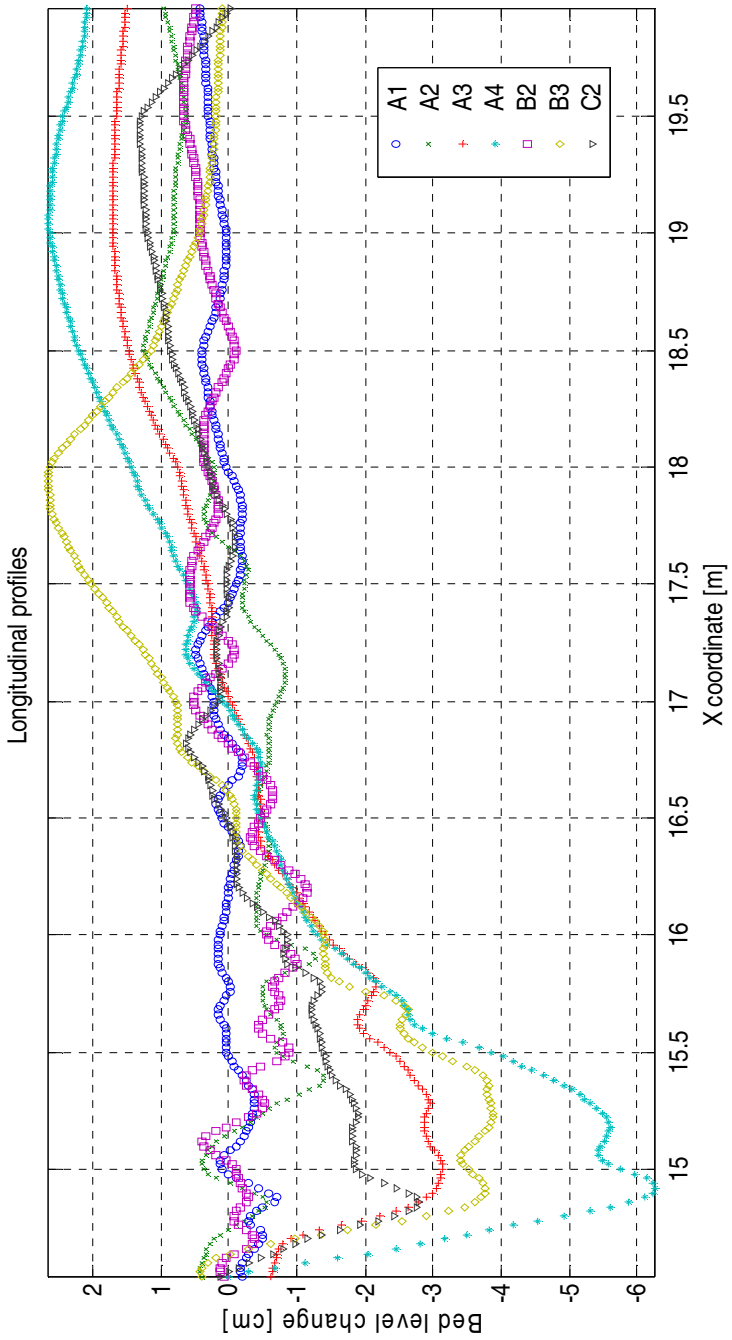

C Bed level contour plots

C.1 Experiment A4

Vane height 12 cm, angle of attack 40 degrees

C.2 Experiment B3

Vane height 6 cm, angle of attack 30 degrees

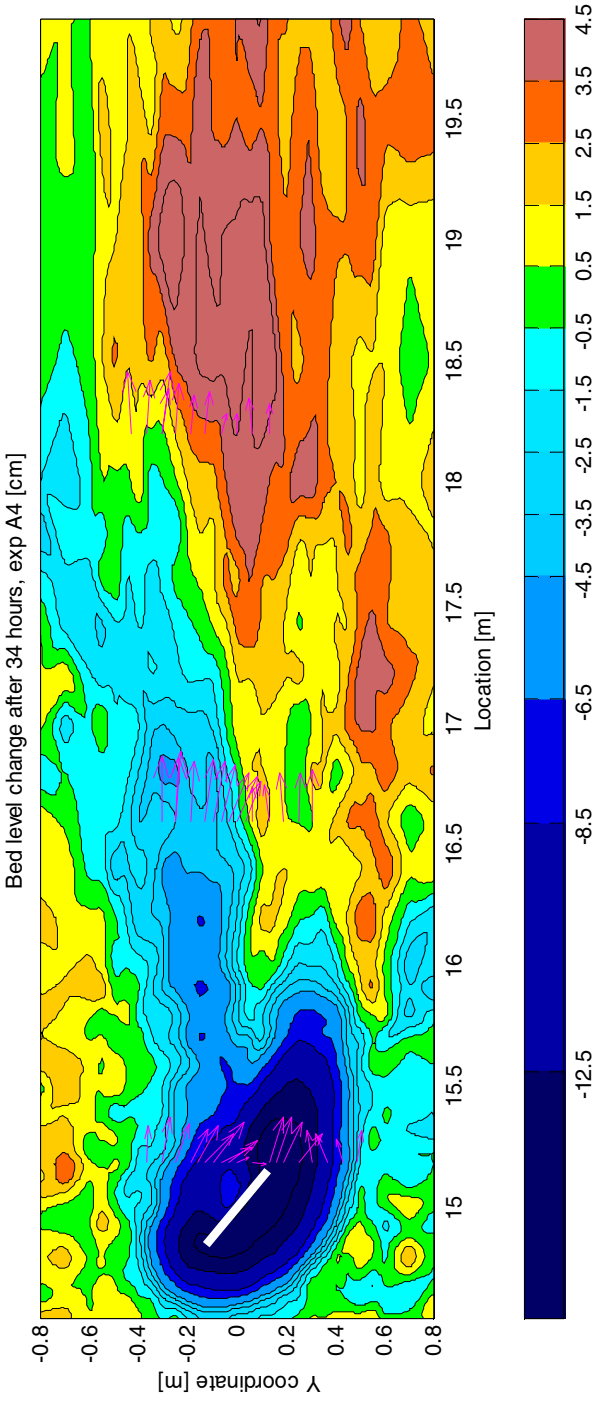

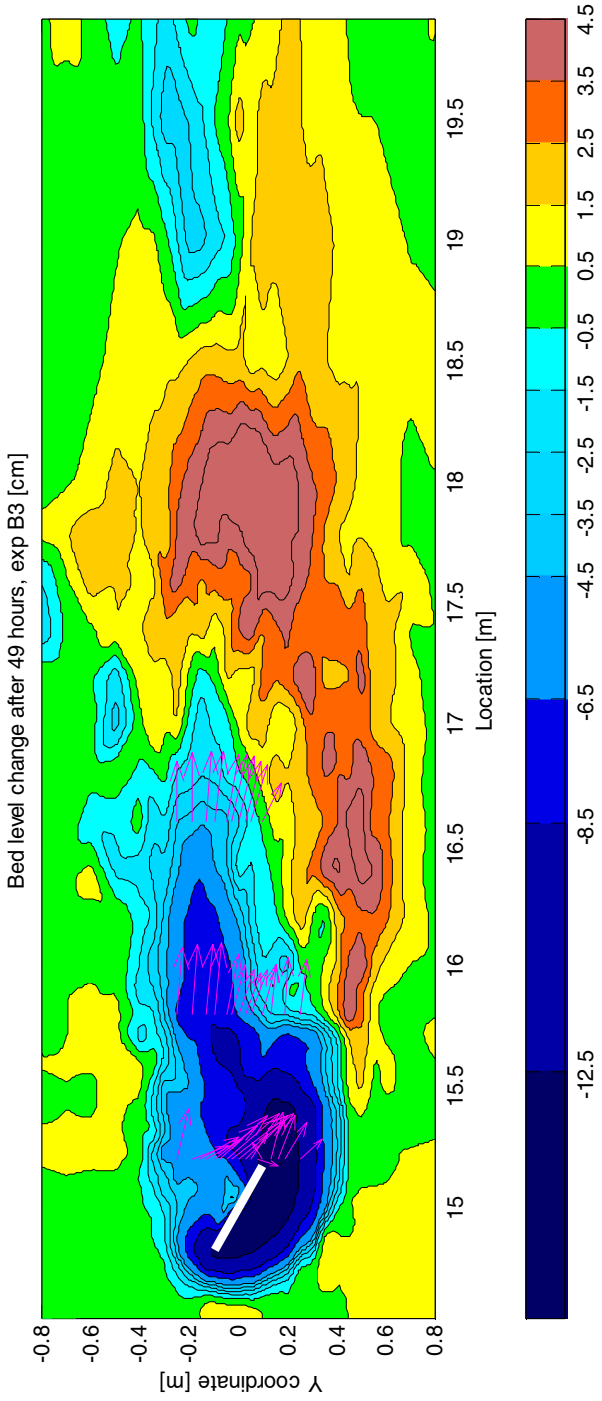

C.3 Experiment A3

Vane height 12 cm, angle of attack 30 degrees

Remark: A3 was the first experiment. The left figure was measured after 8 hours of flow. The right picture, after the experiment had ended (42 hours). However, the measuring density was smaller.

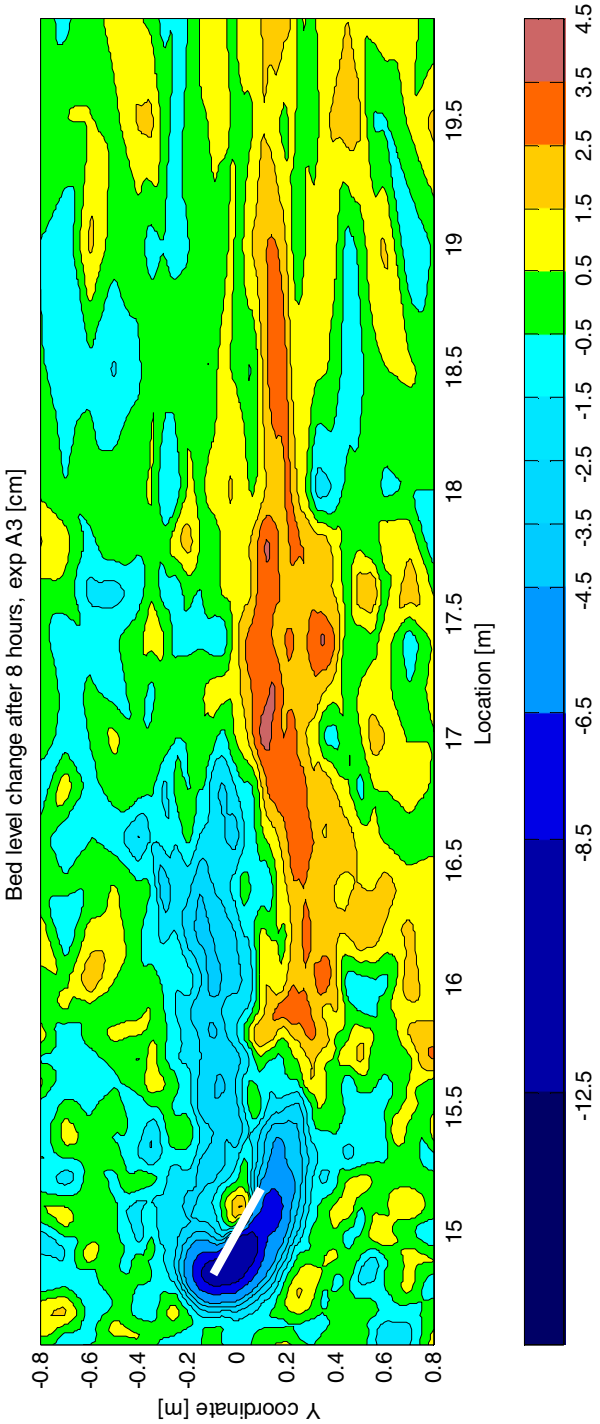

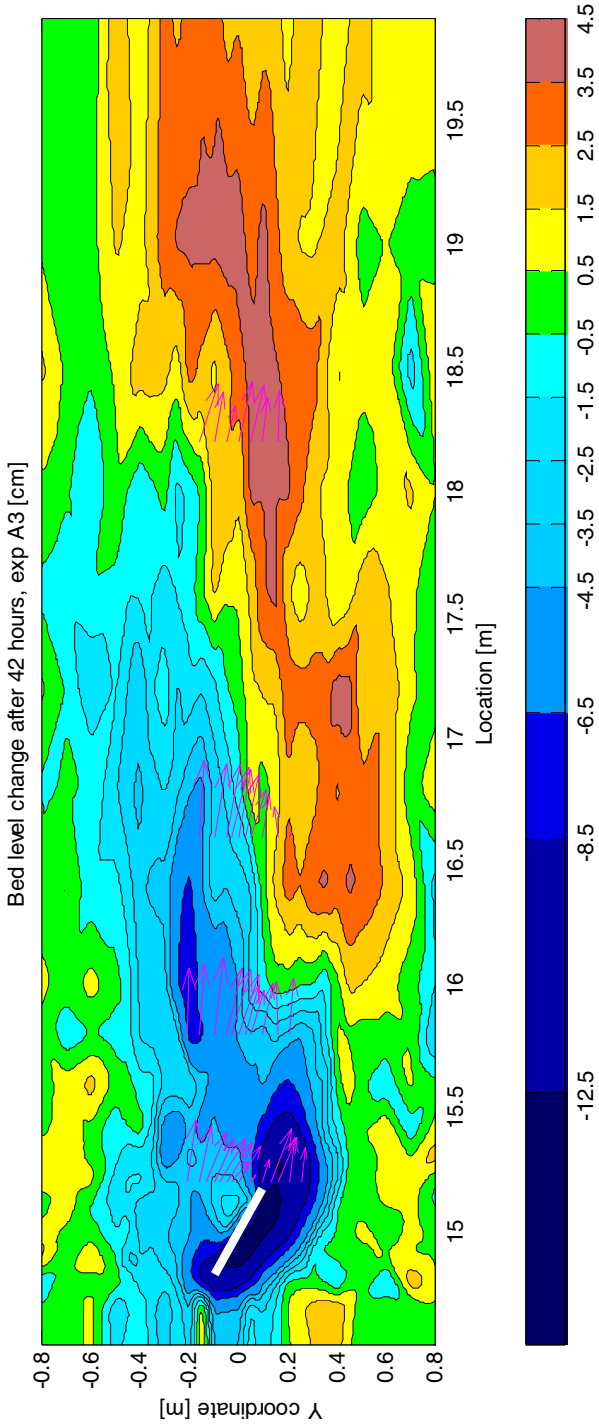

C.4 Experiment A1

Vane height 12 cm, angle of attack 10 degrees

C.5 Experiment A2

Vane height 6 cm, angle of attack 20 degrees

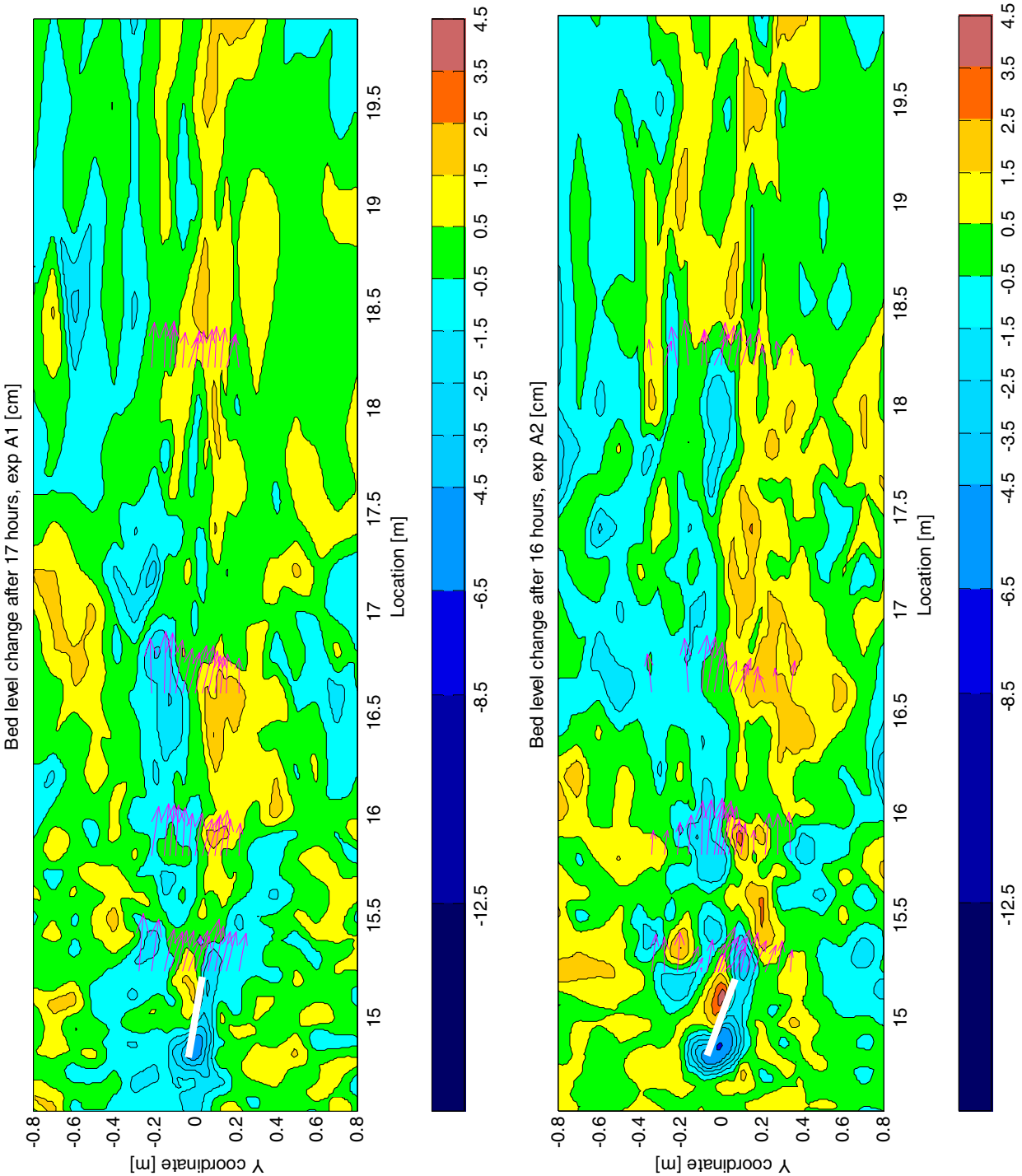

C.6 Experiment B2

Vane height 12 cm, angle of attack 20 degrees

C.7 Experiment C2

Vane height 18 cm, angle of attack 20 degrees

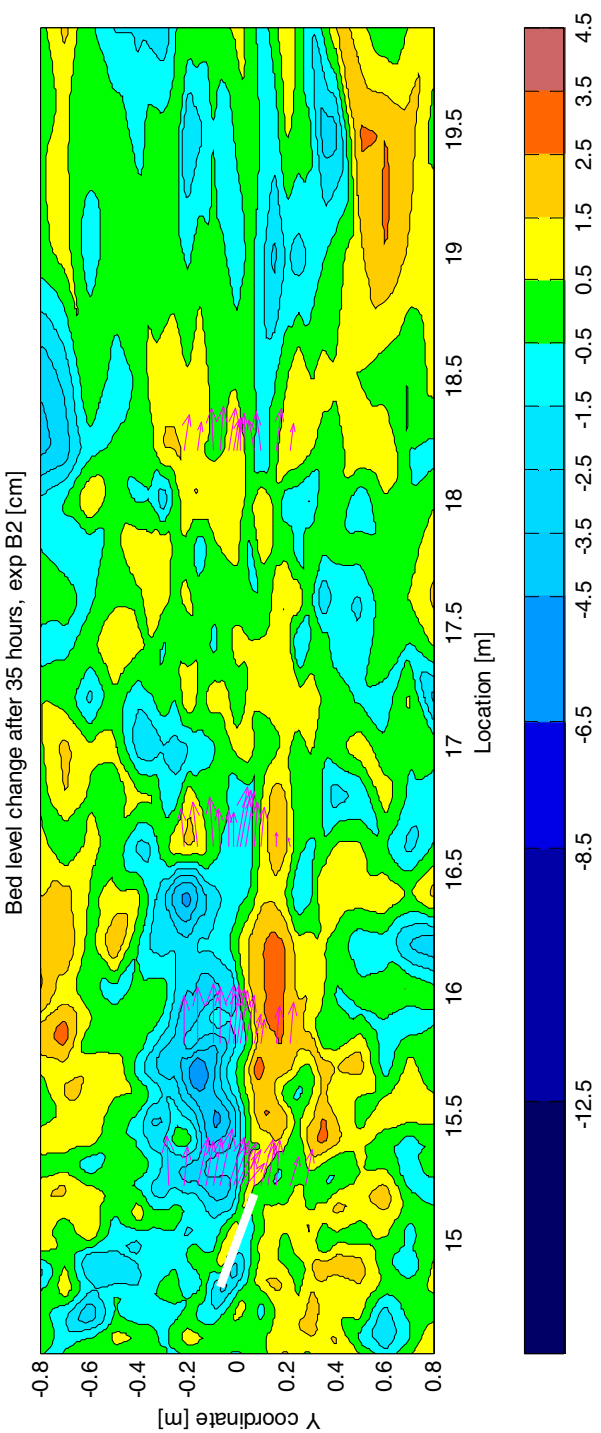

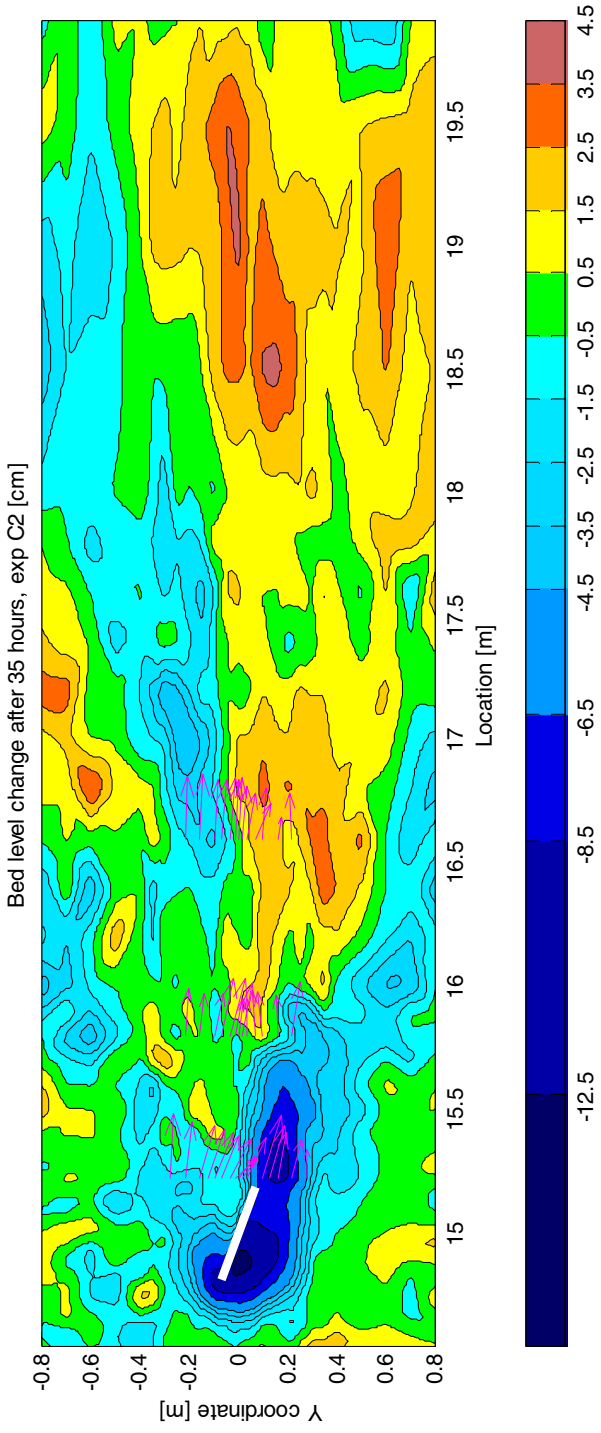

D Cross-sectional bed level plots

D.1 Average x = 14.54 – 19.96 m.

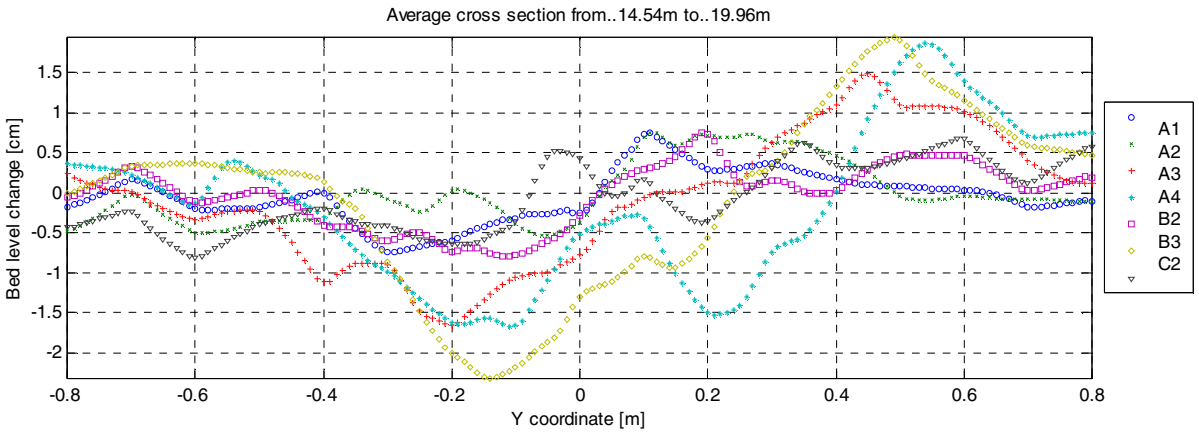

Note: vertical scale times 2 !!

D.2 Average x = 14.80 – 15.20 m.

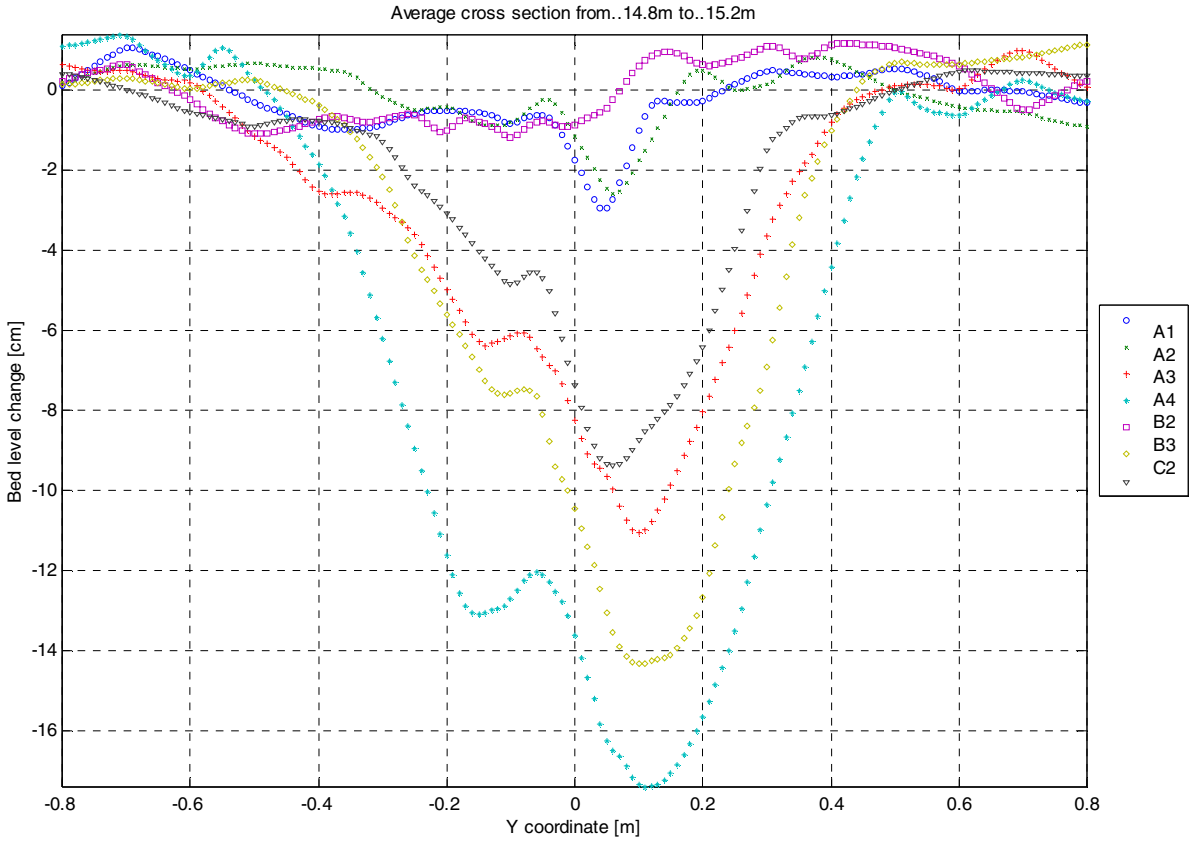

D.3 Average x = 15.20 – 15.60 m.

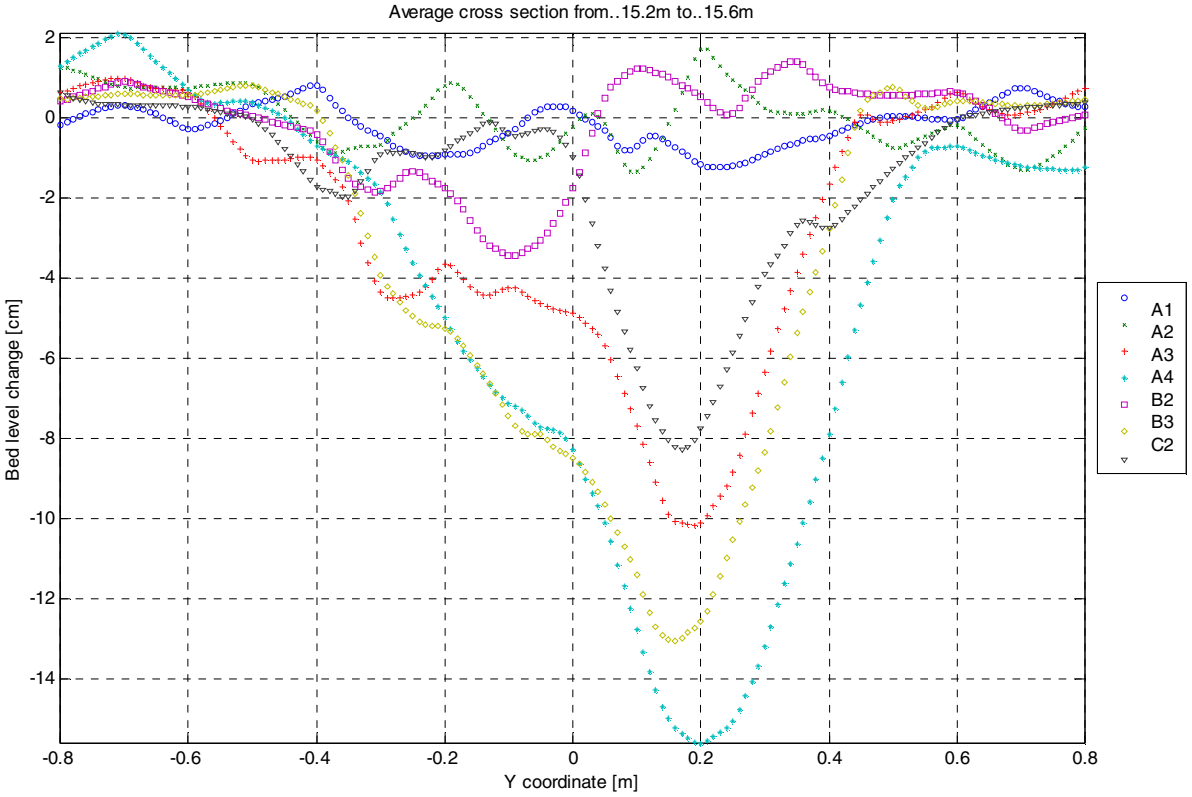

D.4 Average x = 15.60 – 16.20 m.

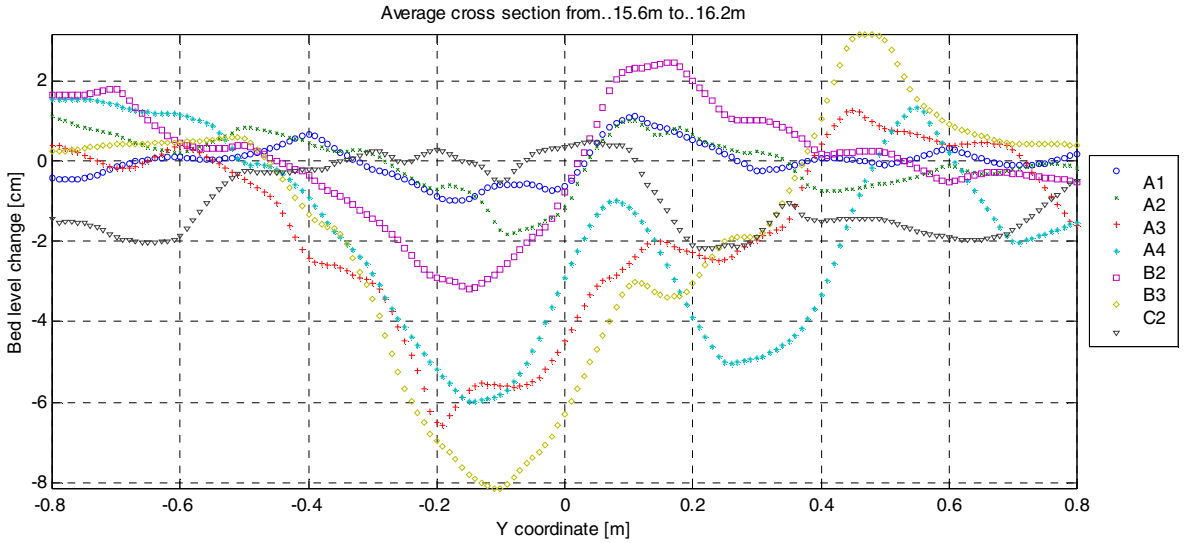

D.5 Average x = 16.20 – 17.20 m.

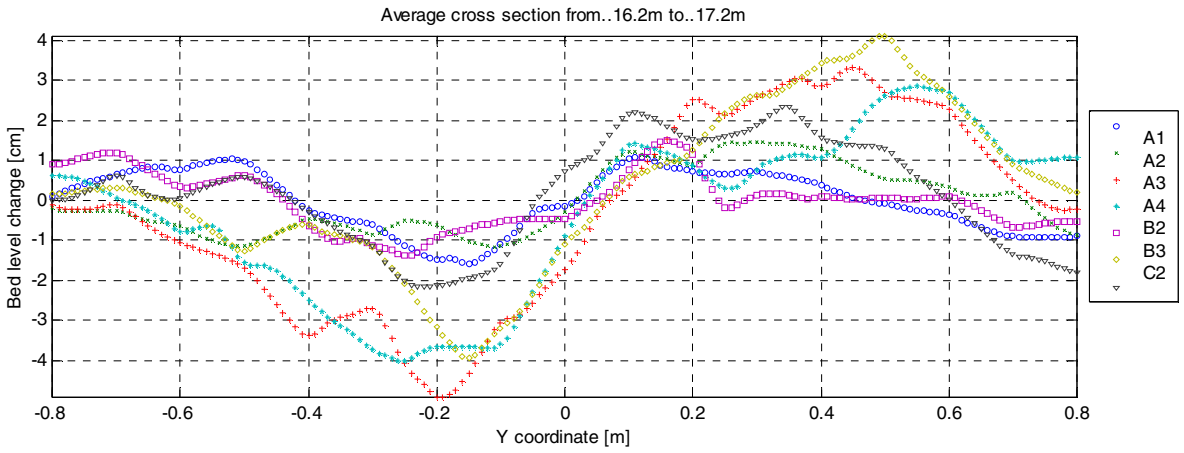

D.6 Average x = 17.20 – 18.50 m.

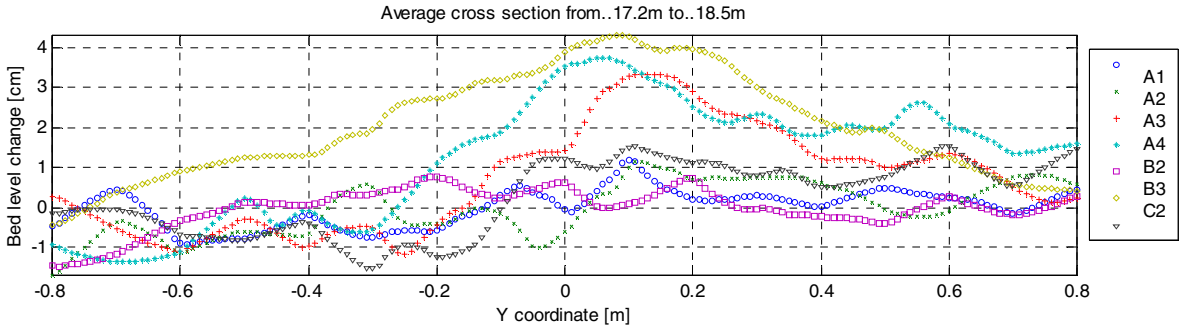

E Experiment A1 and A2 'early' measurements

Like experiment A3, the bed levels of experiment A1 and A2 were both measured already after a few hours of flow (resp. 17 and 16 hours). Like experiment A3 checks were performed on the bed level measurement after the experiment had ended. In the case of exp. A3 it was visually clear that the bed had changed and therefore the measurements were repeated on coarse grid. But for experiment A1 and A3 the changes were not so clear and only a few checks were performed. It was believed that small angles of attack, like 10 and 20 degrees would have reached their equilibrium after 2 days. During analyses, great differences were observed between the result of B2 and A2. Experiment B2 had far greater effect, while the opposite was expected. Taking a better look at the bed level checks of experiment A2 showed the changes of the bed in the period between 16 and 41 hours of flow. Unfortunately, not enough measurements are available to use this data for the analysis of the whole bed. For experiment A1 no measurements behind the vane are available. This appendix shows the measurements for experiment A2 after 41 hours that are available.

E.1 Contour plot experiment A2 after 41 hour

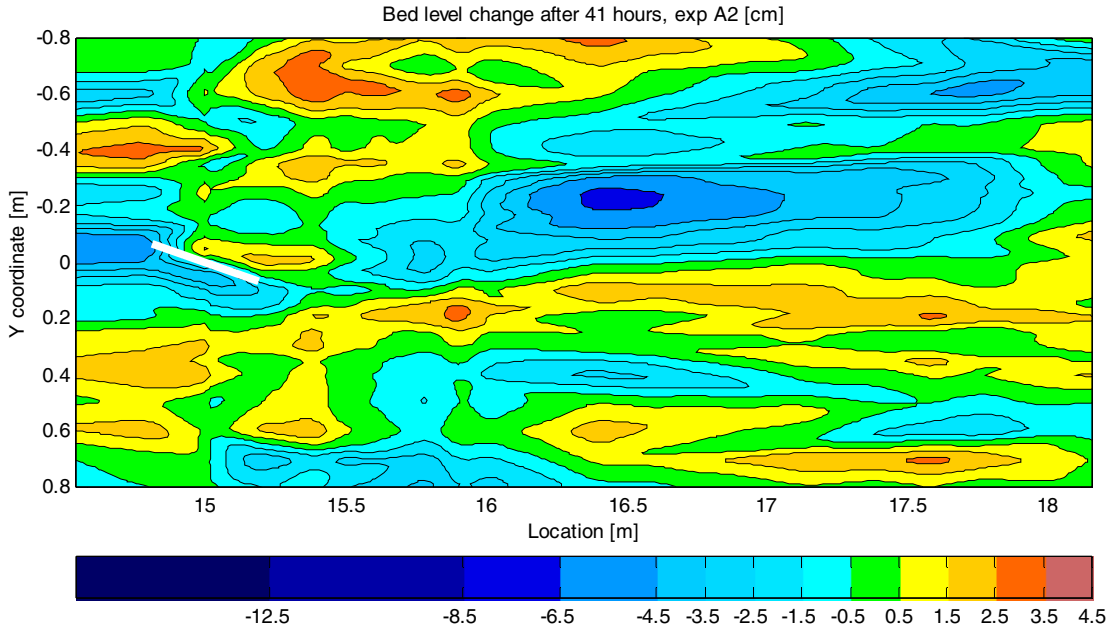

E.2 Comparison cross-sectional plot A2 after 16 and 41 hours of flow

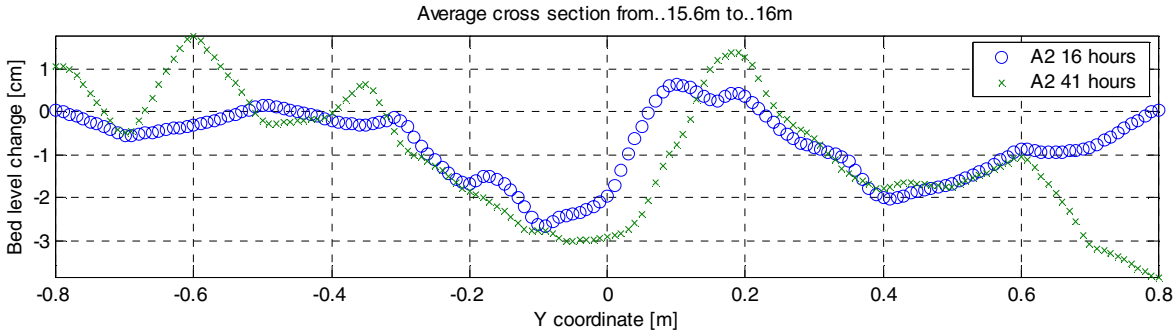

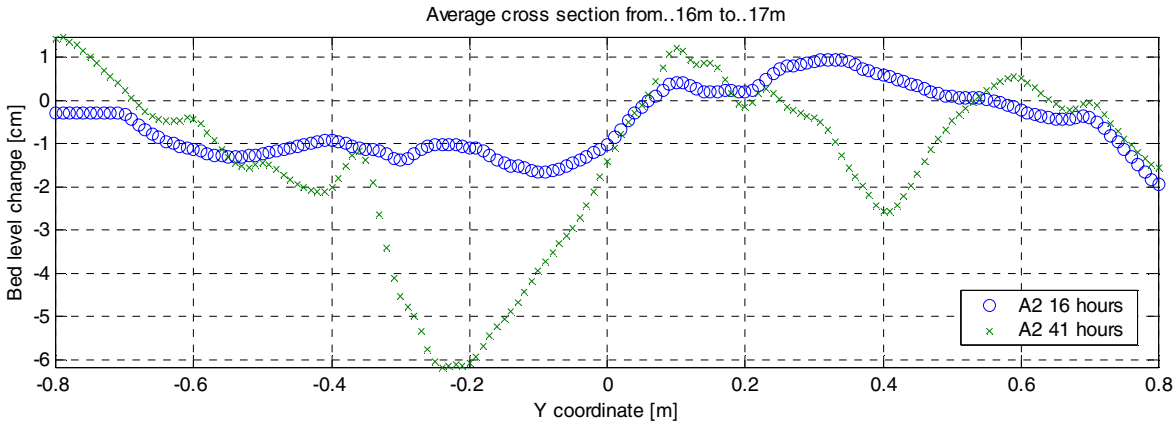

F Bed photographs

F.1 Experiment A3

A ruler with a length of one meter was photographed together with the bed. The vane is in all cases 0.4 meters. Unfortunately for A3 no good picture of the far-field is available as the digital camera was not available at that time yet.

Downstream view

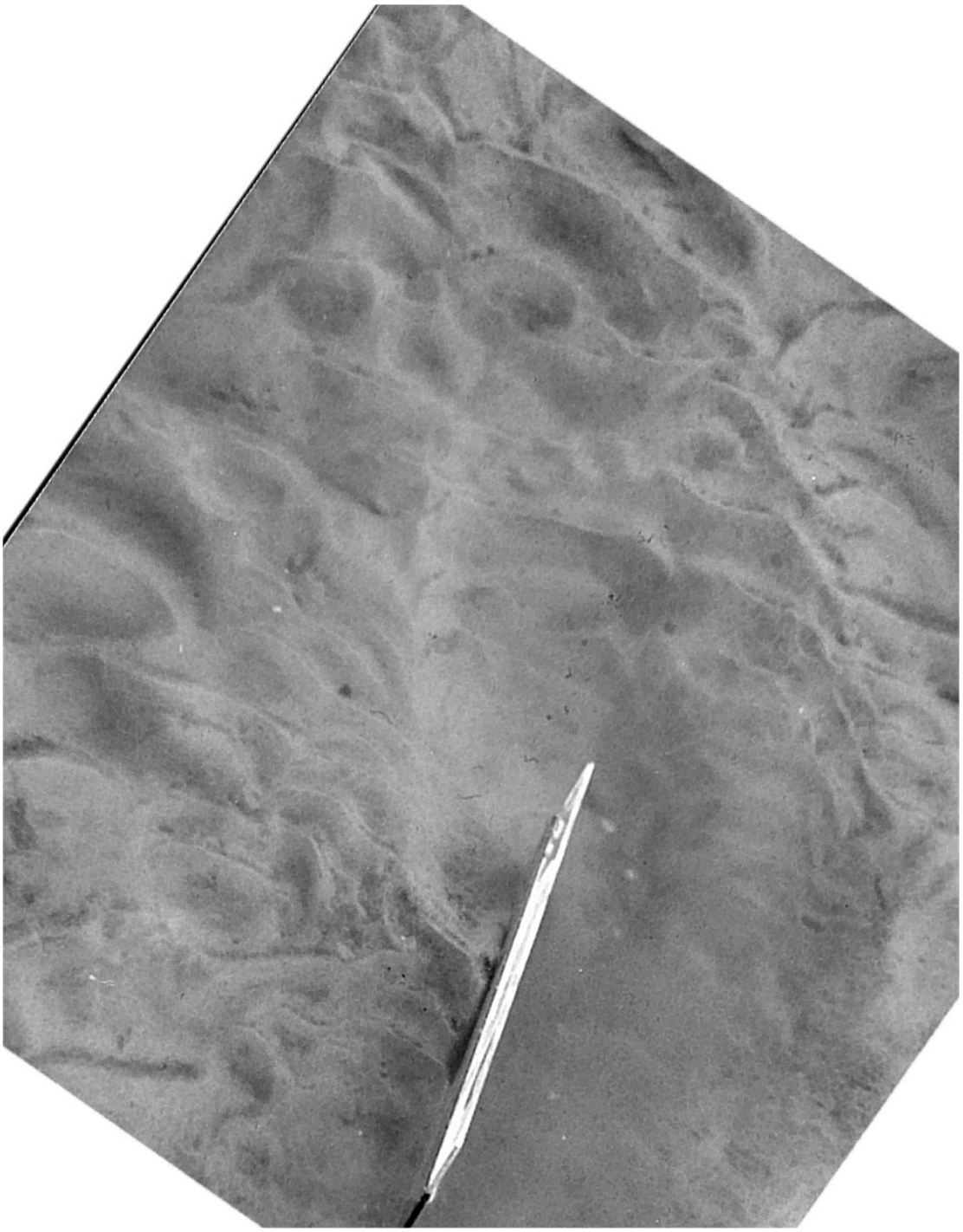

F.2 Experiment A1

Downstream view

F.3 Experiment A4

Downstream view

F.4 Experiment A2

Upstream view

F.5 Experiment B2

Downstream view

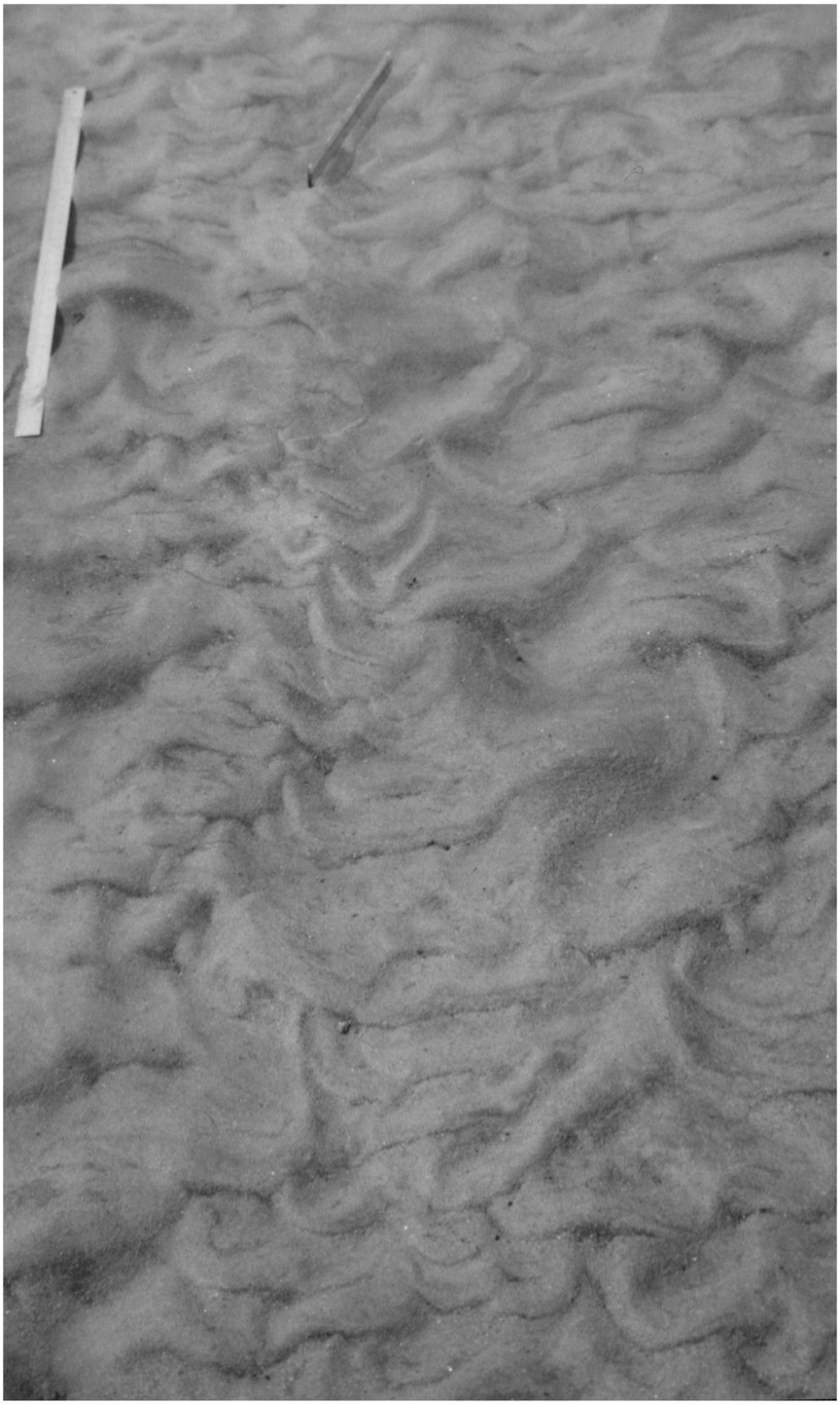

F.6 Experiment C2

Downstream view

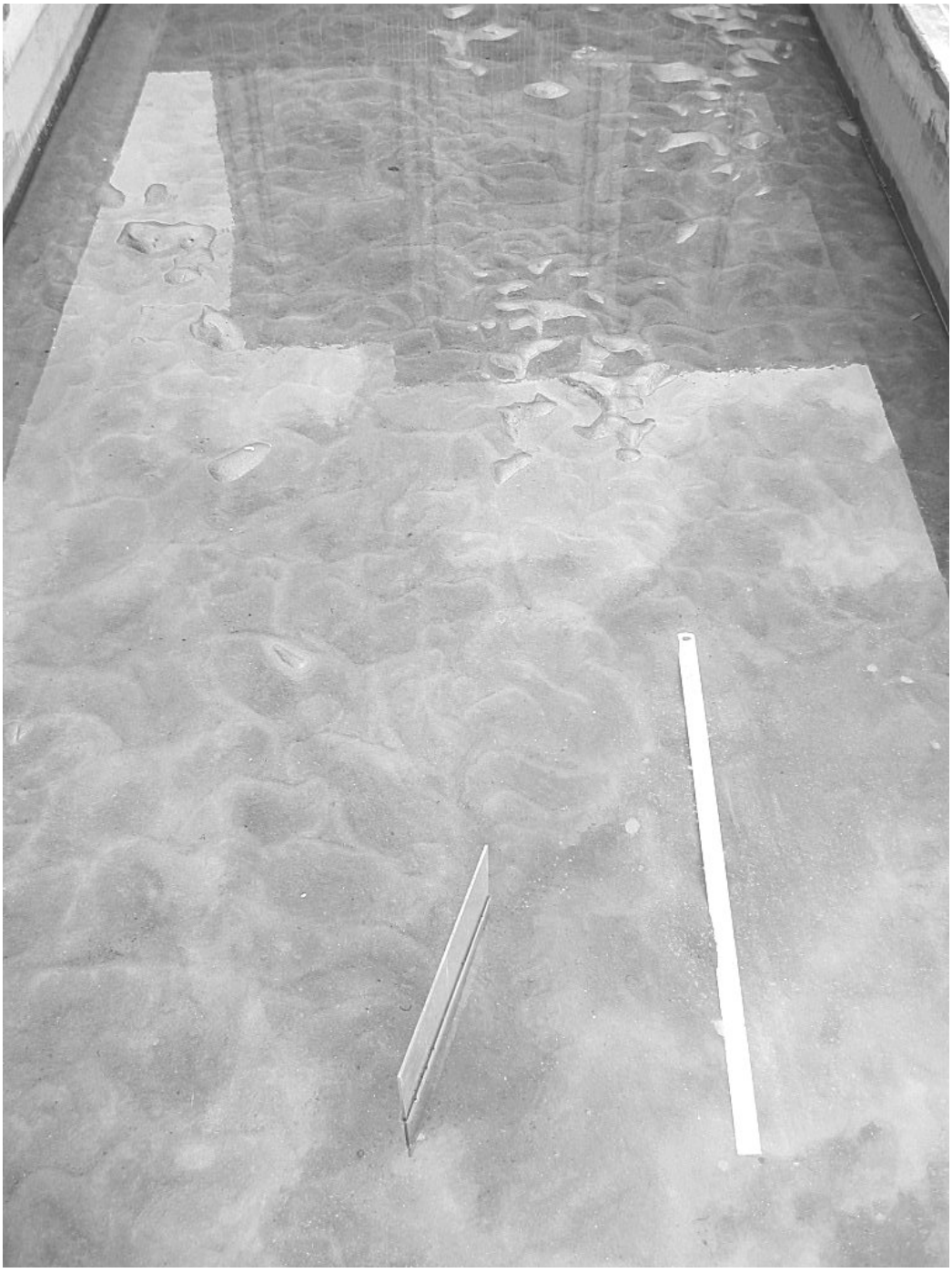

F.7 Experiment B3

Downstream view

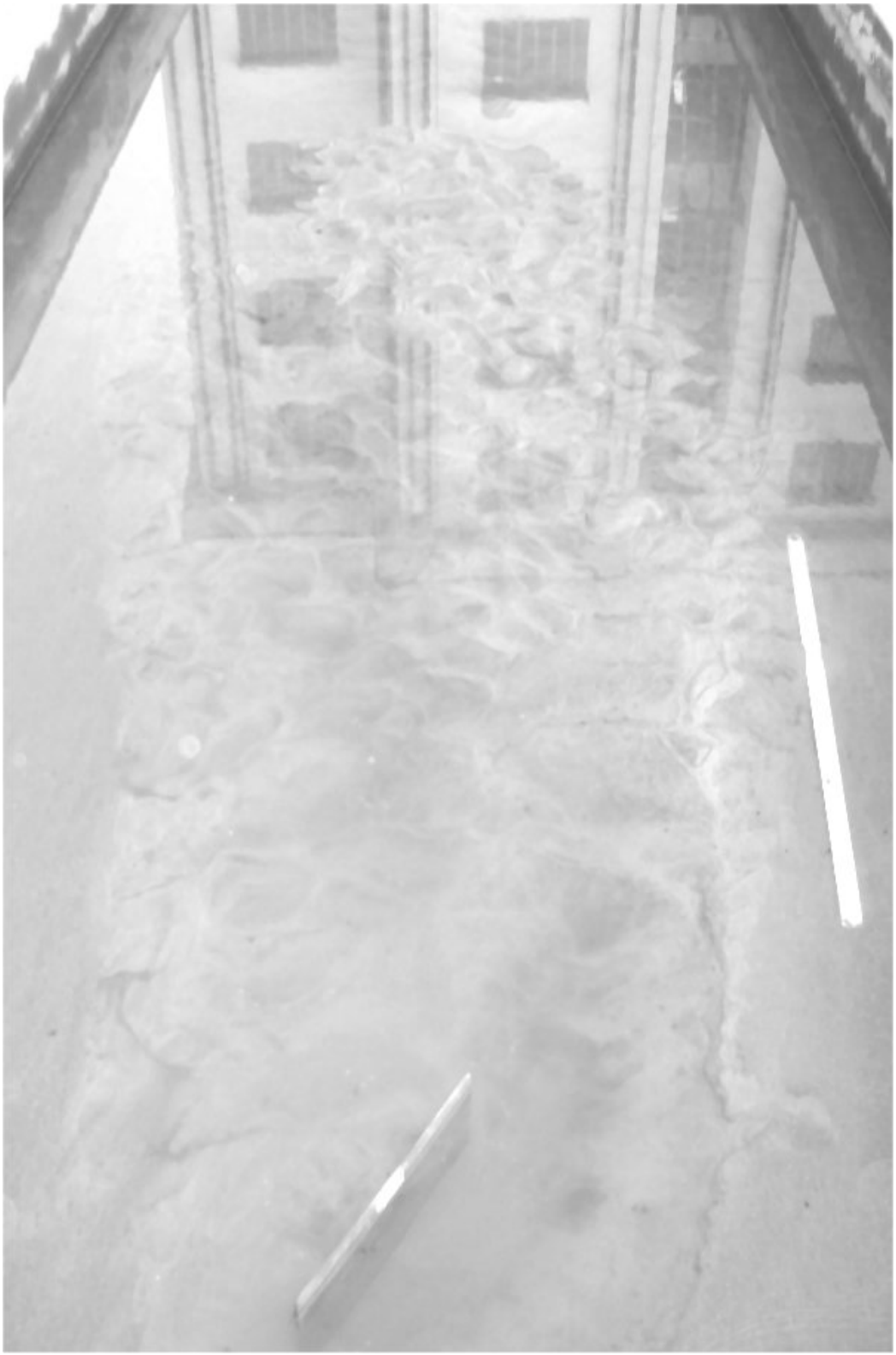

G Transverse flow velocity measurements

G.1 Experiment A3, X=15.20, 15.80 and 16.60 m.

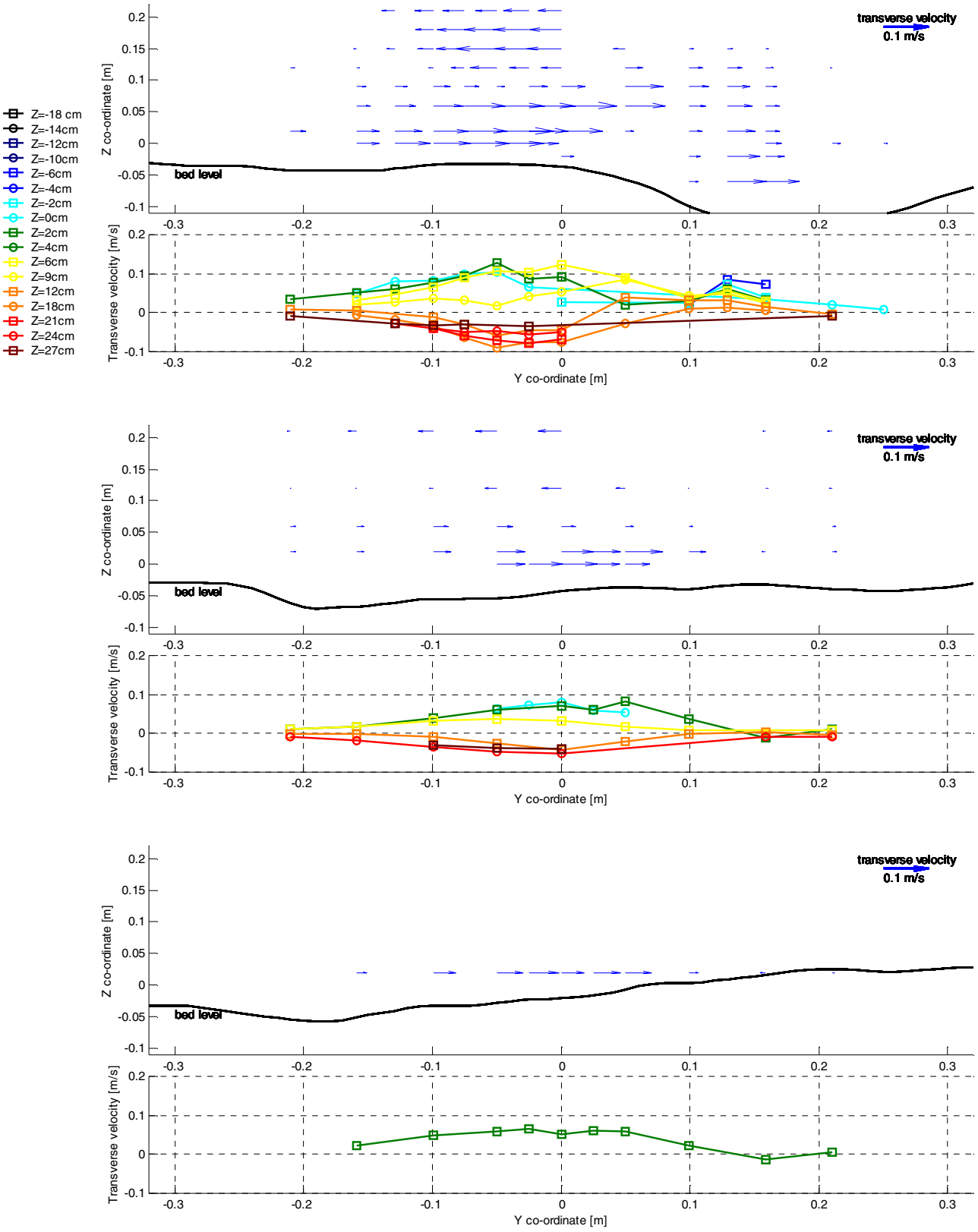

G.2 Experiment A1, X=15.20, 15.80 and 16.60 m.

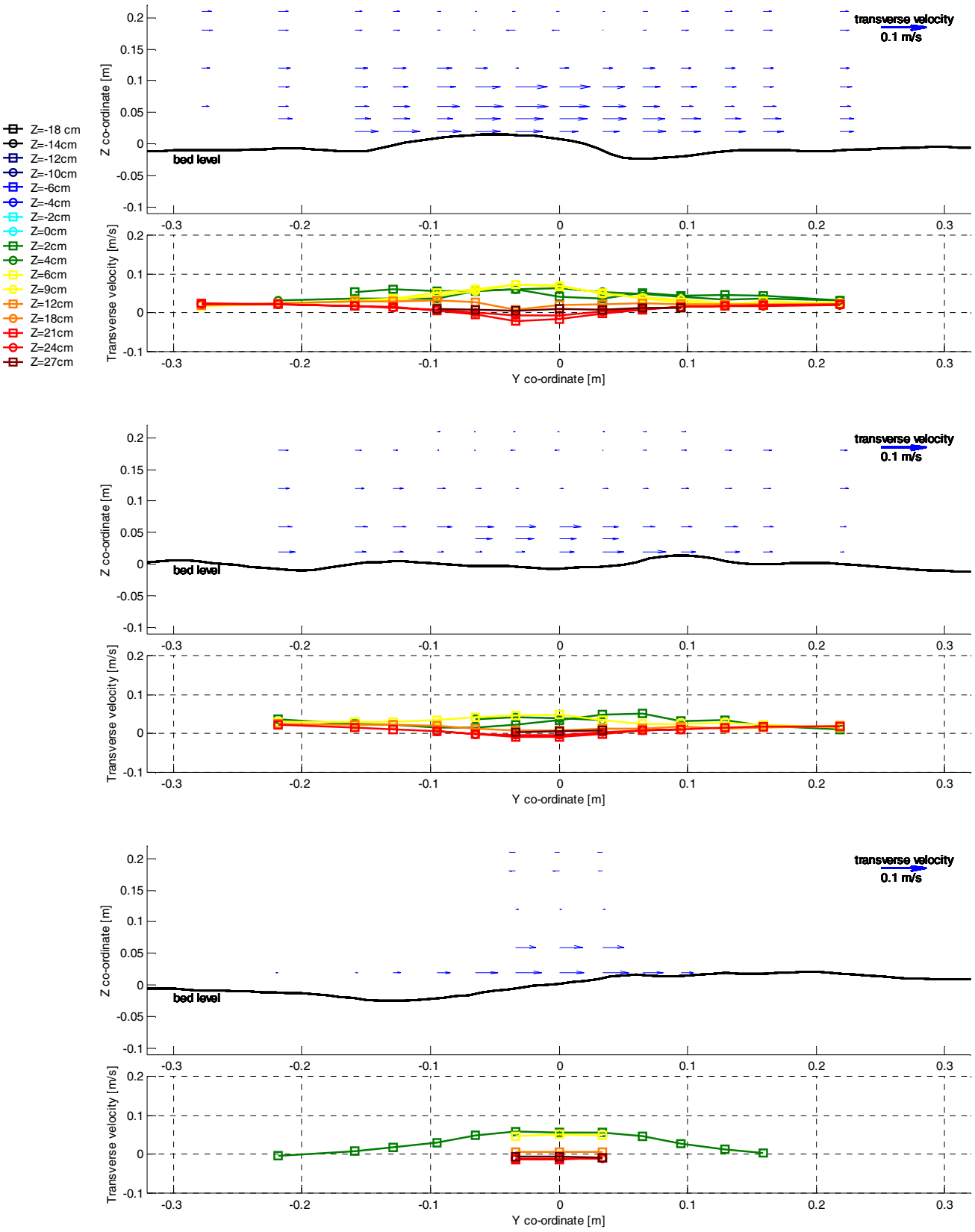

G.3 Experiment A4, X=15.20, 15.80 and 16.60 m

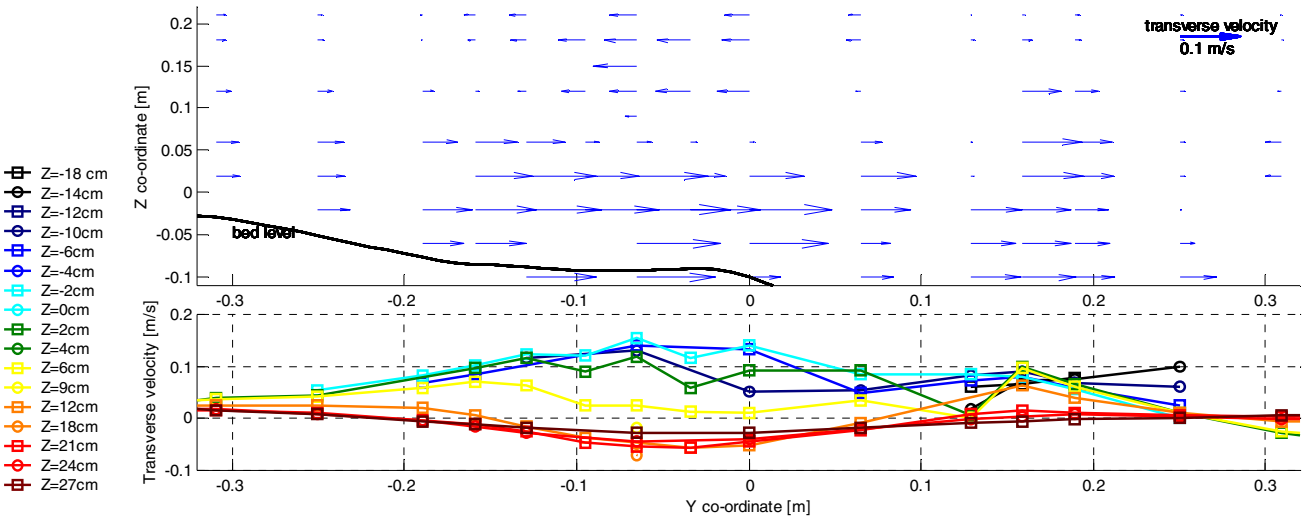

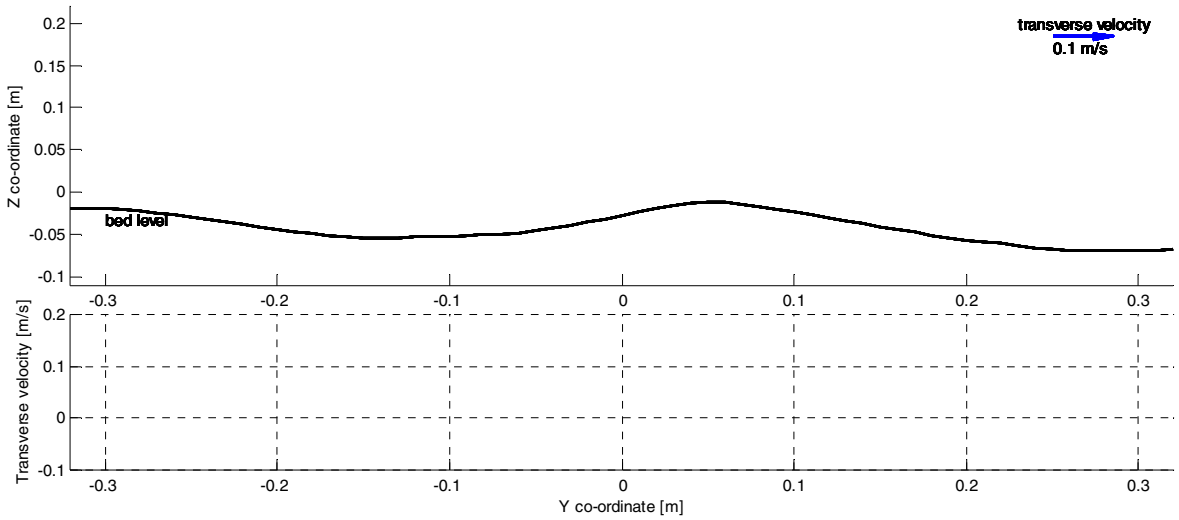

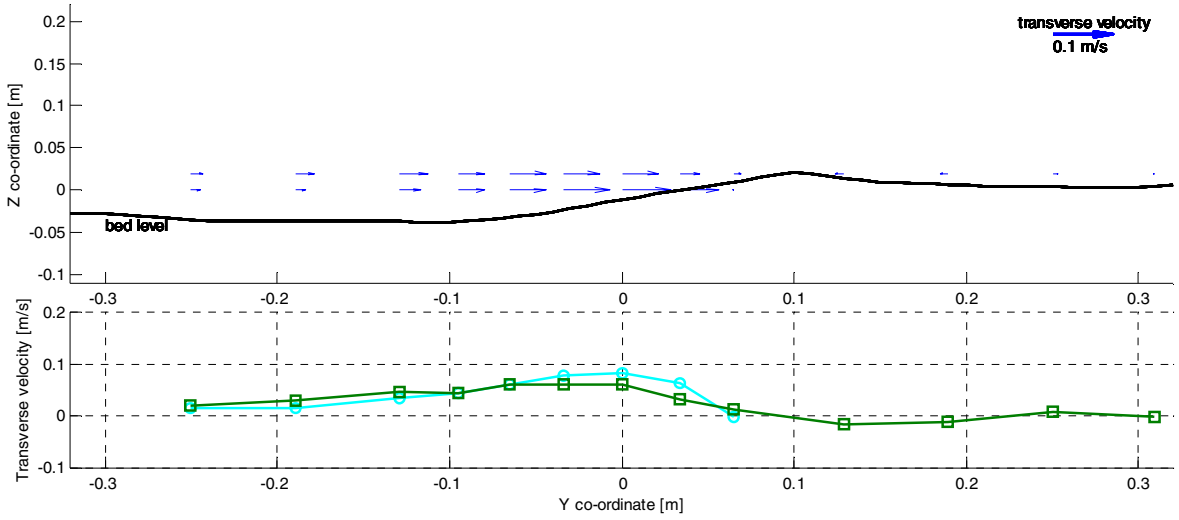

G.4 Experiment A2, X=15.20, 15.80 and 16.60 m.

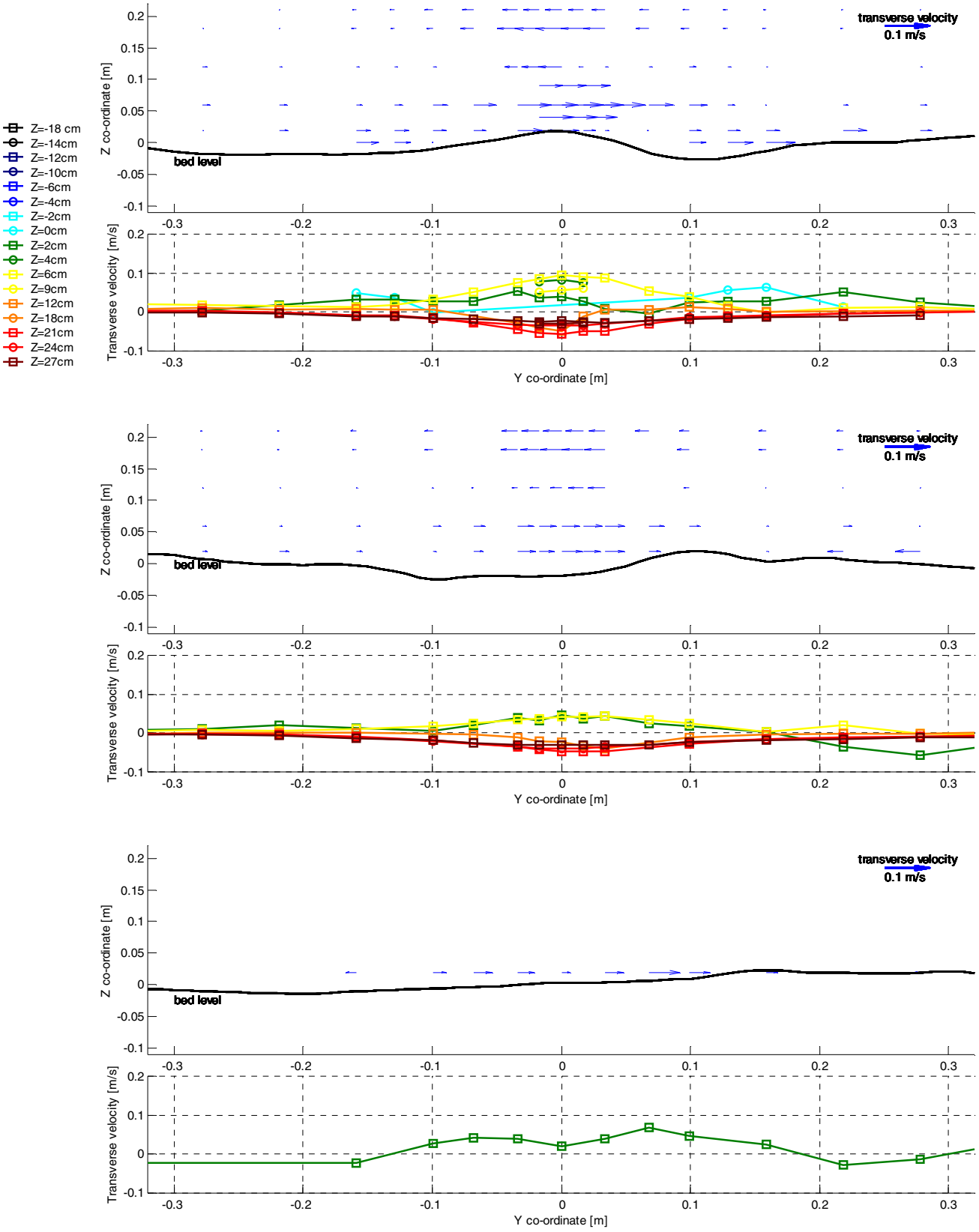

G.5 Experiment B2, X=15.20, 15.80 and 16.60 m.

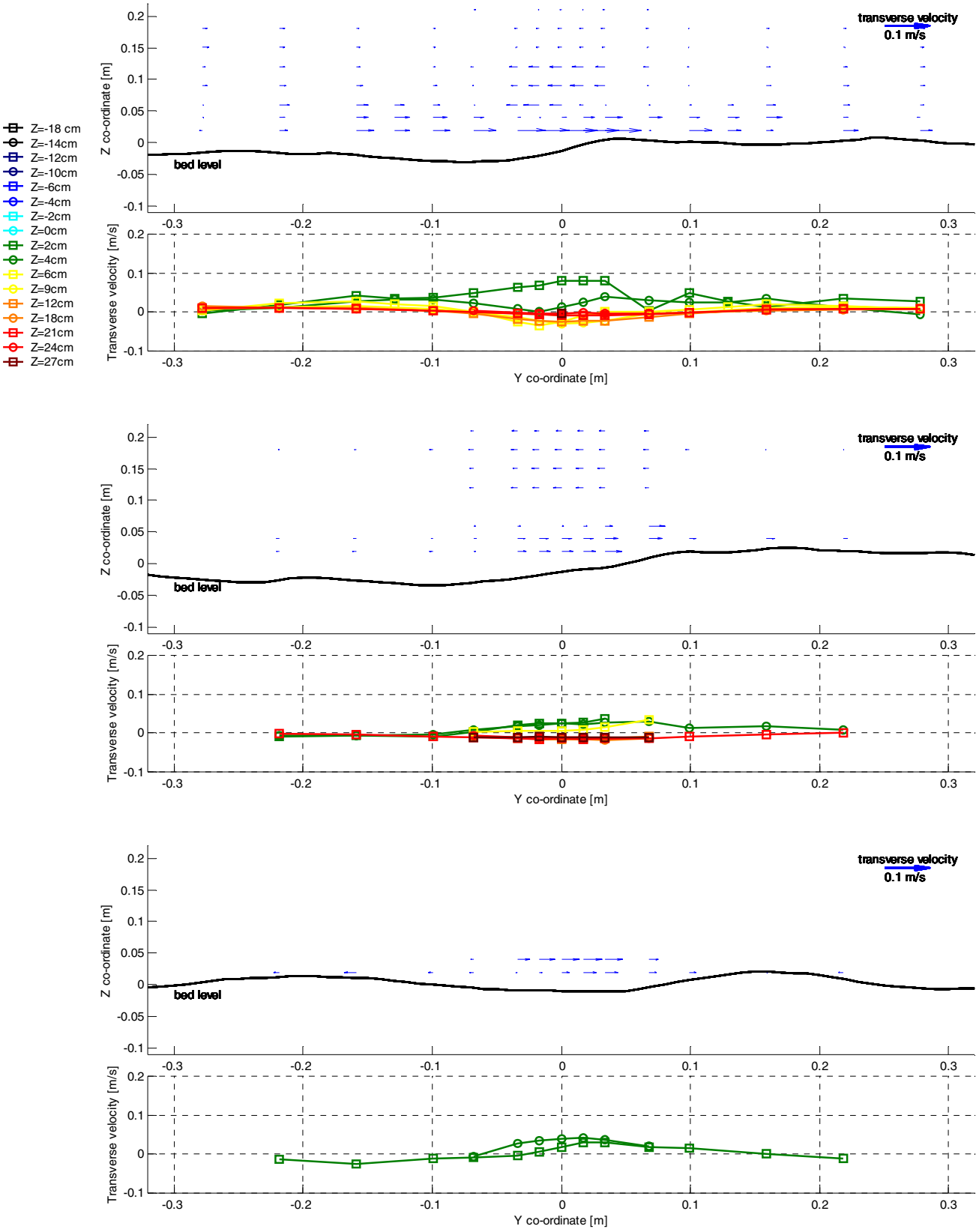

G.6 Experiment C2, X=15.20, 15.80 and 16.60 m.

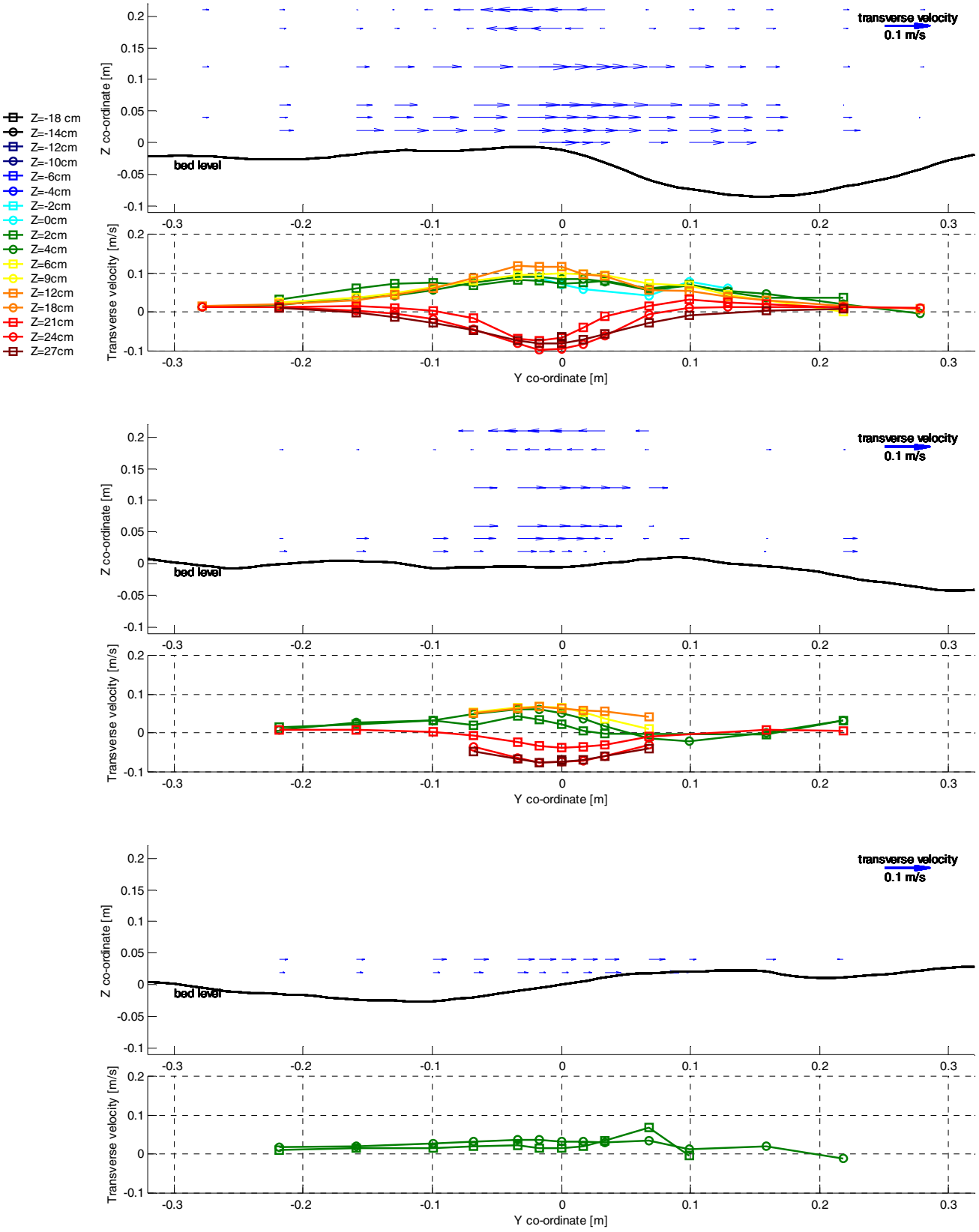

G.7 Experiment B3, X=15.20, 15.80 and 16.60 m.

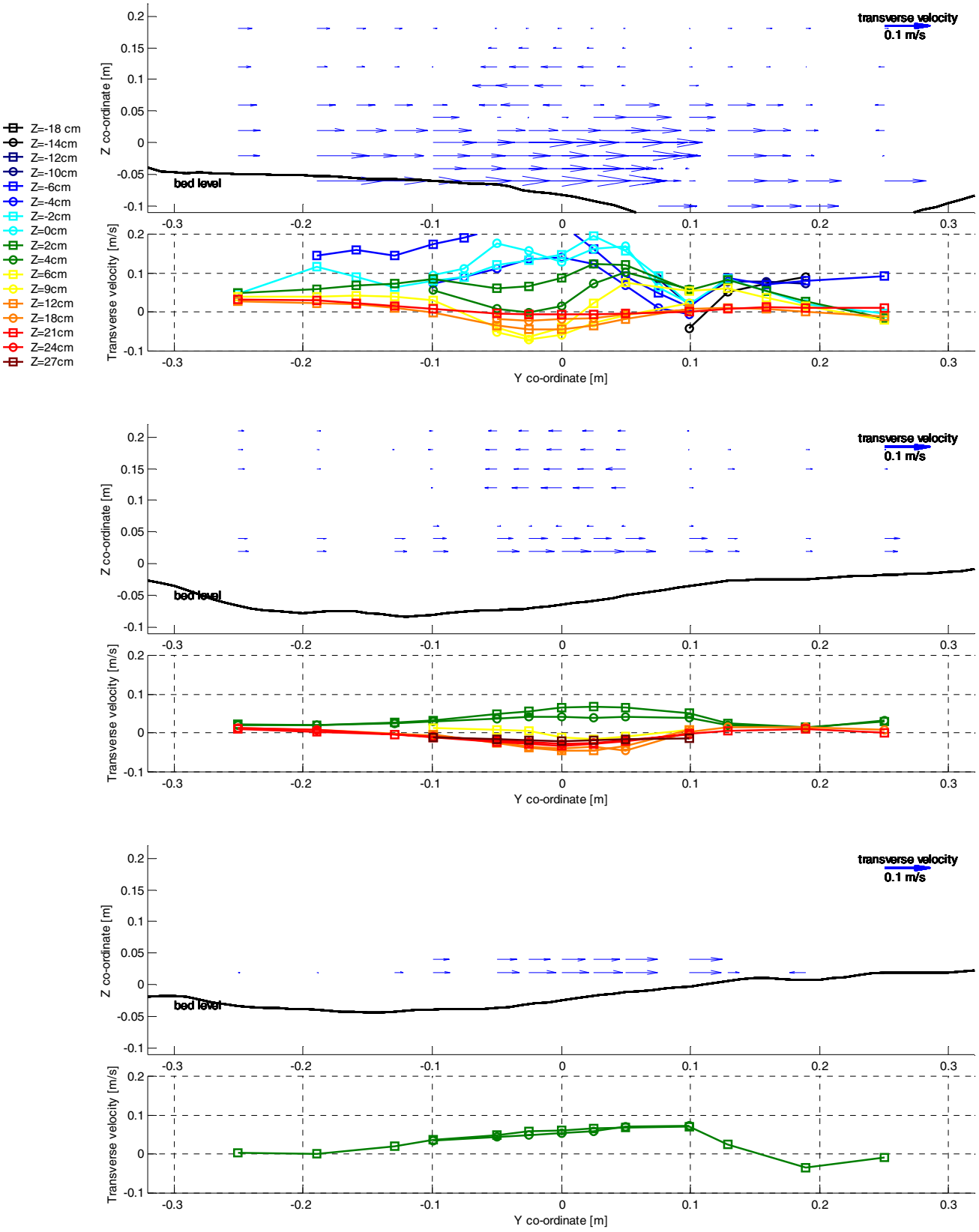

H Longitudinal flow velocity measurements

The longitudinal flow velocity has been plotted at the cross-section x = 15.80 m. For experiment A4 no data was available in this cross-section, so this appendix contains six plots.

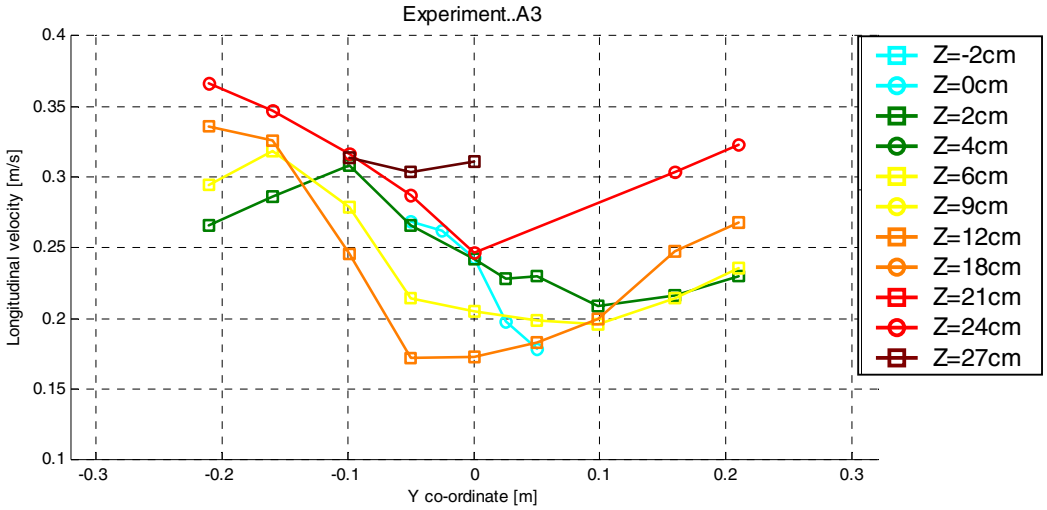

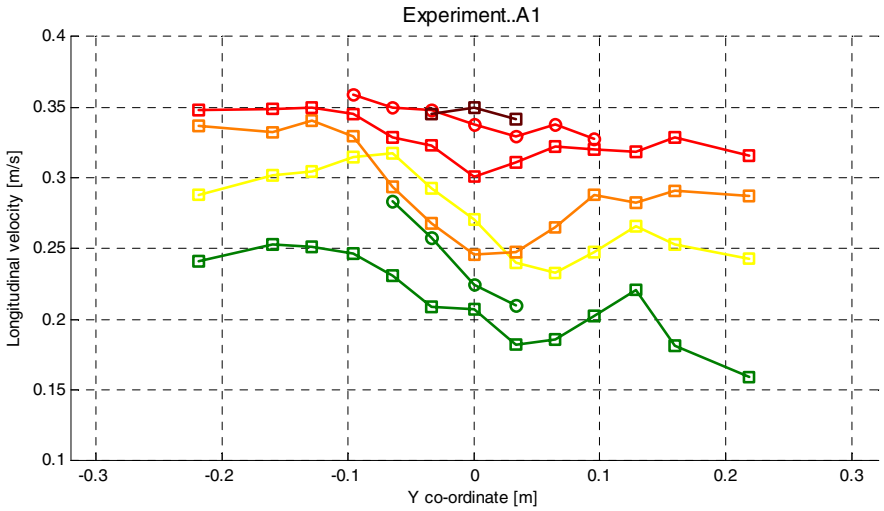

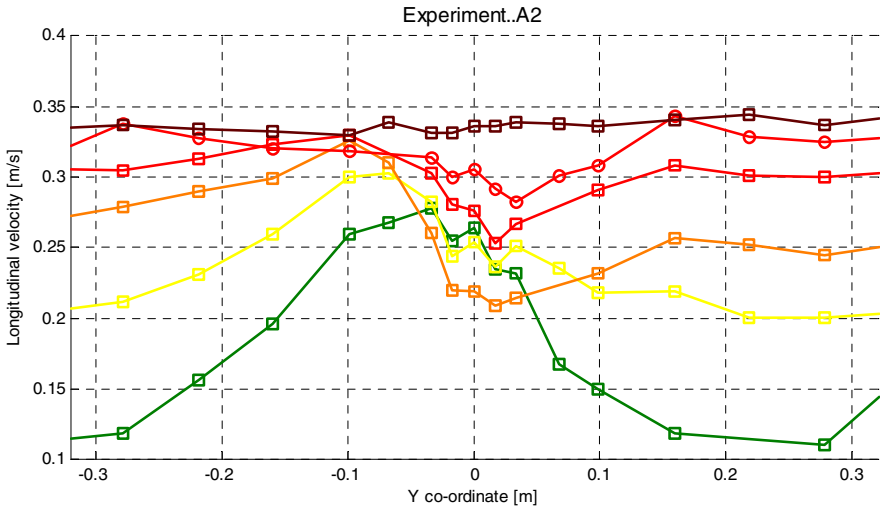

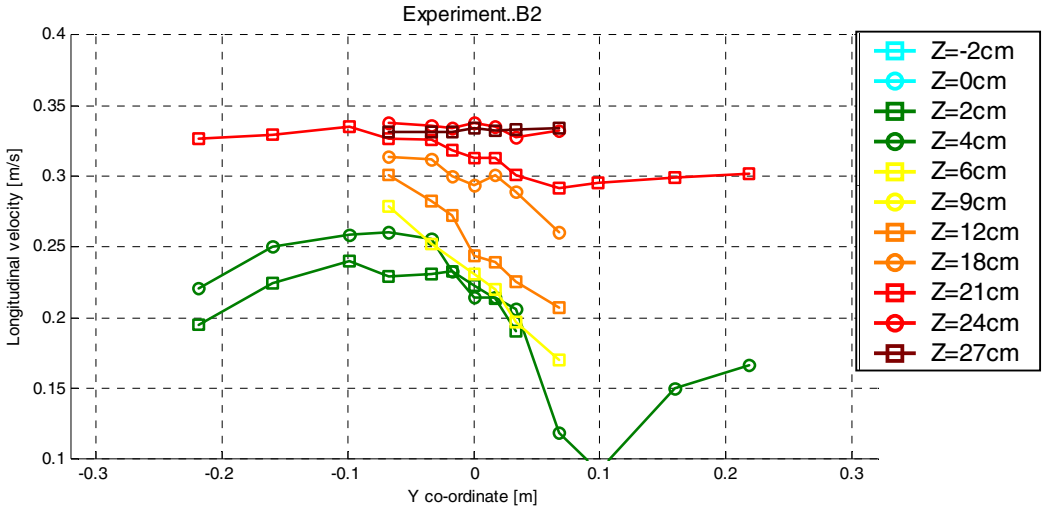
Experiment..B2
Longitudinal velocity [m/s]
Y co-ordinate [m]
Z=-2cm
Z=0cm
Z=2cm
Z=4cm
Z=6cm
Z=9cm
Z=12cm
Z=18cm
Z=21cm
Z=24cm
Z=27cm

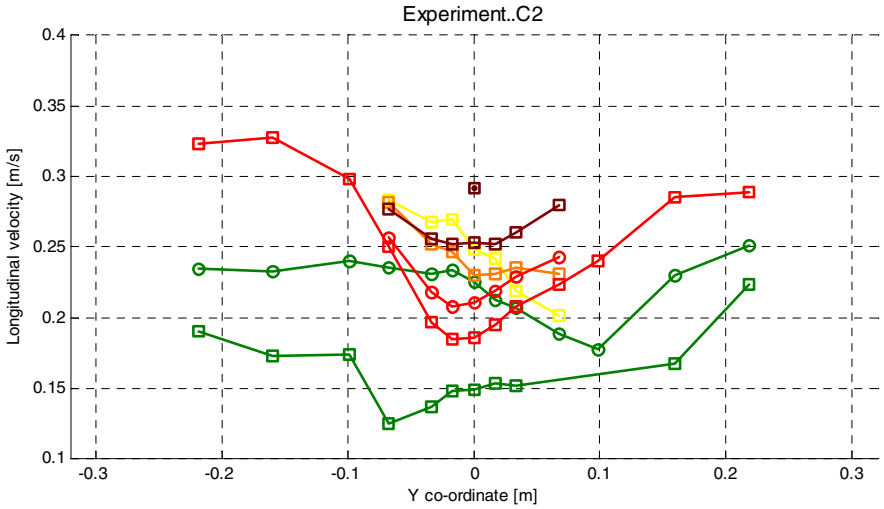
Experiment..C2
Longitudinal velocity [m/s]
Y co-ordinate [m]

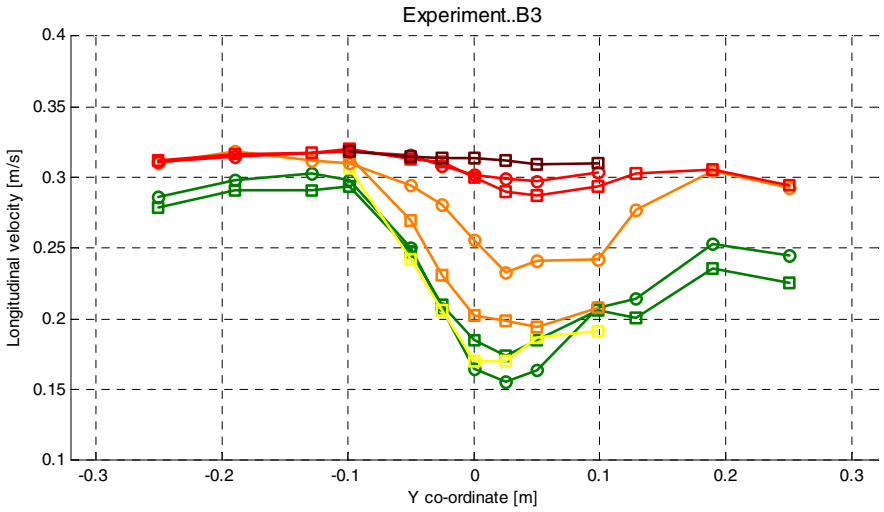
Experiment..B3
Longitudinal velocity [m/s]
Y co-ordinate [m]

I Delft3D-MOR simulations

I.1 Reference simulation, no vane

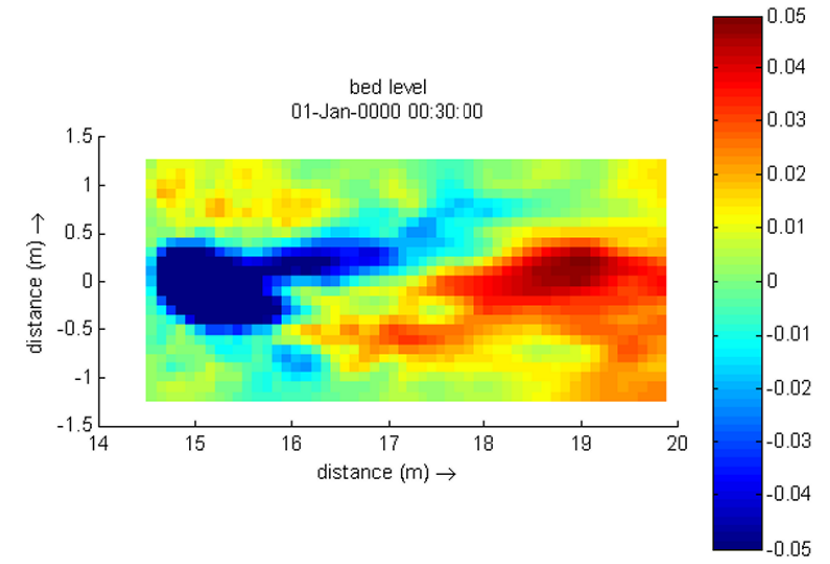

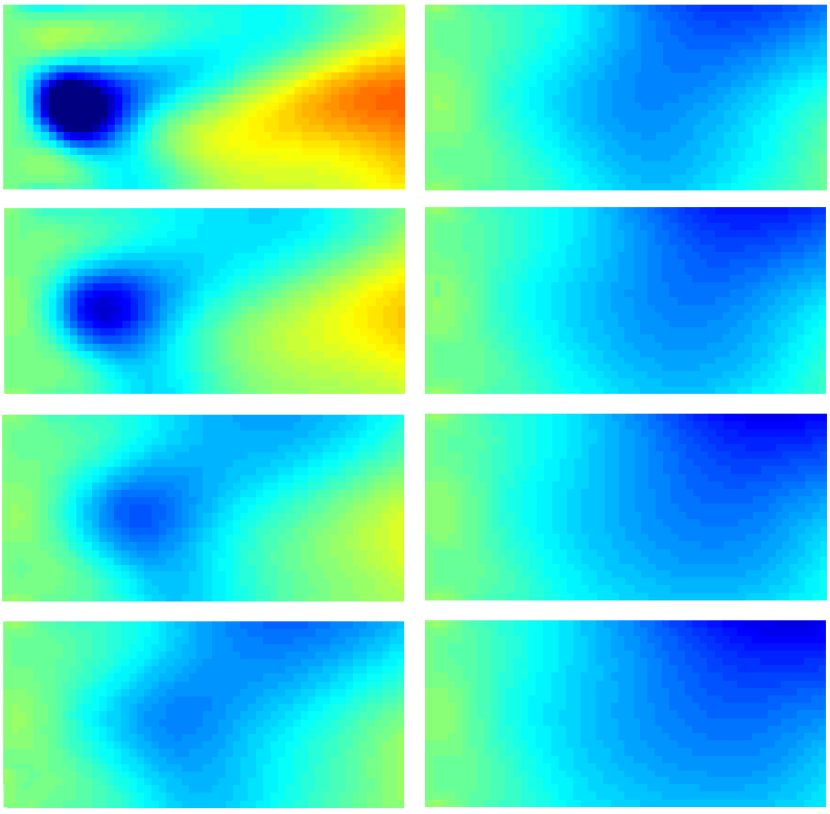

I.2 Type I, initial flat, comparison vortex-line model

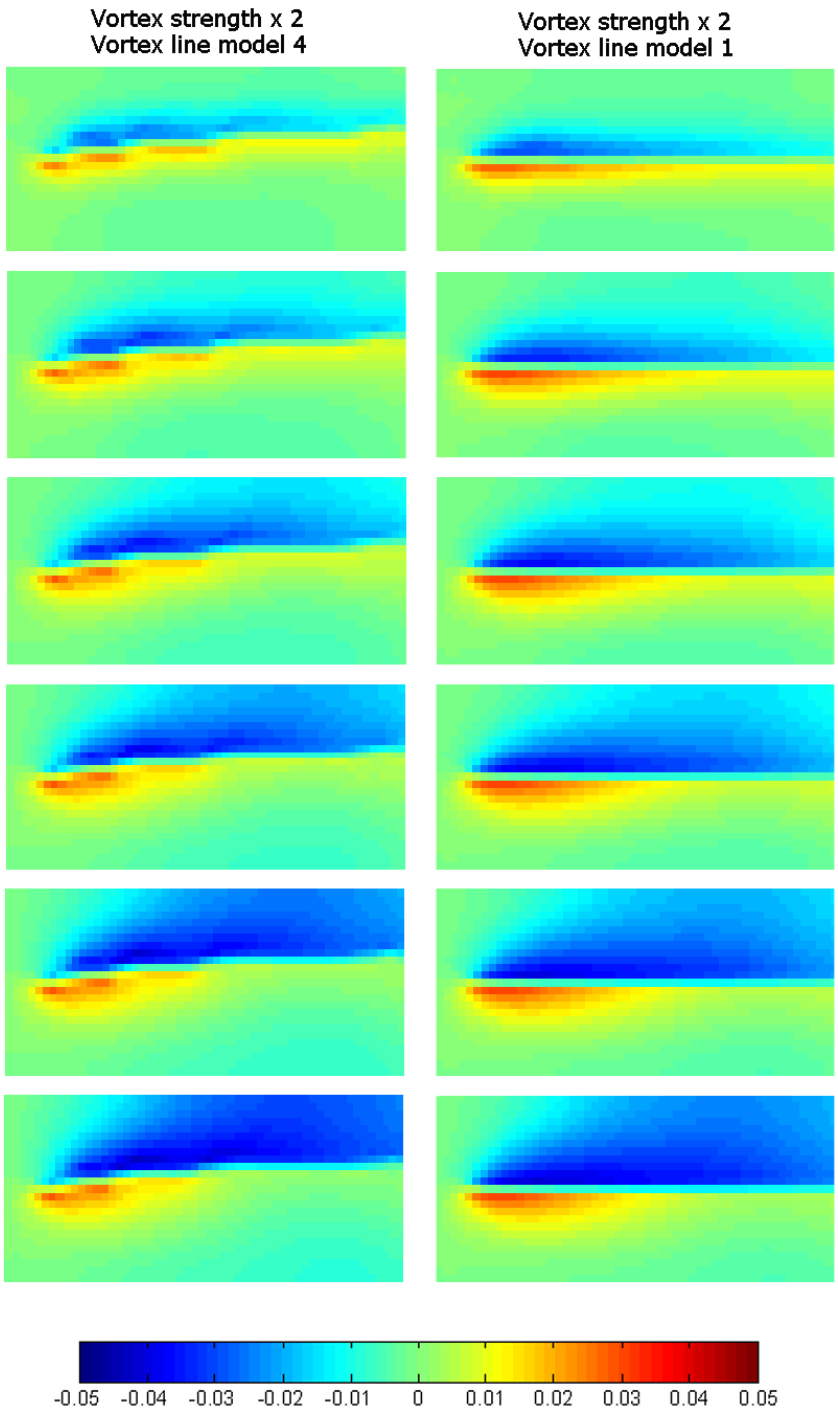

I.3 Type I, initial flat bed, comparison initial vortex

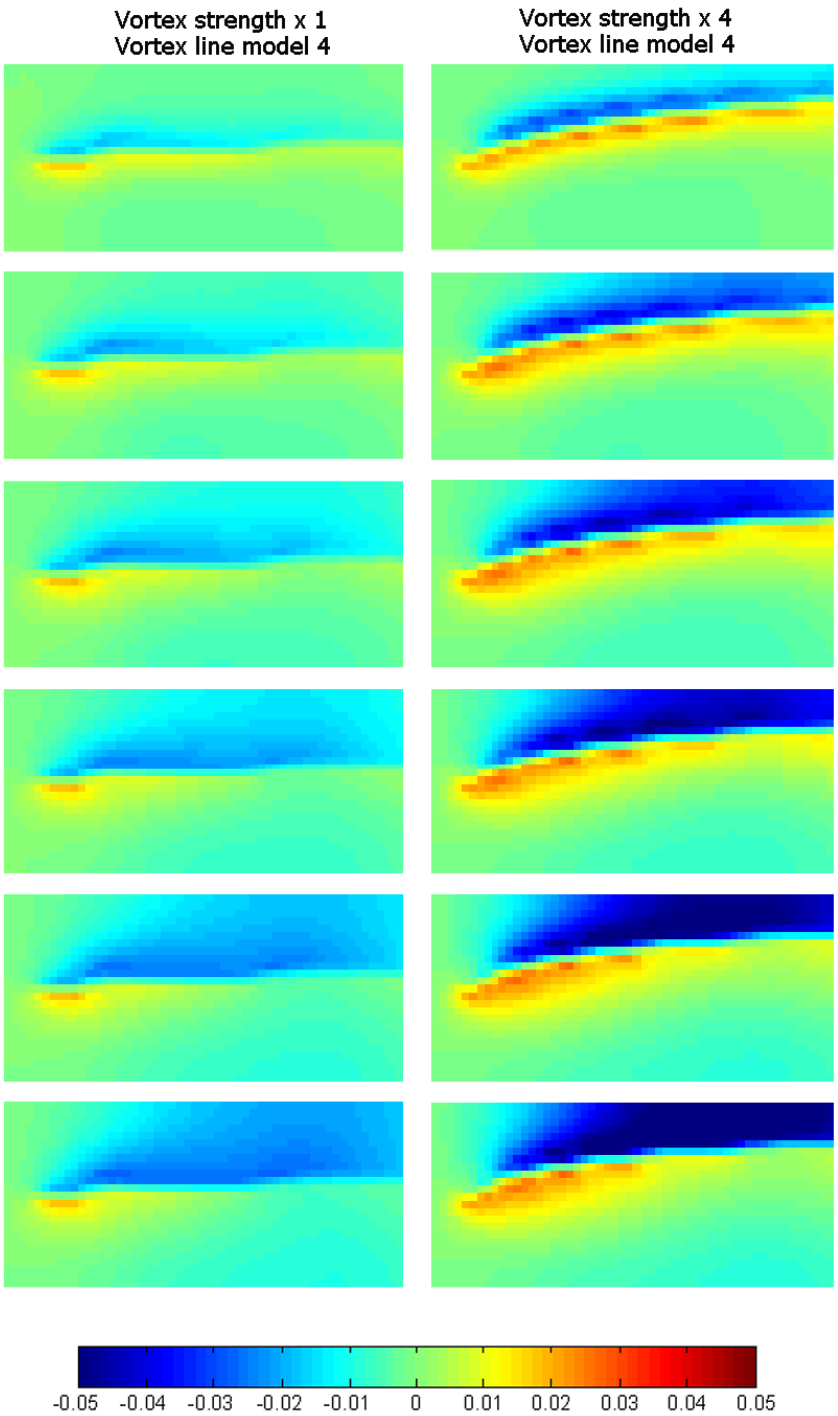

I.4 Type I, initial bed experiment A4

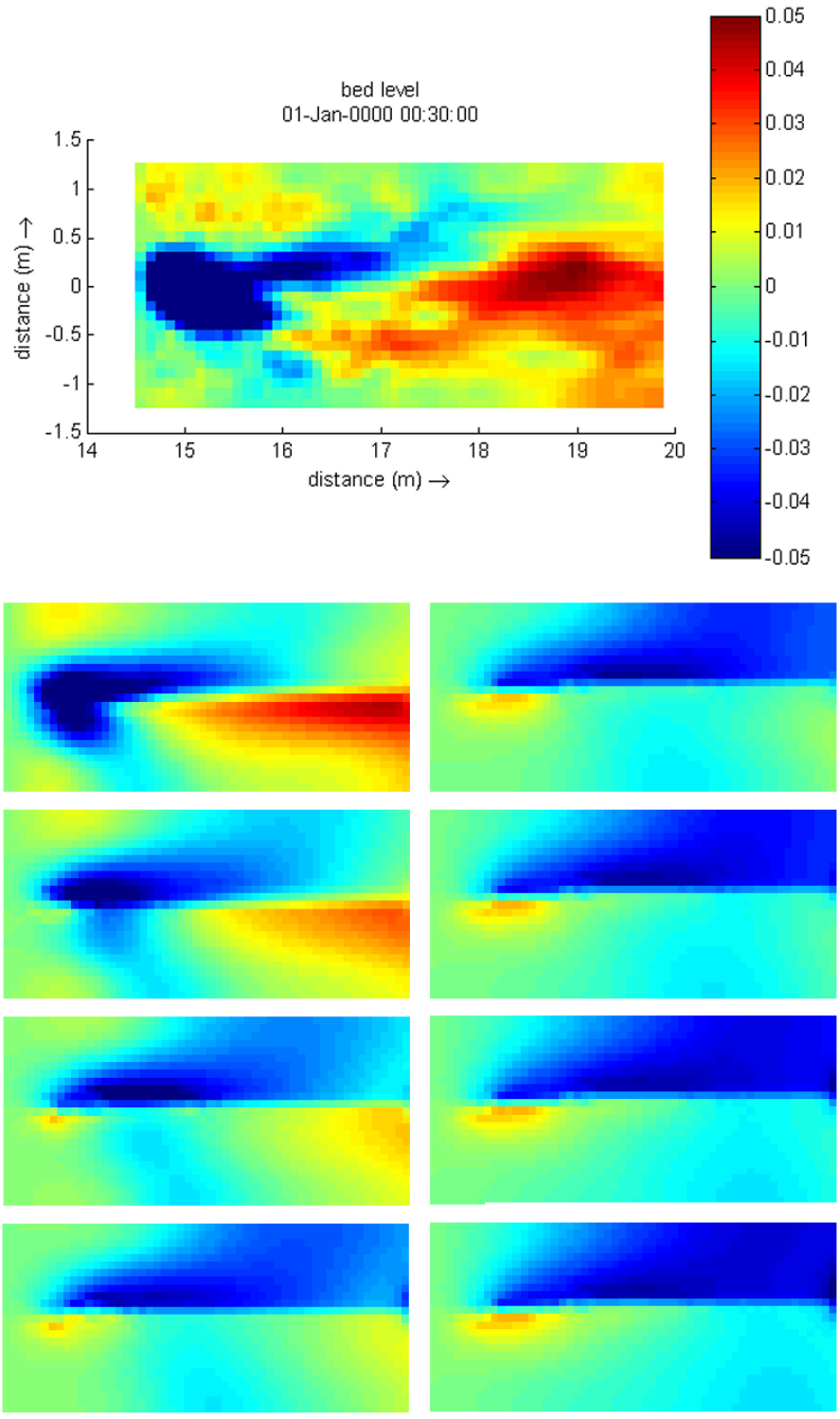

I.5 Type I, initial bed experiment B3

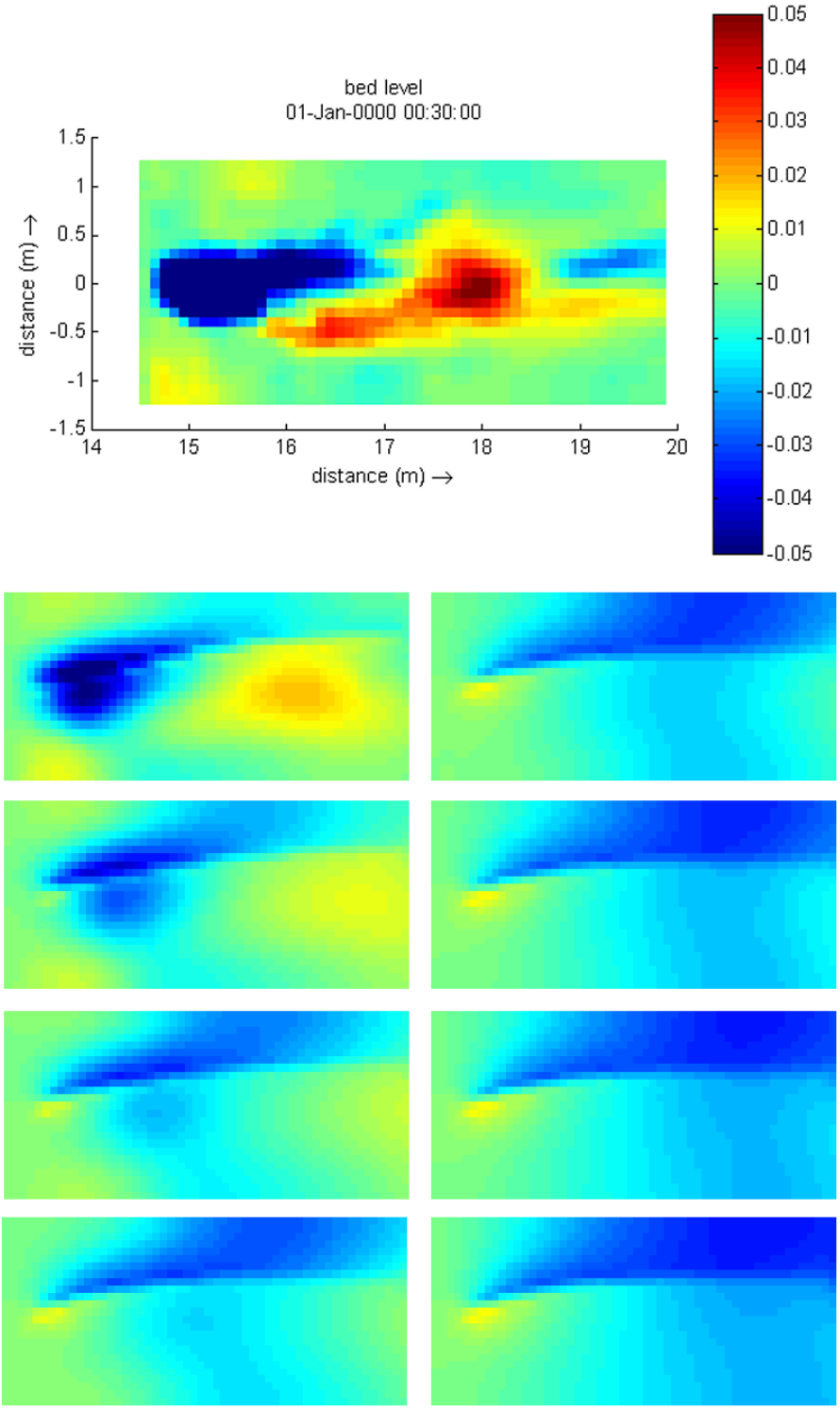

I.6 Type I, initial bed experiment A4, sediment withdrawal

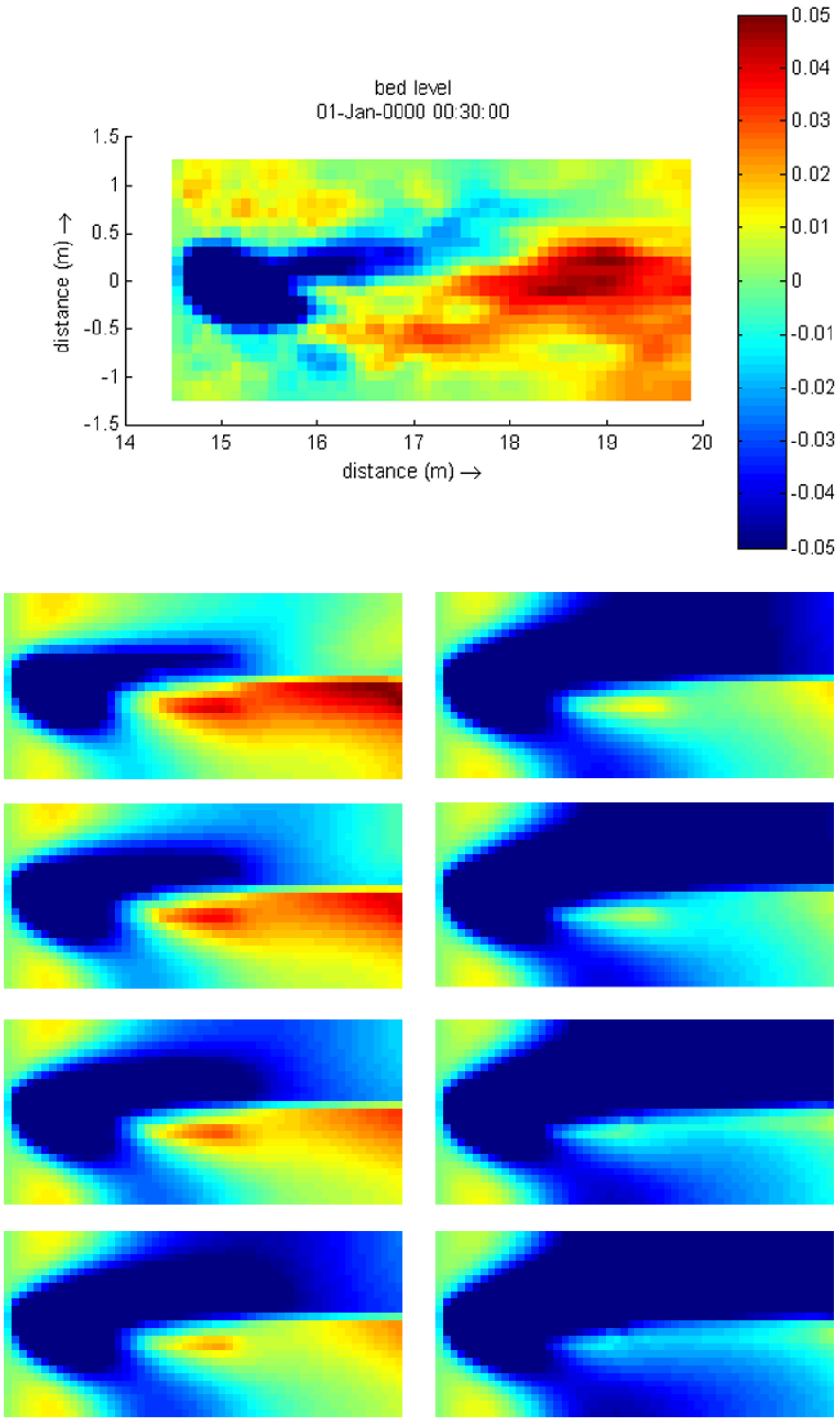

I.7 Type II vane, initial bed experiment A4

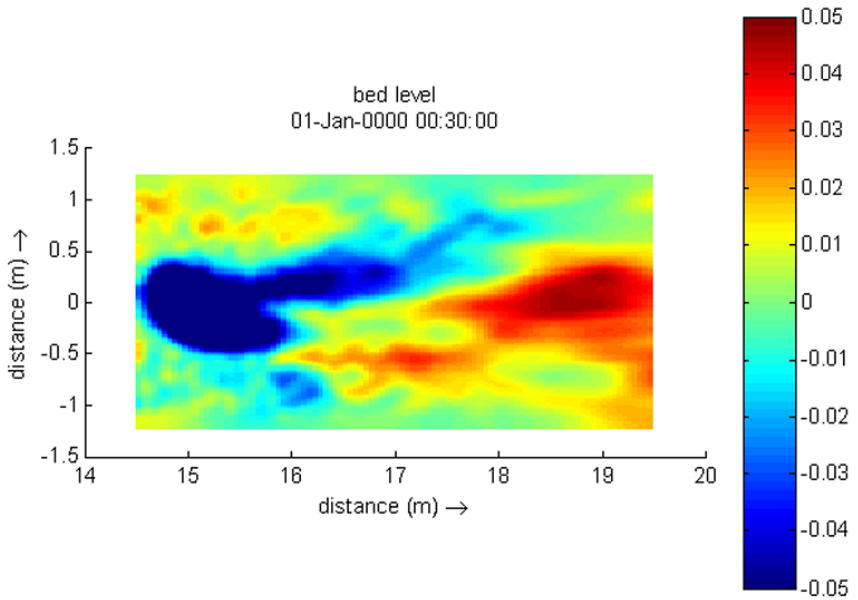

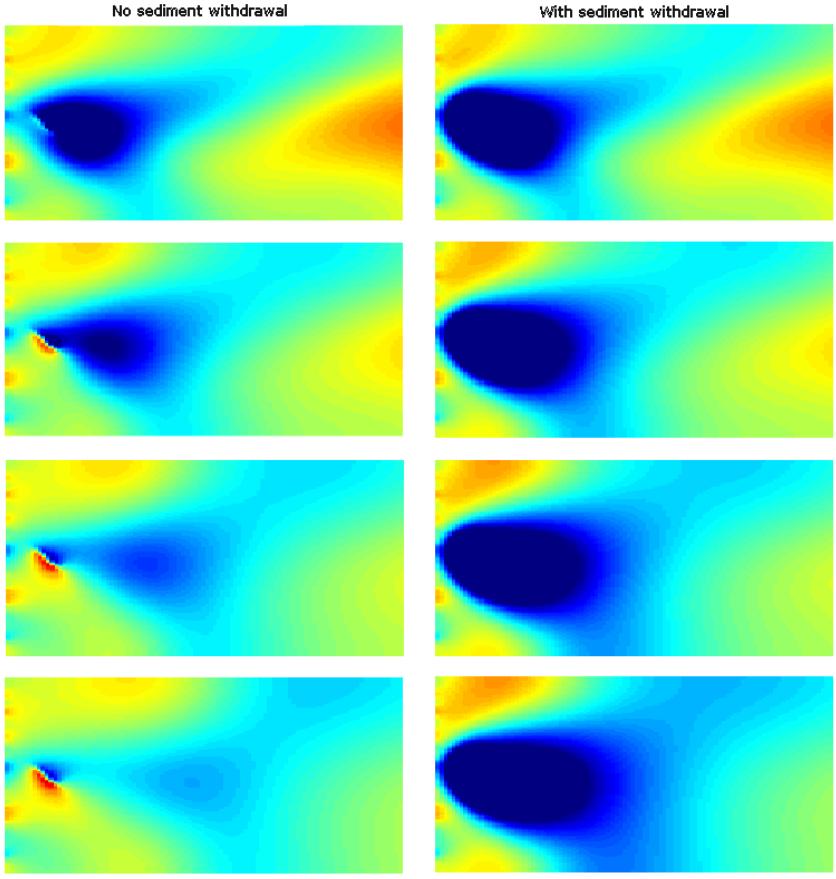

J Alternate bars

By defining two parallel channels in a straight flume and describing the interaction of water movement and sediment transport between the two channels, alternate bars can be explained as an oscillatory response of the system to an internal instability or a forced disturbance [Struiksma & Crosato, 1989]. The following equations contain the original equation and its solution.

$$\frac{T_m}{\lambda_w}\left(\frac{\partial^2 H}{\partial t \partial x}+\frac{1}{\lambda_w}\frac{\partial H}{\partial t}\right)-\frac{\overline{d}}{\beta_x}\frac{\partial^3 H}{\partial x^3}+\left(1-\frac{\overline{d}}{\beta_x \lambda_w}\right)\frac{\partial^2 H}{\partial x^2}+\left(\frac{1}{\lambda_s}-\frac{b-3}{2\lambda_w}\right)\frac{\partial H}{\partial x}+\frac{H}{\lambda_w \lambda_s}=\frac{H_{ce}}{\lambda_w \lambda_s} \qquad \text{(I.1)}$$

$$H' = \hat{H} e^{-k_r x+\omega_r t}\cos(k_i x + k_B y + \omega_i t) \qquad \text{(I.2)}$$

With,

$$\omega_i = \frac{2\pi}{T}, k_B = \frac{m\pi}{B},\ k_r = \frac{1}{L_D},\ k_i = \frac{2\pi}{L_p}$$

In which

ω_r	growth rate
T_m	morphological time scale
ω_i	wave frequency
k_B	cross-sectional wave number
m	Fourier mode in cross-sectional direction
B	width of the channel
k_r	spatial damping number
L_D	damping length
k_i	wave number
L_p	wave length
β_x	coefficient for influence of longitudinal slope on sediment transport
λ_w	characteristic length scale water movement
λ_s	characteristic length scale sediment movement
$\overline{d}$	average water depth
b	power in sediment transport formula

The interaction parameter (IP) is defined as λ_s / λ_w and can be written out into the following equation:

$$IP = \frac{\lambda_s}{\lambda_w} = \frac{\frac{\beta_y}{8}\left(\frac{B}{\overline{d}}\right)^2 \overline{d}}{\frac{C^2}{2g}\overline{d}} = \frac{\beta_y g}{4C^2}\left(\frac{B}{\overline{d}}\right)^2 \qquad \text{(I.3)}$$

In which,

β_y	coefficient influence cross-sectional slope on sediment transport
C	Chézy roughness coefficient

Substituting the solution (Equation (I.2)) into the original Equation (I.1) under certain assumptions, where these assumptions are based on a certain expected behaviour, solves the differential problem. The first solution is obtained by assuming a stable bar pattern by neglecting the damping of the solution ($k_r = 0$). This solution describes free alternate bars that move through a system. The other solution describes forced alternate bars that are on a fixed position is the system and damp out. This solution is obtained by neglecting the wave frequency and growth rate.

J.1 Free alternate bars

The first solution has been worked out in the handouts CTwa5311 [de Vriend, Wang & Havinga, 2001]. The elaboration results in the following equation describing the growth rate of alternate bars.

$$\omega_i T = \frac{-1}{k_i \lambda_w + 1}\left[\left(\frac{1}{IP} - \frac{b-1}{2} + \frac{\overline{d}}{\beta_x \lambda_w}\right)\left(k_i \lambda_w\right)^2 + \frac{\overline{d}}{\beta_x \lambda_w}\left(k_i \lambda_w\right)^4 + \frac{1}{IP}\right] \tag{I.4}$$

The presence of these free alternate bars can also be determined on base of the marginal stability curve [Columbini, Seminara & Tubino, 1987, Mosselman & Wang, 1994]. The curve describes the boundary value of IP for which alternate bars will start developing.

$$\frac{\lambda_s}{\lambda_w}(=IP) = \frac{2\left(\frac{C^2}{g}\right) f(\theta) X \left(X+1\right)^2 (\xi X + \left(\frac{g}{C^2 f(\theta)}\right))}{(b-1)X(2X+1) - (X+2)^2 (\xi X + \left(\frac{g}{C^2 f(\theta)}\right))} \tag{I.5}$$

with,

$$X = \left(\frac{k_i}{k_B}\right)^2 = \left(\frac{k_i B}{m\pi}\right)^2$$

In which

ξ	coefficient influence longitudinal slope on sediment transport
$f(\theta)$	coefficient influence gravity on cross-sectional slopes based on the shields parameter.

Equation (I.3) and (I.5) are graphically presented in Figure J.2 and Figure J.1 below. The flume characteristics have been used, and are: $\lambda_s = 1.1$, $\lambda_w = 13.8$, b = 5, and m = 1. The influences of the cross- and longitudinal slope have been defined using:

- Cross-sectional slope influence, $\beta_y = \frac{8 f(\theta)}{\pi^2 m}$, $f(\theta) = 0.85\sqrt{\theta}$

- Longitudinal influence, assuming ξ = 0.03, $\beta_x = \frac{1}{\xi}\frac{g}{C^2}$

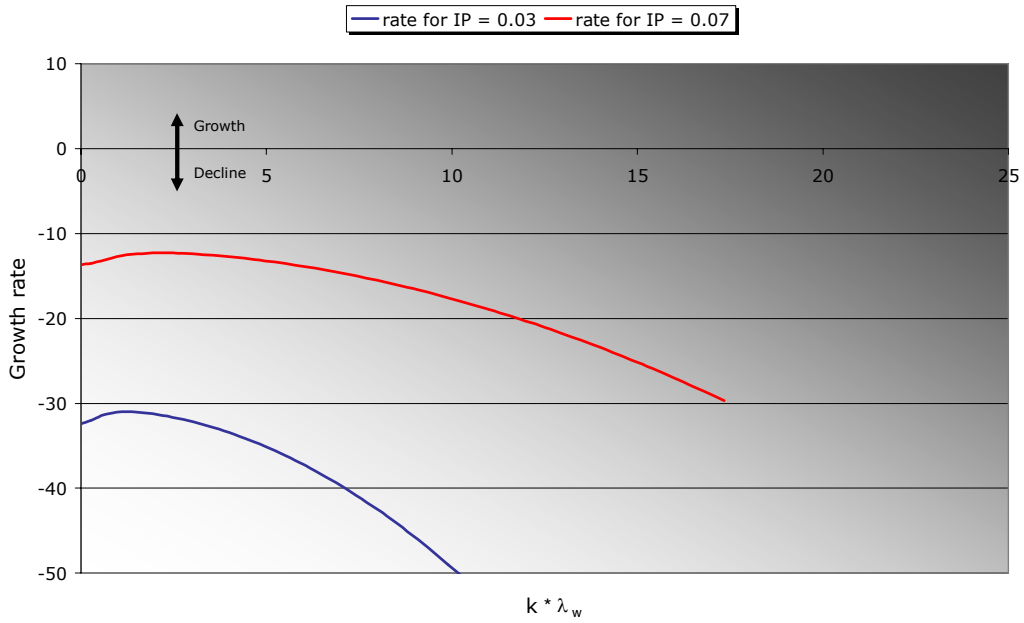

Figure J.1: Growth rate of alternate bars

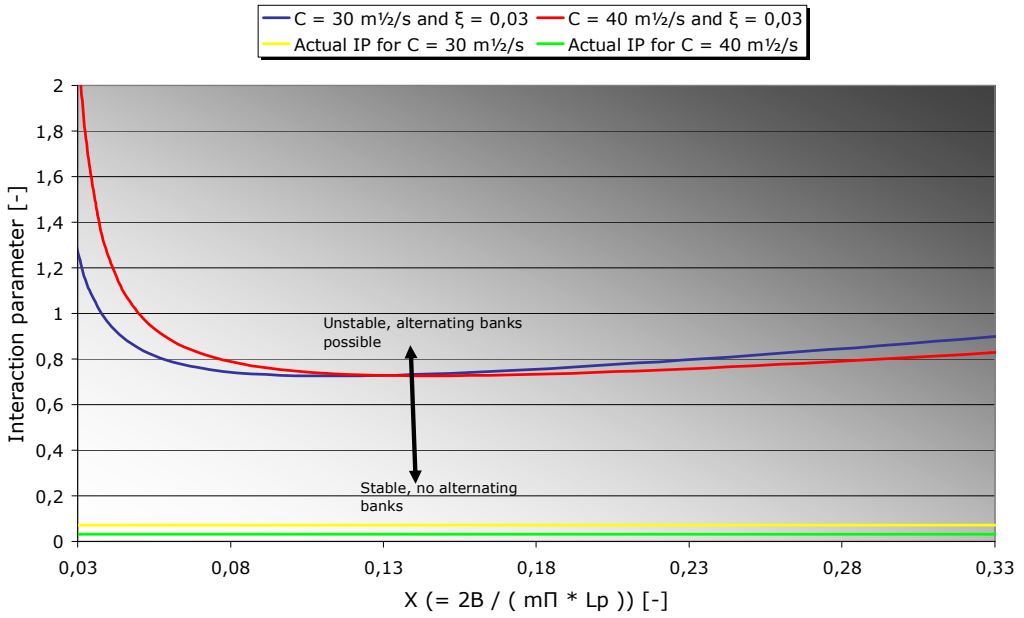

Figure J.2: Marginal stability curve alternate bars

Figure J.1 shows that the growth rate for alternate bars is strongly negative, and Figure J.2 shows that instability can only occur for IP>0.7. So both figures clearly indicate that free alternate bars are absent.

J.2 Forced alternate bars

Placing the vane in the flume might somehow force an alternate bars pattern. In this case the bars are not migrating, but are on a fixed position and are present as a response to the local disturbance by the vane.

By neglecting the time dependency of Equation (I.2), the equation reduces to:

$$H' = \hat{H}\cos(k_r x)e^{-k_i x} \tag{I.6}$$

Substituting this equation into the original differential equation reveals the following expressions for damping length, $L_D\left(=\frac{1}{k_r}\right)$ and the wavelength, $L_p\left(=\frac{2\pi}{k_i}\right)$ [de Vriend, Wang & Havinga, 2001]:

$$L_D = \frac{4\lambda_w}{2\frac{\lambda_w}{\lambda_s} - b - 3}, L_p = \frac{4\pi\lambda_w}{\sqrt{\frac{b^2+7}{4} - \left(\frac{\lambda_w}{\lambda_s} + \frac{b+1}{2}\right)^2}} \tag{I.7}$$

Using λ_s=1.1, λ_w=13.8, and b = 5 results in L_D = 2.3 m and a non-existent solution for L_p. Physically this means that there in no oscillatory solution and the solution damps or grows exponentially according to $e^{-\frac{x}{L_D}}$. So the flume is also not sensitive for forced alternate bars. The solution has also been obtained by solving Equation (I.5) in Matlab with initial conditions $H(0) = 0.1$ and $\frac{\delta H}{\delta x} = 0$ (value function and derivative). Figure J.3 below shows the solution.

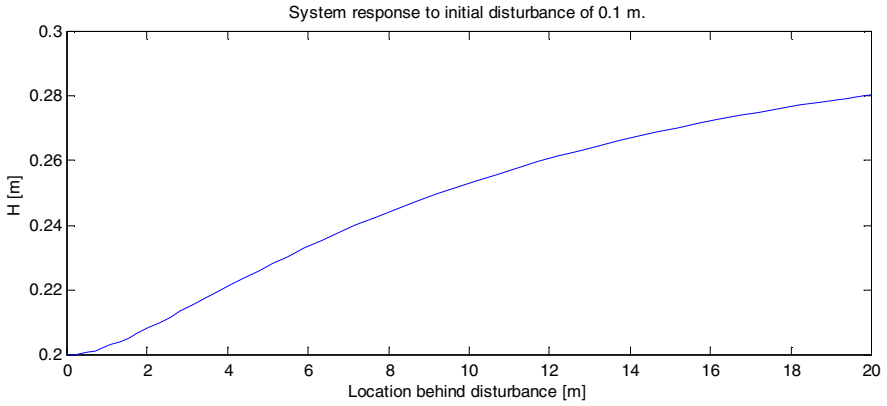

Figure J.3 Flume response to initial disturbance

Analysis was done for a width of 2.5 meter, the flume width. For smaller widths, the stability of the system only increases; so alternating patterns are excluded for those cases too.